Meso- and Nano-scaled Polymer Fibers and Tubes

Fabrication, Functionalization, and Characterization

Dissertation

zur

Erlangung des Doktorgrades

der Naturwissenschaften

(Dr. rer. nat.)

dem

Fachbereich Chemie der Philipps-Universität Marburg

vorgelegt von

Jun Zeng

aus Hunan, China

Marburg / Lahn, 2003

Von Fachbereich Chemie der Philipps-Universität Marburg
als Dissertation angenommen am 06. 03. 2003

Erstgutachter: Prof. Dr. A. Greiner
Zweitgutachter: Prof. J. H. Wendorff

Tag der mündlichen Prüfung am 07. 03. 2003

Wissenschaft in Dissertationen

Band

Meso- and Nano-scaled Polymer Fibers and Tubes

Fabrication, Functionalization, and Characterization

von

Jun Zeng

Verlag Görich & Weiershäuser GmbH
Marburg / Lahn
2003

Zugl.: Marburg/L, Diss.2003

Druck: Görich & Weiershäuser GmbH, Marburg / Lahn

Printed in Germany

ISBN

Für meine lieben Eltern
und meine liebe Familie
in Dankbarkeit.

Table of Contents

Structures, expressions, and abbreviations

Structures	Expressions	Abbreviations
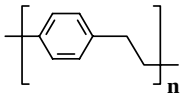	Poly (p-xylylene)	PPX or Parylene N
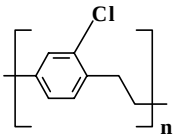	Poly (p-chloroxylylene)	Parylene C
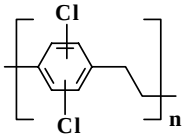	Poly (dichloro-xylylene)	Parylene D
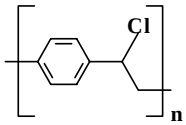	Poly (chloro-p-xylylene)	PPX-Cl
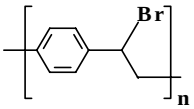	Poly (bromo-p-xylylene)	PPX-Br
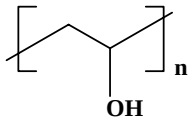	Polyvinyl alcohol	PVA
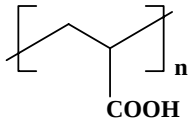	Polyacrylic acid	PAA
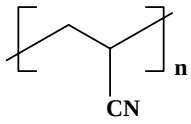	Polyacrylonitrile	PAN
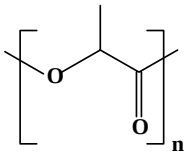	Polylactide	PLA
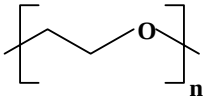	Polyethylene oxide	PEO

Structures, expressions, and abbreviations

Structures	Expressions	Abbreviations
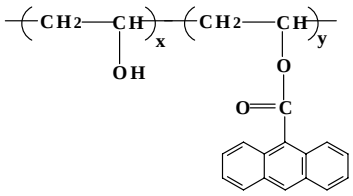	PVA derivative containing anthracene substituent	PVA-Anth
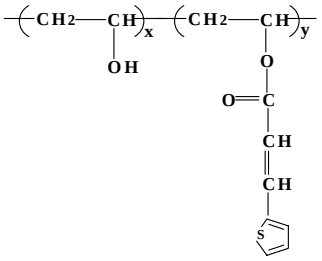	PVA derivative containing thienyl acrylate substituent	PVA-Thio
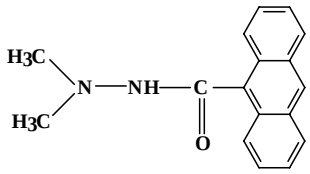	Tert-amine compound containing fluorescent substituent	Tert-amine
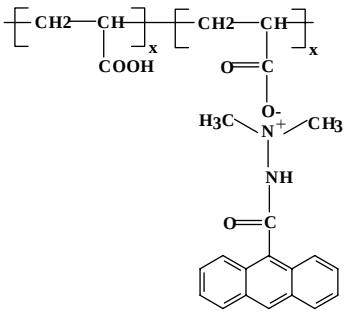	PAA-tert-amine salt containing anthracene substituent	PAA-tert-amine

Abbreviations

A	Absorbance
ArC	Aromatic carbon
ArH	Aromatic hydrogen
BSA	Bovine serum albumin
cps	counts per second
Conc.	Concentration
Cond.	Conductivity
CVD	Chemical vapor deposition
d	day
diam.	diameter
DMF	N, N-Dimethylforamide
DSC	Differential Scanning Calorimetry
Econd.	Electrical conductivity
GC	Gas Chromatography
GPC	Gel Permeation Chromatography
hr	hour
IR	Infrared Spectroscopy
m	middle
min	minute
M_n	Number average molecular weight
MS	Mass Spectrometry
M_w	Weight average molecular weight
nm	nanometer
NMR	Nuclear Magnetic Resonance Spectroscopy
Pa·s	Pascal second
PF	pyridinium formiate
ppm	parts per million
RT	room temperature
s	strong
SFT	Surface tension
SDS	sodium dodecylsulfate
T	temperature

t	time
TGA	Thermogravimetry Analysis
THF	tetrahydrofuran
T_g	Glass temperature
T_m	Melting point
TOS	p-toluene sulfonate
UV	ultraviolet
Vis	visible
Visc.	viscosity
w	weak
WAXS	Wide-angle X-ray Scattering
λ	Wavelength
$\tilde{\nu}$	Wavenumber

1 Introduction

Since Richard Feynman's famous statement in 1959 that "There's plenty of room at the bottom", a new field of nanostructures, which have dimensions between 1 nm to 100nm, has been opened. The continuously increasing interests in nanostructures result from their numerous potential applications in various areas such as biomedical sciences [1], electronics, optics, optoelectronics [2], magnetism [3], energy storage [4], filtration [5, 6], separation [7, 8], electroanalysis [9], catalysis [10], and sensors [11, 12]. Ultra-small building blocks have been found to exhibit a broad range of enhanced properties, such as enhanced mechanical, optical [13], optoelectronic, magnetic [14, 15], and electronic properties [16] compared to coarser-grained matter of the same chemical composition. These unique, enhanced properties are attributed to size effects, which are well understood in terms of "quantum confinement" in nanostructures.

Nano-scaled fibrils and tubules, as a class of low-dimensional nanostructures, have attracted extensive research interests due to their high anisotropy and huge specific surface area. During the past decade, great progress has been made in fabrication techniques for nanofibrils and nanotubules. Among the numerous chemical methods, a so-called "template synthesis" method has been paid tremendous attention due to its generality and versatility, which was developed by the group of C.R Martin [1, 6, 9, 17-23]. The "template synthesis" method entails synthesizing the desired material within the pores of a nanoporous membrane. The membranes employed have cylindrical pores of uniform diameter (Fig. 1.1), and nanocylinders of the desired materials are obtained in each pore. Depending on the material and the chemistry of the pore wall, the nanocylinders may be solid (nanofibrils) or hollow (nanotubules). A representative "template synthesis" process utilizing electrochemical deposition methods is schematically shown in Fig. 1.1 a-b.

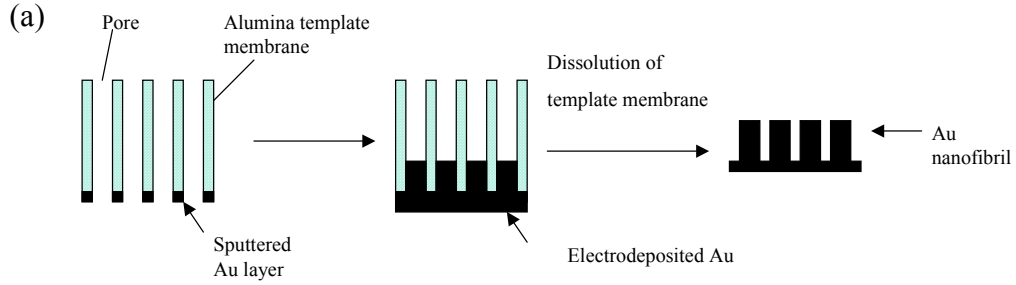

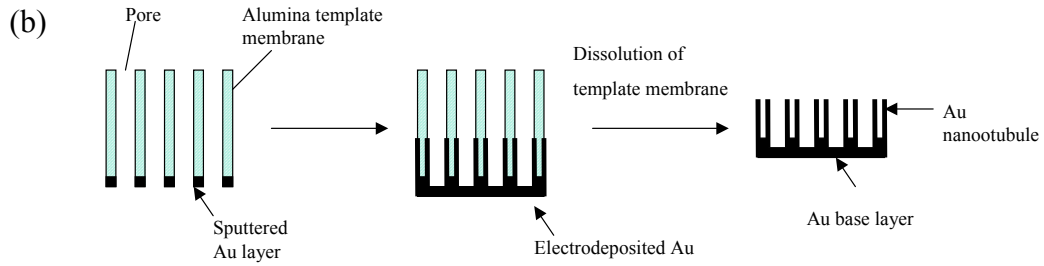

Fig. 1. 1 Fabrication procedure of Au nanostructures by means of Martin's template synthesis technique. (a) Au nanofibril; (b) Au nanotubule

The most commonly employed porous templates are alumina membranes, which have uniform, cylindrical, and parallel pores with diameters ranging from 20 nm to 200 nm (commercially available in Whatmann, Anotech etc.). Alumina membranes with desired diameters (as small as 5 nm) can be prepared by means of electrochemical method [24]. Alternatively, "track-etch" polymeric membranes, which contain randomly distributed nanochannels with uniform diameters, are also good template candidates. A wide range of pore diameters (down to 10 nm) are available for this type of membranes. Typical representatives of the "track-etch" membranes are polycarbonate and polyester filtration membranes. In addition, mesoporous silica membranes [25, 26], aluminosilicate membranes [25, 27], mesoporous zeolites [28-30], and carbon nanotubes [31-33] have also been used as templates.

Depending on the materials of the nanostructures to be synthesized within the pores, various synthesis methods have been developed, including electrochemical deposition [14, 19], electroless (i.e. chemical) metal deposition [34], chemical polymerization [17], electropolymerization [3, 11, 35-37], sol-gel deposition [38, 39], and chemical vapor deposition (CVD) [40-43]. For example, conductive polymer nanostructures (e. g. polyaniline, polythiophone, polypyrrole, and their copolymer) have been synthesized by electrochemical polymerization [36, 37, 44] or chemical polymerization [17]; nanometals (e.g. Au, Ni, Co, Fe, Pt, Cu etc) have been produced by electrochemical [19] or chemical ("electroless") reduction of the appropriate metal ion [45], carbon nanofibers or nanotubes have been obtained by chemical vapor deposition [4, 41, 46, 47], semiconductors (e.g. TiO_2, ZnO, MnO_2, WO_3) [48] and oxides (Al_2O_3, SiO_2, ZrO_2) [49] have been yielded by the sol-gel method, and various composite nanostructures (TiS_2 /

Au, ZnO / Au, TiO_2 / Au, ZrO_2 / Ni, Co / polyaniline [14]) have been prepared by means of the combination of the above synthesis methods [50].

In addition to the above chemical synthesis methods, a simple and versatile physical method for fabrication of polymer nanotubes within porous templates has been recently reported by Wendorff et al. [26]. This method makes use of the wetting phenomena of polymer solutions or melts on the pore walls. When porous templates are brought into contact with polymer solutions or melts, a thin surface film will cover the pore walls. Complete filling of the pores can be prevented by thermal quenching in case of melts or solvent evaporation in case of solutions, resulting in the formation of nanotube structures. Any melt-processable polymers (e.g. polytetrafluoroethylene, polystyrene, and polymethyl methacrylate etc.), blends, or multi-component polymer solutions can be formed into nanotubes with a wall thickness of a few tens of nanometers. The template-wetting technique is proved to be a promising approach for providing customized polymer nanotubes.

Despite its general and versatile features, the membrane-based template synthesis method has also limitations, such as too low yield for practical applications, no free - standing fibrils or tubules, limited fibril or tubule length by the membrane thickness, and poor mechanical strength etc.

Greiner et al. have recently developed a fiber-based template technique by which meso- and nanotubes can be fabricated in a large scale [51, 52]. The method is termed the TUFT process (tubes by fiber templates), which consists of three steps: 1. preparation of polymer fiber templates by electrospinning, 2. coating of the fiber templates with a polymer layer by means of e. g. chemical vapor deposition (CVD), and 3. removal of the template fibers by thermal decomposition or solvent-extraction. The TUFT process is shown schematically in Fig. 1. 2.

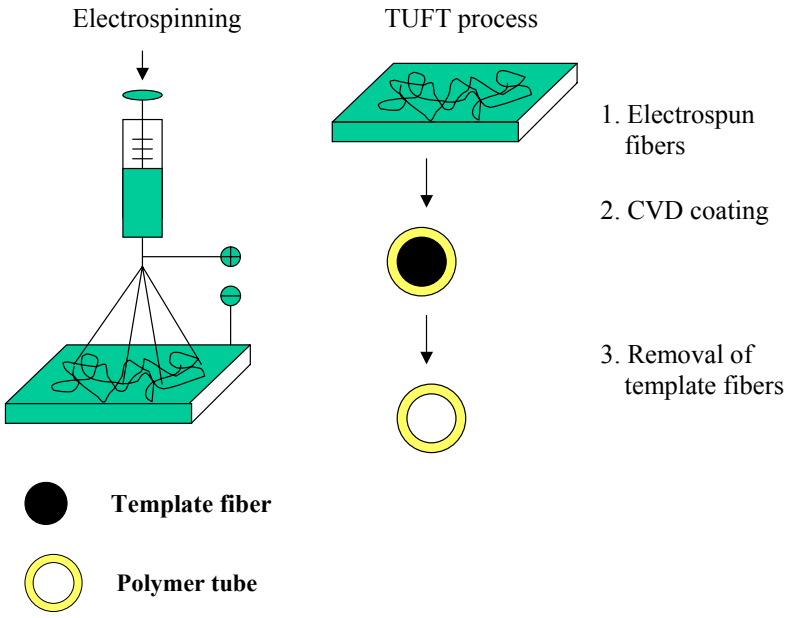

Fig. 1. 2 Fabrication of polymer meso- and nanofibers by electrospinning and polymer nanotubes by means of the TUFT process

The TUFT process has redundant characteristic features. It can produce nanotubes in a large scale; it can present free-standing polymer nanotubes or nanotube webs; the inner diameter of the tubes can be manipulated in a broad range from a few nanometer to several microns; the tube length and the wall thickness can be controlled at will. For example, the tubes can be continuous or of a random length, and the thickness of the tubes can range from nanometer scale to micron scale, depending on the amount of the coating material.

In the TUFT process, two crucial techniques are involved. One is the electrospinning technique, and the other is the PPX coating by chemical vapor deposition (CVD).

Electrospinning is a process that produces continuous polymer fibers through the action of an external electric field imposed on a polymer solution or melt. So far, meso- and nano-scaled polymer fibers have been electrospun from a wide range of polymers, including textile fiber polymers such as nylon [53], polyacrylonitrile [54], polyvinyl alcohol [55] etc., biodegradable or bioabsorbable polymers [56-59], elastomers [60, 61], liquid crystalline polymers [62], conductive polymers [63-66], protein [67], peptide [68-

72], DNA [73], natural silk [74, 75] etc. Various further treatments on the polymer nanofibers result in special nanofibers, such as carbon [63] or ceramics nanofibers [76].

The obvious advantage of the electrospinning technique is that, it produces ultra-fine fibers with huge surface-to-volume ratio, which have great application potentials in many fields such as protective clothing [77, 78], air filtration [5, 79], [5], sensors [12, 80, 81], drug delivery system [82], tissue engineering [56, 83, 84], fiber-reinforced composites [53], [85], and template materials for nanotubes [51]. In addition, inexpensive apparatus, simple operation, possibility of large-scale production of nanofibers, result in the rapid development of electrospinning technique during the recent a couple of years. In this work, we will focus on finding crucial processing parameters for electrospun fibers in order to well control over the fiber diameters.

The second technique involved in the TUFT process is the PPX coating by CVD. The unique film-formation process of PPX by CVD was firstly reported by Gorham in 1967 [86]. In this process, a cyclic dimer, [2,2] paracyclophane, is pyrolysed at 700 - 800ºC under vacuum (lower than 2 Torr) and the polymerization takes place on a cold substrate (<30ºC), resulting in the formation of a conformal, pinhole-free film on the surface of the substrate.

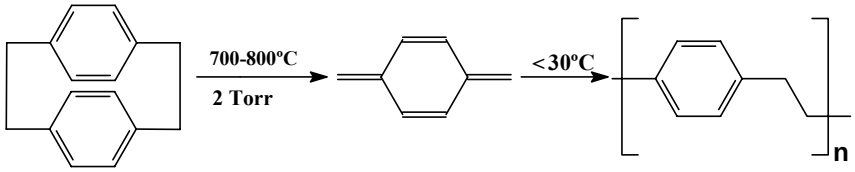

Fig. 1. 3 Chemical vapor deposition of paracyclophane (Gorham, 1966)

The unique features of the PPX coating process by CVD are that it produces extremely pure material with exceptional conformity without any solvents, additives, or catalysts.

By means of the TUFT process, meso- and nano-scaled PPX tubes with inner diameter ranging from 5 nm to several microns have been prepared [51]. Due to the huge surface-to-volume ratio the tubes are promising in the applications in many fields, such as filtration, separation, catalysis, controlled drug delivery, sensors, and other applications concerned with size confinement effects. However, due to the chemical inertness of PPX,

the applications of the PPX tubes are limited. One of the aims in this work is to functionalize the PPX tubes in order to expand their applications.

To functionalize the PPX tubes, various modification approaches have been developed in this work, including the preparation of PPX / polymer or PPX / metal composite tubes; the preparation of PPX / metal hybrid tubes or PPX-encapsulated metal nanowires; the fabrication of PPX-coated functional fibers; surface modification by chemical attachment of functional groups or surface grafting by means of atom transfer radical polymerization (ATRP); hydrophilication of the PPX tubes etc.

The application of the functionalized PPX tubes in the field of controlled drug delivery has been explored. As a model of small molecular drug systems, the release behavior of NaCl from NaCl-incorporated PPX tubes was studied. Furthermore, as a model of protein drug systems, the release behavior of protein BSA from PPX-coated PVA / BSA fibers was investigated. Due to the excellent biocompatibility of PPX, the drug delivery system based on PPX-coated fibers will be promising.

2 Theoretical background

2.1 Electrospinning

2.1.1 Introduction

Electrospinning (also called electrostatic spinning) is a process that utilizes electrical force to produce polymer fibers from polymer solutions or melts. Although the behavior of electrically driven liquid jets and electrically charged liquid drops have been of interest since the late 1800's [87], electrospinning was paid attention only during the recent several decades. An early patent on electrospinning of polymer fibers was issued by Formhals [88] in 1934, followed by the study on electrostatic spinning of acrylic microfibers which was performed by Baumgarten [89] in 1971. The fiber diameter was in the range between 500 - 1100 nm. Later, Larrondo and Manley [90-92] described the electrospinning of polyethylene and polypropylene fibers from the melts in air. Since 1990s, electrospinning was investigated in detail particularly by Reneker and co-workers [62, 73, 85, 93-96], Vancso et al. [53] as well as Greiner and co-workers [51, 52, 58, 59, 97].

During the recent few years, extensive investigations on electrospinning process have been conducted in the aspects of theoretical simulation [96, 98], fiber formation mechanism, influence factors for fiber size and morphology [99] and so on. Meso- and nanofibers of various materials have been fabricated, including ordinary polymers, conducting polymers [65, 100], carbon [63], spider silk, protein [71, 72], and DNA [73]. The as-spun fibers have diameters ranging from as small as a few nanometer to several micrometers and therefore possess huge surface-to-volume ratios, resulting in their great application potentials in a broad of fields, such as separation, filtration [77, 79], catalysis, fiber-reinforced composites [101], tissue engineering [56, 82-84], drug delivery system [82], sensors [12, 80, 81], protective textile [78], and as fiber templates for preparation of nanotubes [51]. At present, studies on electrospinning center on precise control over fiber size and morphology by changing process parameters, modeling of electrospinning process, and practical applications of electrospun fibers.

In this work, the effect of process parameters on fiber size and shape has been systematically investigated, and various polymer nanofibers such as poly (L-lactide), polyacrylonitrile, nylon, polyethylene oxide, polyvinyl alcohol, and polyacrylic acid have been fabricated with controllable size and shape. In addition, functional nanofibers have also been produced, including protein / polymer composite fibers, inorganic salt-incorporated fibers, water-stable PVA fibers, fluorescence nanofibers, and metal compounds-incorporated fibers.

2.1.2 Principle

In the electrospinning process, fibers are spun under a high voltage electrical field. The setup is shown in Fig.2.1. A polymer solution (or melt) is contained in a syringe, which is equipped with a piston and a stainless steel capillary serving as an electrode. A grounded counter electrode (a round metal plate) is placed down against the capillary and a high voltage is applied between the capillary and the counter electrode.

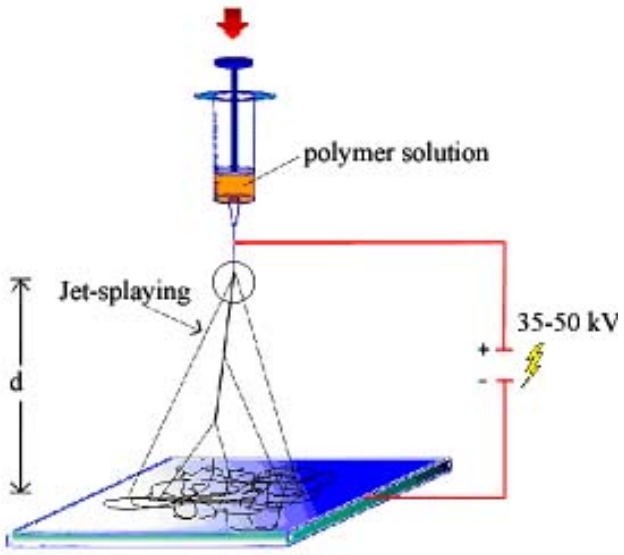

Fig. 2. 1 Setup for Electrospinning

Under controlled velocity the piston on the syringe was driven down by a motor and a droplet of polymer solution is suspended by its surface tension at the tip of the capillary. If the free surface of the solution is subjected to an electrical field, charge and /or dipolar orientation will be induced at the air-solution interface. The charge (or dipolar) repulsion causes a force that opposes the surface tension. If the voltage surpasses a threshold value, electrostatic forces overcome the surface tension, resulting in that jets are ejected from

the solution and move towards the counter electrode. During the travel to the counter electrode, the solvent in the jets evaporates and the solidified fibers are deposited on a substrate located above the counter electrode.

So far, fibers with diameters ranging from as low as 5 nm to several micron have been produced. It is found that the morphology and dimension of the electrospun fibers are dependent on the process parameters, including solution concentration and viscosity, electrical conductivity of the solution, surface tension of the solution, polymer molecular weight, molecular weight distribution of the polymers, vapor pressure and boiling point of the solvent, flow rate, intensity of electrical field, distance between the capillary and the substrate, temperature, humidity and atmosphere etc.

2.1.3 Processing parameters

In the electrospinning process, three main forces are involved:

1. Surface tension: favor to produce as few as possible polymer jets in order to decrease surface area of polymer droplets
   Corresponding process parameter: Surface tension of polymer solution (SFT)

2. Electrical repellent force derived from electrical charged polymer droplets: favor to form as many as possible polymer jets
   Corresponding process parameter: conductivity of polymer solution

3. Viscoelastical force coming from polymer: against the deformation of polymer droplets.
   Corresponding process parameter: solution viscosity

These three parameters play very important roles in the formation of the fibers. In this work an attempt has been made to accomplish a systematic investigation on these process parameters and to find the crucial parameters for electrospun fibers in order to well control the fiber morphology and dimension. The results will be discussed in detail in **Chapter 3 - Electrospun fibers**.

2.2 PPX and PPX coating by chemical vapor deposition

2.2.1 Synthesis of PPX

PPX is an important aromatic polyhydrocarbon consisting of a strictly alternating sequence of p-phenylene moieties and ethylene moieties. There are mainly two classes of synthesis methods for PPX. One is vapor phase pyrolysis / CVD method; the other is solution-based synthesis route.

The early synthesis of PPX by pyrolysis was reported by Szwarc in 1947 [102-104]. p-Xylene, as staring material, was pyrolysed at very high temperature (1100ºC) under vacuum (2 Torr), resulting in yellow-colored, insoluble (crosslinked) PPX (3). Szwarc postulated the reaction mechanism as shown in Fig. 2. 2.

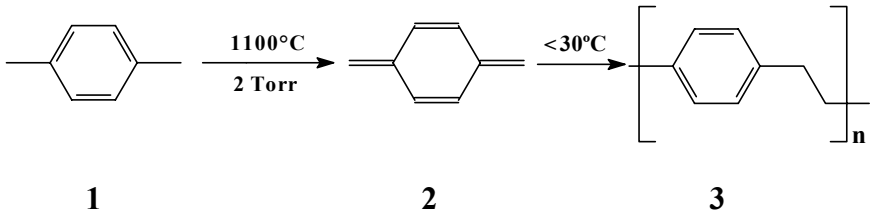

Fig. 2. 2 Synthesis of PPX (3) by means of pyrolysis of p-xylene (1) through p-quinodimethane intermediate (2).

Szwarc studied the stability of p-quinodimethane (2) in the gas phase and liquid phase, respectively, and confirmed, that the biradical is stable in the gas phase but immediately polymerizes in the liquid phase, which results in insoluble PPX (3).

Improved PPX synthesis by pyrolysis, which is also called chemical vapor deposition (CVD), was invented by Gorham in 1966. In the Gorham process, [2, 2] paracyclophane, instead of p-xylene, was used as starting material. The pyrolysis was performed at much lower temperature (about 700°C) under vacuum (2 Torr), resulting in the formation of linear and soluble PPX films. The resulting PPX is characterized by high melting point and excellent chemical inertness against organic and inorganic reagents, and thus attracted extensive investigation interests. The Gorham process was soon technically realized by Union-Carbide. The process is schematically shown in Fig. 2.3.

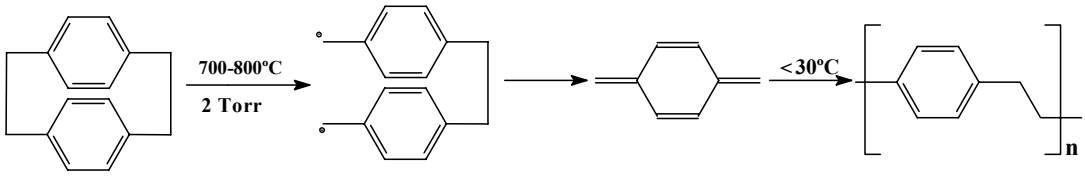

[2, 2] paracyclophane p-quinodimethane PPX

Fig. 2. 3 Gorham process for the formation of PPX film

The solution-based synthesis routes for PPX were represented by the Gilch-route, which was published by Gilch in 1966 [105]. In the Gilch-route, a strong base, potassium tert-butylate, was used as initiator and p-quinodimethane (5) was formed by means of a base-induced 1, 6-dehalogenation of substituted α-haglogen-p-xylene (4) (Fig. 2. 4).

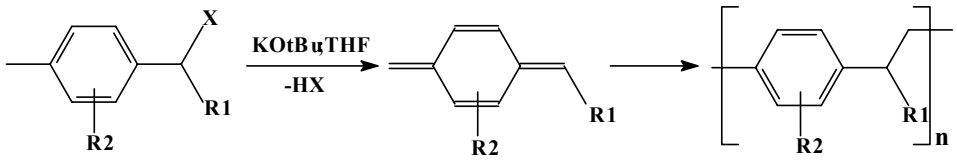

4 5 6

Fig. 2. 4 Synthesis of substituted PPX (6) by the Gilch-route

By introducing different substituents in the aromatic ring, various soluble PPX derivatives can be obtained by means of the Gilch-route.

In this work, we focus on the Gorham process as it presents conformal, uniform, and pinhole-free PPX films with high melting point, which are ideal wall materials for our nanotubes.

2.2.2 Polymerization mechanism of PPX

All the above described synthesis routes of PPX involved the formation of p-quinodimethane intermediate. The presence of p-quinodimethane as intermediate was verified by means of spectroscopy method and its reaction with iodine to form α, α'–diiodo-p-xylene [106, 107]. p-Quinodimethane is highly reactive. In addition to its singulett form (7 a), it exists also in triplett form (7 b), which is a biradical species. The

energy difference between the two forms is 50 kJ/mol. At room temperature the singulett form of p-quinodimethane is the dormant species.

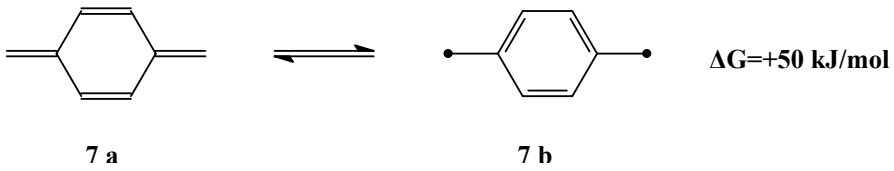

Fig. 2. 5 Equilibrium between singulett and triplett form of p-quinodimethane

So far, the exact polymerization mechanism of PPX is still not clear. However, it is commonly thought that the biradical species in the above equilibrium initiates the polymerization. One biradical reactes with one p-quinodimethane, resulting in the formation of another biradical species. Consequently, the propagation of the chain proceeds in two directions (Fig. 2. 6).

Start reaction:

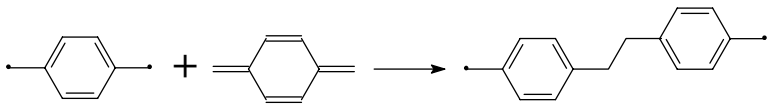

Propagation reaction:

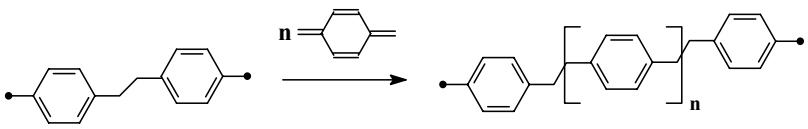

Termination reaction:

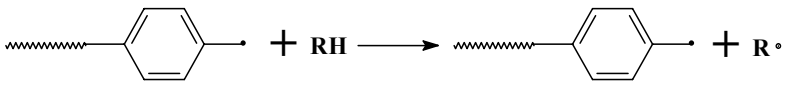

Fig. 2. 6 Supposed mechanism for the polymerization of PPX

2.2.3 PPX coating by CVD

As described above, PPX film can be produced by means of the Gorham process (CVD process). The set up of the CVD process is shown in Fig 2. 7. The starting material, [2, 2] paracyclophane, is firstly evaporated in a sublimed zone at high vacuum (<1 mbar), and pyrolysed at about 700°C in the vapor phase, resulting in the formation of p-

quinodimethane intermediate. Once physically condensing on cold substrates (<30°C), p-quinodimethane immediately polymerizes and a thin polymer film is formed on the surface of the substrate. As the solid polymer is formed directly from the gaseous monomer during deposition without any liquid phase as intermediate, it is possible to produce almost defect-free coatings with uniform thickness on the substrate – even on those showing complicated surface profiles.

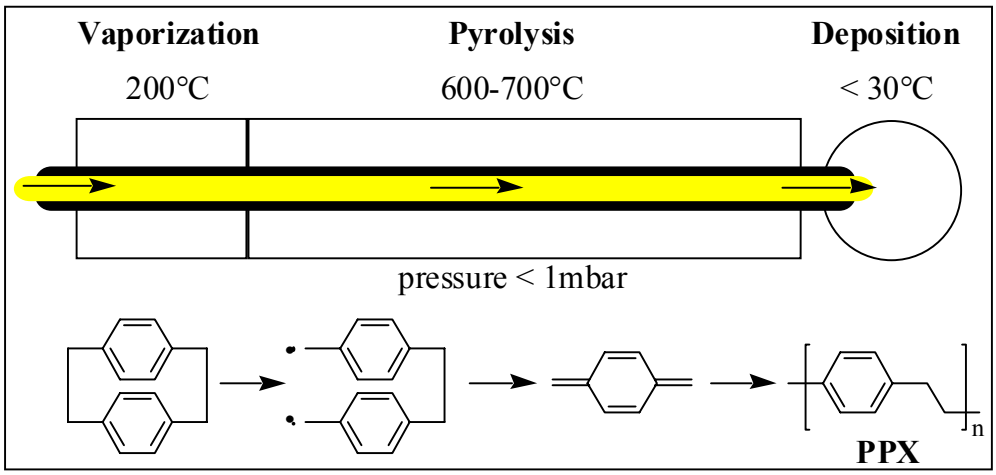

Fig. 2. 7 Formation of PPX films by means of CVD process

Alternatively, with α, α'-dihalogen-1, 4-xylene as monomer, substituted PPX with halogen substituent in the ethylene segments (PPX-X) can be obtained by means of CVD [108]. This monomer is cheaper and easier to evaporate than paracyclophane. The pyrolysis is performed at 700°C, and polymerization and deposition takes place on a substrate with a temperature of 50 - 70°C. The process is shown in Fig. 2. 8.

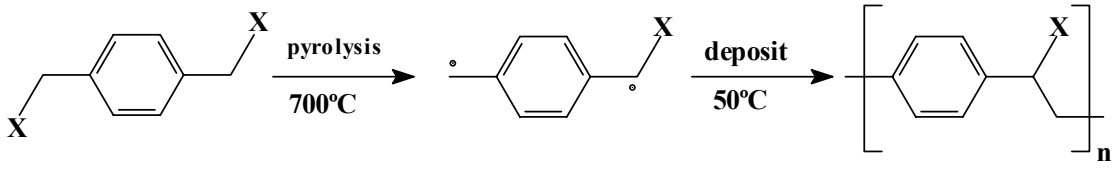

Fig. 2. 8 Formation of halogen-substituted PPX films by the CVD process. X is Cl or Br.

The as deposited PPX-X film is light yellow-colored in case of PPX-Cl and dark yellow-colored in case of PPX-Br. The presence of the C-X bonds in the polymer chain, which are relatively chemically active, allows further reactions with other functional compounds. As will be described in the later chapter, some of the functionalization approaches of PPX tubes are just based on the reactivity of PPX-X.

During the past decades, the CVD process of PPX film has achieved commercial importance and is attracting increasing attention due to its unique features, such as no use of solvents, catalysts or any additives, no by-products, and presenting extremely pure material with exceptional conformity.

So far, there are four kinds of PPX commercially available: unsubstituted Parylene N, mono-chloro substituted Parylene C, di-chloro substituted Parylene D, and high temperature PPX (HT Parylene) with four fluorine substituents in the ethylene segments.

2.2.4 Properties of PPX films

PPX films produced by the Gorham process possess excellent physical and chemical properties, some of which are summarized in Table 2. 1.

Table 2.1 Properties of PPX [109]

Properties	PPX
General properties	
Refractive index	1.669
Density (g/cm^3)	1.110
Thermal properties	
Glass transition temperature (ºC)	80
Melting Point (ºC)	420
Electrical properties	
Dielectrical constant	
60 Hz	2.65
1 MHz	2.65
Dissipation factor	
60 Hz	$2*10^{-4}$
1 MHz	$6*10^{-4}$
Hydrophobility	
Contact angle against water (º)	95,4

The PPX obtained by the Gorham process is a transparent, insoluble at RT, and partially crystalline film. It is soluble only above 250ºC in exotic solvents such as chlorinated biphenyls, α-chloronaphthaline, or benzyl benzoate. PPX has excellent thermal stability

[110]. Its glass transition temperature (T_g) is 80ºC and the crystalline melting point (T_m) is about 420ºC (PPX starts to decompose at this temperature). PPX exhibits two kinds of crystalline morphologies: α- and β-modification. The major peaks of α-modification is at $2\theta = 16.79^\circ$ and 22.52° and that of β-modification is at $2\theta = 20^\circ$. The transition from the α- to the β-modification is observed at 220ºC and is irreversible [111].

The mechanical properties of the PPX or substituted PPX films are characterized by high Young's modulus and rather low elongation at break, as shown in Table 2. 2. The Young's moduli of PPX films drops significantly at 200ºC.

Table 2. 2 Mechanical properties of PPX and halogen substituted PPX films [112]

Properties	PPX	Cl-PPX	Br-PPX	Cl_2-PPX
At room temp. Young's modulus (Gpa)	2.41	3.17	2.76	2.76
Elongation at break (%)	10 - 15	220	30	5 - 10
At 200ºC Young's modulus (Gpa)	0.17	0.17	0.14	0.17

The gas- and water vapor-permeability of PPX and substituted PPX films is very low compared to other synthetic polymers. The best barrier properties were observed with chloro- and bromo-substituted PPX (Table 2. 3). Therefore, PPX film is an excellent barrier material and has been extensively used as anti-corrosion coatings.

Table 2. 3 Permeability properties of PPX and halogen substituted PPX films [112]

Polymer	H_2 [a]	CO_2 [a]	O_2 [a]	N_2 [a]	H_2O [b]
PPX	250	225	30	9	6.0
Cl-PPX	200	21	8	1	0.6
Br-PPX	75	6	4	0.1	0.6
Cl_2-PPX	-	130	30	4.5	5.0

[a] Permeability at 25ºC, cm^3 (STP) - mil/100 in^2 – 14 h

[b] Moisture vapor permeability at 20ºC, g-mil / atm.100 in^2

What is worthy of note is the interesting electrical properties of PPX. Its high dielectric constant of 2.65 and low dissipation factor of 0.0002 makes it suitable for applications in the field of microelectronics [113].

2.3 The TUFT process

Based on the electrospinning technique and CVD technique, the so-called TUFT process for preparing polymer meso- and nano-tubes consists of three steps:

1. Preparation of degradable polymer template fibers by electrospinning
2. Coating the template fiber with the desired wall materials by different deposition techniques
3. Removal of polymer template fibers by degradation or by solvent extraction

The polymer tubes prepared by this way have the inner diameters ranging from 5 nm to 2000 nm, depending on the diameter of the template fibers. The TUFT process is schematically shown in scheme 2. 1.

Scheme 2. 1 The TUFT process

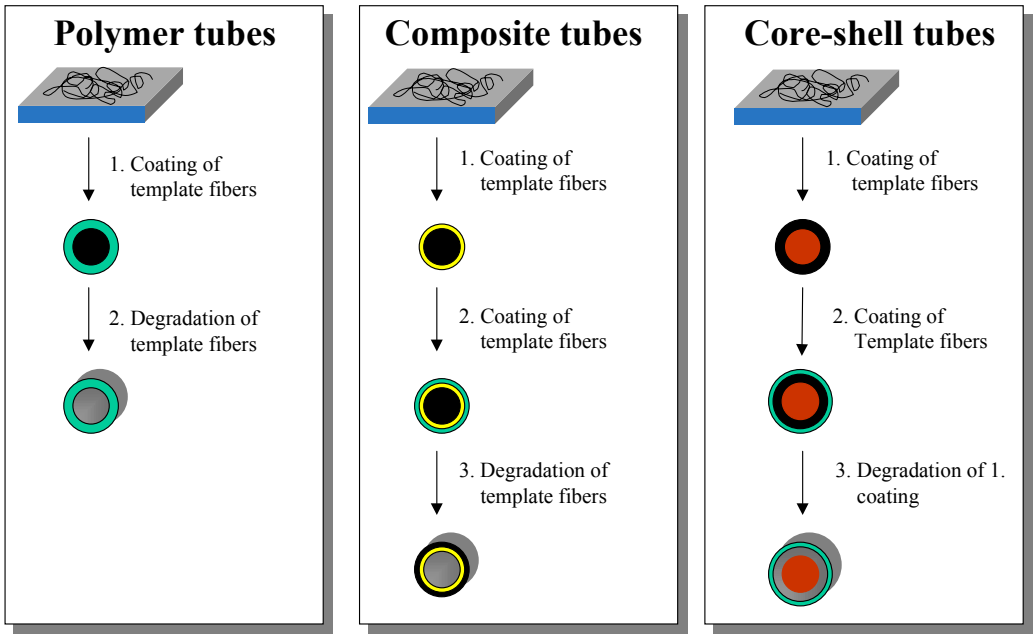

2.3.1 Template fibers

According to the TUFT process, the polymers, which are suitable as template fibers, should meet the following requirements:

1. They should be fiber-processable;
2. They are stable during the coating conditions;
3. They are solvent-extractable or thermal-degradable at the temperature lower than the decomposition temperature of the wall materials.

Among a variety of polymers electrospun by our group, poly (L-lactide) (PLA) is a suitable template candidate due to its thermal degradability at sufficiently low temperature, its excellent electrospinning-processable properties and good mechanical properties. By adjusting the concentration of PLA solution in dichloromethane and using proper additives, smooth PLA fibers with diameters ranging from 5 nm to several micrometers can be obtained. Fig. 2. 9 demonstrates the thermal decomposition process of PLA fibers under nitrogen. At 280°C PLA starts to decompose and at 365°C the decomposition rate reaches a maximal value.

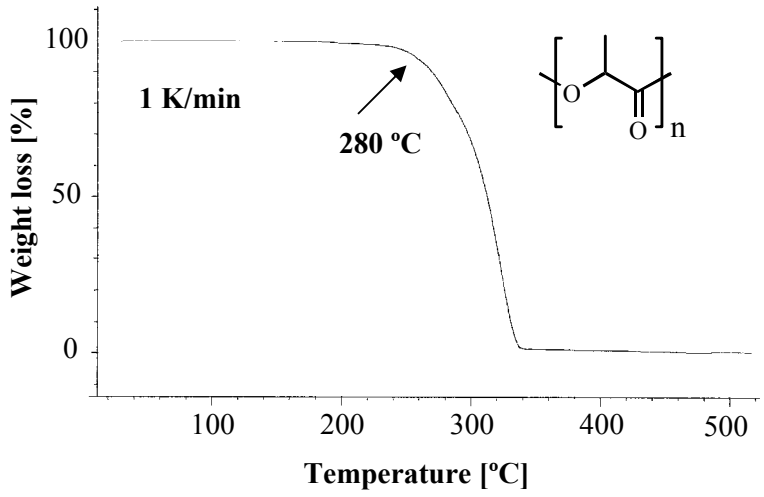

Fig. 2. 9 Thermal degradation of poly (L-Lactide) in nitrogen atmosphere

In addition to PLA, other polymers, which can be readily electrospun into fibers and extracted with suitable solvents or thermally degraded under heat, are also good template candidates. For example, nylon 4,6 and nylon 6 were used as template fibers with formic acid as extracting solvent, poly(ethylene oxide) (PEO) with chloroform as extracting

solvent or by means of thermal degradation at 370°C, polyacrylonitrile (PAN) with DMF as extracting solvent.

Moreover, a variety of multi-component fibers were also used as template fibers so that polymer tubes with special structures and functions can be produced. For example, composite fibers consisting of two different polymers, hybrid fibers consisting of polymer and metal compounds such as palladium acetate, silver acetate, copper acetate etc., and inorganic salt-incorporated polymer fibers.

2.3.2 Wall materials

Wall materials should be stable during removal of template fibers. Different types of materials can be used as wall materials, including metal, ceramic, glass, semiconductor, and polymers. For example, gold- or aluminum-coated polymer fibers can be prepared by means of physical vapor deposition of the corresponding metal. Further pyrolysis of aluminum-coated fibers resulted in Al_2O_3 / Al hybrid tubes. By means of sol-gel technique, glass- or TiO_2- coated fibers were obtained [114]. Here we focus on polymers as wall materials.

Due to the unique properties of the PPX coatings by CVD, it can be an ideal wall material. Its good thermal stability (melt point at about 420°C) and excellent chemical inertness against all kinds of reagents and solvents allows the realization of the third step in the TUFT process, removal of the template fibers, without any problem. Another very important advantage of PPX coatings is, that it can form very conformal, pinhole-free coating layers with uniform thickness on the substrates, even on very delicate articles like butterfly wings while preserving their original structures [115]. This ensures that the PPX coating on nano-scaled template fibers is uniform and keeps the original shape of fibers. As the PPX formation by CVD is almost quantitative, it is possible to manipulate the thickness of PPX coating by controlling the amount of starting materials.

2.4 Atom transfer radical polymerization

2.4.1 Principle of ATRP

Atom transfer radical polymerization (ATRP) is one kind of controlled / "living" radical polymerization, which was developed by Matyjaszewski in 1995 [116]. As it allows well controlled radical polymerization to give rise to predictable molecular weights with low polydispersities, ATRP has attracted extensive research interests during the recent years [117-124].

A typical ATRP requires an alkyl halide (R-X) as initiator, a transition metal in a lower oxidation state, and a ligand that complexes with the metal. Of various metals used for ATRP chemistry, copper appears to be the most promising in terms of price and versatility. The ligands are usually dipyridyl derivatives or tertiary amines. A general mechanism for ATRP is shown in Scheme 2. 2.

Scheme 2. 2

Initiation:

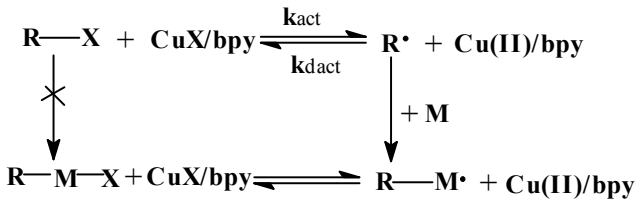

Propagation:

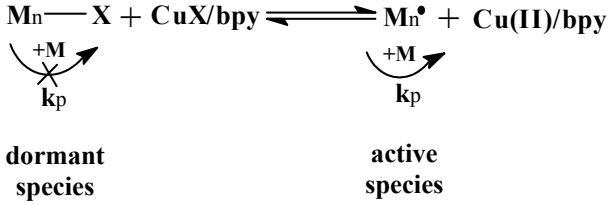

(X = Cl or Br)

The radicals, or the active species, are generated through a reversible redox process catalyzed by a transition metal complex (M_t^n-Y/Ligand). The resulting radical $R^{\cdot}$ can then add to the monomer unit, followed by reaction with the oxidized form of the

catalyst, leading to a dormant chain. The repetition of this process results in high polymer chains.

An important variation of ATRP chemistry is reverse ATRP, which requires a conventional radical initiator such as a peroxide or azobisisobutyronitrile (AIBN), a transition metal in a higher oxidation state, and a ligand for metal solubilization. The initiation step is the decomposition of the radical initiator. The resulting radical can then react with the monomer to create a growing chain or directly with the catalyst to form the reduced species. The situation then becomes the same as in a classical ATRP , as shown in Scheme 2. 3.

Scheme 2. 3

Initiation:

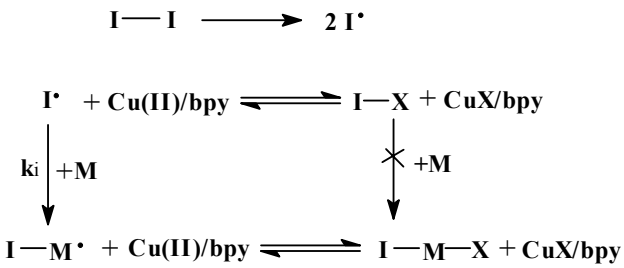

Propagation:

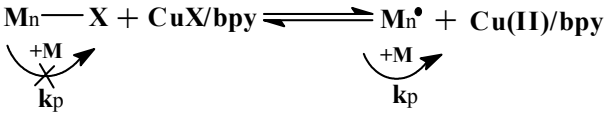

The reverse ATRP has been applied successfully in many different systems [125]. For example, styrene was recently polymerized by reverse ATRP using peroxide initiators to give polymers with predictable molecular weights and low polydispersities (1.14 - 1.21) [126]

Monomer

Various monomers have been successfully polymerized using ATRP: styrene and its derivatives, methacrylates, methacrylamides, dienes, acrylonitrile, and other monomers which contain substituents that can stabilize the propagating radicals [121].

Initiator

Typical ATRP initiators are alkyl halides, including halogenated alkanes like $CHCl_3$, CCl_4, benzylic halides (e.g. Ph_2CHCl, Ph_2CCl_2), α-haloesters, α-haloketones, α-halonitriles, and sulfonyl halides. Among the halogens in the halides, bromine and chlorine are most frequently used.

Transition metal

Transition metal complexes are perhaps the most important components of ATRP. To generate growing radicals, the metal center should undergo an electron transfer reaction with the abstraction of a (pseudo)halogen and expansion of the coordination sphere. In addition, to differentiate ATRP from the conventional redox-initiated polymerization and induce a controlled process, the oxidized transition metal should rapidly deactivate the propagating polymer chains to form the dormant species. In addition to copper complexes, complexes of nickel, iron, and Ruthenium have also been studied as ATRP catalysts.

Ligand

The main role of the ligand in ATRP is to solubilize the transition-metal salt in the organic media and to adjust the redox potential of the metal center for appropriate reactivity and dynamics for the atom transfer. Most common ligands are nitrogen ligands, which have been frequently used in copper- and iron-mediated ATRP. In addition, phosphorus-based ligands are used to complex most transition metals (e.g. iron, nickel, palladium, ruthenium, and rhenium etc), but not copper.

Reaction temperature

Although most of the ATRP polymerizations have been perfomed at elevated temperature (e.g. about 100ºC for styrene), ambient temperature ATRP have been successfully realized by several groups. Ying et al conducted ATRP of methacrylates and 2-hydroxy ethyl methacrylate (HEMA) at RT by using a solvent (e.g. acetonitrile) or monomer (e.g. HEMA) with high dielectric constant [122]; Xia et al performed copper-mediated ATRP of acrylates at RT by using multidentate amines as ligands [127]; Baker et al reported ambient temperature ATRP of PMMA grafted from gold surfaces [128].

2.4.2 Surface-mediated ATRP

Covalent attachment of polymer chains to solid substrates is an attractive method for tailoring interfacial properties and functionalizing surfaces. Strategies for attaching polymer brushes to surfaces include the "grafting to" technique, which involves tetheration of preformed polymer chains from solution onto a surface, and "grafting from" technique, which involves polymerization from surface-anchored initiators. The latter results in well-defined surfaces with higher grafting densities and thus becomes the preferred technique.

Numerous recent reports describe the use of controlled polymerization techniques to grow polymer chains from surfaces. ATRP is especially useful because it is remarkably tolerant of a variety of functionalized monomers. Baker et al reported surface-initiated ATRP of methyl methacrylate (MMA) [128] and hydroxyethyl methacrylate [129] on gold surface. Matyjaszewski et al immobilized homopolymers and block copolymers on silicon surfaces by using ATRP [119].

In this work, the ATRP techniques were applied to surface-initiated grafting of polymers onto the surface of PPX-X tubes, which is one of the functionalization approaches. The halogen substituted PPX-X (X is Cl or Br) acted as "anchored" initiator, and monomers such as MMA were grafted from the PPX-X surface under the action of the catalyst CuBr / bipyridin.

3 Electrospun fibers

3.1 Influence parameters for electrospun fibers

3.1.1 Solution concentration and viscosity

Solution concentration and viscosity are two closely correlated factors. Increase in solution concentration always results in increase in solution viscosity, and decrease in solution concentration always results in decrease in solution viscosity. Therefore, these two factors were investigated together.

Poly (L-lactide) (PLA, M_w = 670,000 g/mol, M_w/M_n = 1.60) fibers were electrospun from PLA/dichloromethane solution with different concentration. Strong dependence of fiber diameters on solution concentrations was observed, as shown in the SEM images of the PLA fibers (Fig. 3. 1 A-C). Fibers from 5 wt % solutions are cylindrical with diameters ranging from 800 - 2400 nm (Fig. 3.1 C), while fibers from 3 wt % solutions were still cylindrical but showed decreased fiber diameter ranging from 300 - 800 nm (Fig. 3.1 B). Further decrease in the solution concentration resulted in further decrease of the fiber diameters but the formation of beaded fibers was observed (Fig. 3.1 A).

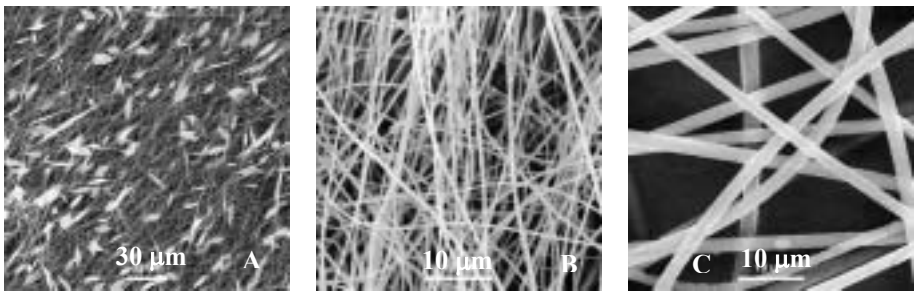

Fig. 3. 1 SEM images of PLA fibers from PLA / dichloromethane solution without additive. Solution concentration: A: 2 %, B: 3 %, C: 5 %

The formation of less beaded fibers by decrease in PLA concentration was also identified with PLA/DMF solution [57]. Also, the tendency of decreased fiber diameters combined with the formation of beaded fibers by decrease of the polymer solution concentrations is consistent with previous reports for example for polyethylene oxide (PEO) by Reneker et al. [130] and Deitzel et al. [99].

Similar dependence of fiber diameters on solution concentrations was observed with PLA/dichloromethane solutions containing 0.8 wt % pyridinium formiate (PF) as additive (Fig. 3. 2 A-F). PLA fibers with diameters ranging from 600 - 2000 nm were obtained by electrospinning of 5 % PLA / PF / CH_2Cl_2 solution (Fig. 3. 2 F); while PLA fibers with dramatically decreased diameters (50 - 200 nm) were produced by electrospinning of 1 % PLA/PF/CH_2Cl_2 solutions (Fig. 3. 2 D). Further decrease in PLA solution concentration resulted in further decrease in fiber diameters. With 0.8 % PLA solution, fibers of as small as 10 - 70 nm were obtained from (Fig. 3.2 A).

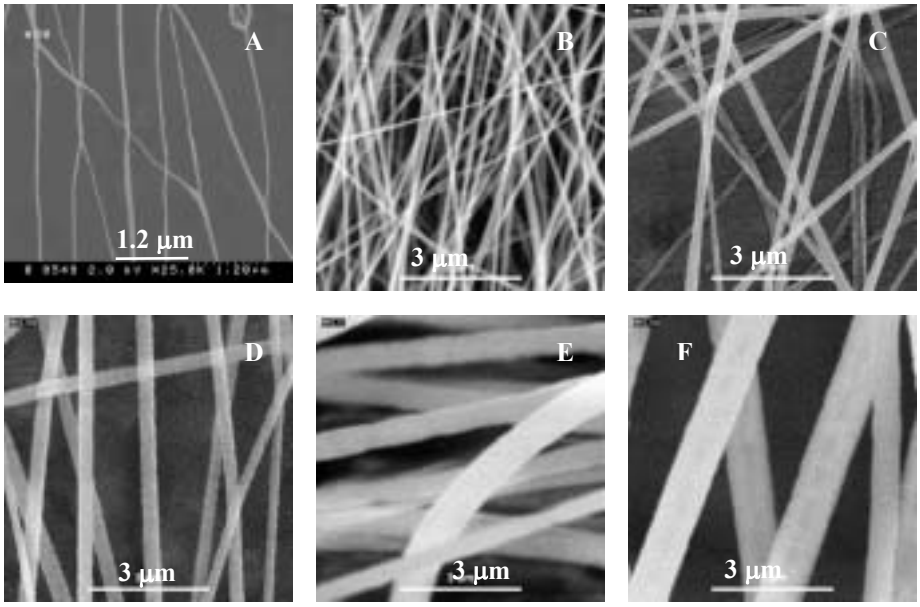

Fig. 3. 2 SEM images of PLA fibers from PLA solution in dichloromethane with 0.8 % PF. Solution concentration: A: 0.8 %, B: 1.0 %, C: 2.0 %, D: 3.0 %, E: 4.0 %, F: 5.0 %

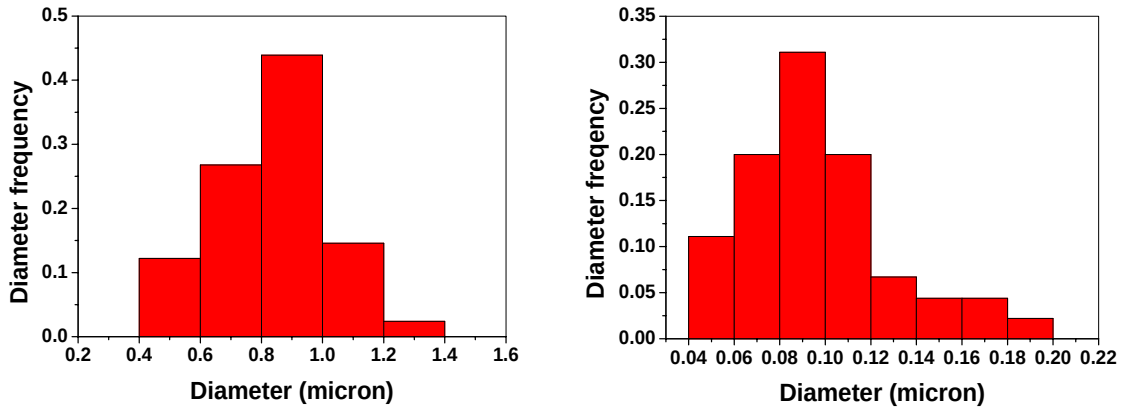

Fig. 3. 3 Diameter distribution of PLA fibers electrospun from PLA solutions in dichloromethane with 0.8 % PF. Solution concentration: left 5 %, right 1 %.

The fiber diameter distribution (Fig. 3. 3) shows clearly the effect of solution concentrations on fiber diameters.

It is worth noting that no beads at all were observed in the fibers electrospun from even very dilute solutions in the presence of the additive, indicating that the additive, pyridinium formiate may play a significant role in fiber shape. The effect of additive will be discussed in detail in **Chapter 3.1.2**.

To get a further insight into the crucial parameters, the detailed characterization of the polymer solutions used for electrospinning was done in terms of viscosity, electrical conductivity, and surface tension. As expected, solution viscosity decreased significantly with decreasing PLA solution concentration, whereas electrical conductivity and surface tension did not vary significantly. The results are summarized in Table 3. 1.

Table 3. 1 Influence of PLA concentration on surface viscosity, electrical conductivity, surface tension, and fiber diameters. All PLA solutions in dichloromethane contain 0.8 % (related to dichloromethane) pyridinium formiate as additive

Conc. PLA [weight %]	Viscosity [mPa·s]	Electr. cond. [µS/cm]	Surface tension [mN/m]	Fiber diameter [nm]
0.8	**1.65**	**1.26**	**28.02**	**10 - 70**
1.0	**3.20**	**1.22**	**28.09**	**50 - 150**
2.0	**11.57**	**1.13**	**28.35**	**100 - 300**
3.0	**32.36**	**1.04**	**28.59**	**150 - 550**
4.0	**120.01**	**0.99**	**28.96**	**400 - 700**
5.0	**139.45**	**0.73**	**29.13**	**500 - 1200**

The result proves that solution viscosity plays very important role in the size of electrospun fibers. Decrease in solution viscosity results in the formation of smaller but “beaded” fibers. The addition of additives seems to be helpful to decrease the beads in the fibers

3.1.2 Electrical conductivity of polymer solutions

As described above, the presence of PF in PLA/CH_2Cl_2 solution favors the formation of smooth and cylindrical fibers. It was also found, that addition of proper additives in PVA/water and PEO/water/ethanol systems, mostly some organic or inorganic salts, could inhibit the formation of "beaded" fibers. Similar results have been reported for PEO/water system and PLA/DMF system [57, 130]. A common feature in these systems is that electrical conductivity of these solutions increased after addition of the additives.

To further understand the effect of the additive on fiber shape and size, 2 wt % PLA/CH_2Cl_2 solutions containing different amount of PF was investigated. The SEM images (Fig. 3. 4) show clearly that formation of bead defects was prohibited by increase in PF concentration. In case of no PF, the fibers electrospun from 2 % PLA solution exhibited many beads along the fibers (Fig. 3. 4 A); with increase in PF concentration, beads in the fibers decreased gradually. With 0.8 % PF, PLA fibers without any beads at all were obtained (Fig. 3. 4 F). The influence of PF on fiber diameter was less dramatic for dilute PLA solution (2 %). Fiber diameters ranging from 100 - 500 nm and 100 - 300 nm were observed for 0.2 % PF (Fig. 3. 4 B) and 0.8 % PF (Fig. 3. 4 F), respectively.

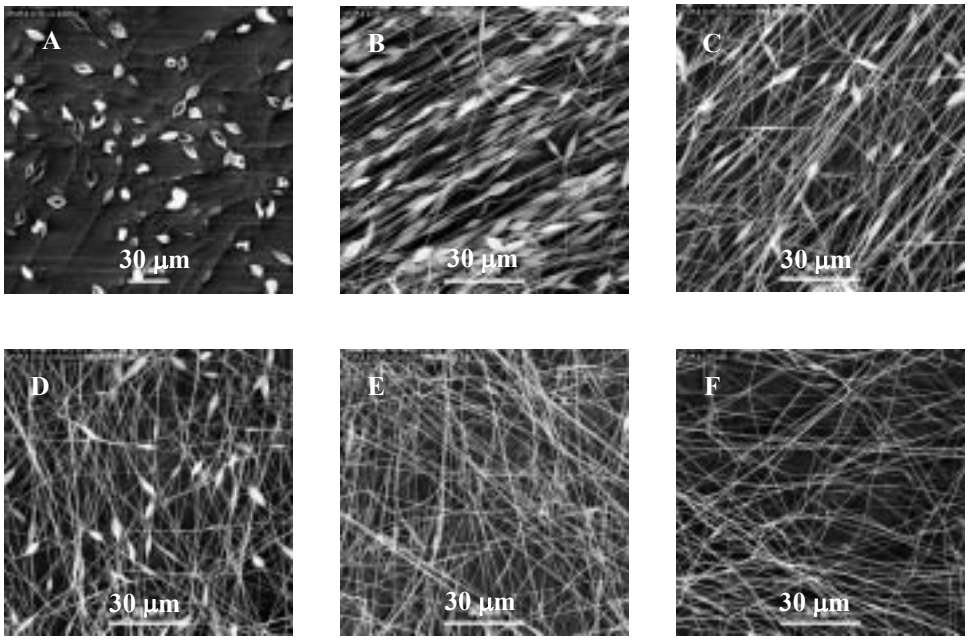

Fig. 3. 4 SEM images of PLA fibers from 2 % PLA solution in dichloromethane with different concentration of PF:. A: 0%, B: 0.2 %, C: 0.3 %, D: 0.4 %, E: 0.6 %, F: 0.8 %

Table 3. 2 Influence of additive (pyridinium formiate, PF) in PLA / dichloromethane solutions on solution viscosity, electrical conductivity, surface tension, and fiber diameters.

Conc. PF [weight %]	Viscosity [mPa·s]	Electr. cond. [μS/cm]	Surface tension [mN/m]	Fiber diameter [nm]
0.2	11.378	1.7	28.48	100 - 500
0.3	11.514	1.8	28.42	100 - 450
0.4	12.214	1.9	28.37	100 - 400
0.5	11.302	2.0	28.29	100 - 400
0.6	11.981	2.6	28.33	100 - 350
0.8	10.734	3.6	28.33	100 - 300

However, in case of concentrated PLA solution (e.g. 5 % PLA solution), a significant effect of PF on the fiber diameter was observed. Fibers with diameter ranging from 800 - 2400 nm were obtained for 5 % PLA solution without PF (Fig. 3. 5 a), whileas fibers with diameter ranging from 500 - 1200 nm were obtained for 5 % PLA solution with 0.8 % PF (Fig. 3. 5 b).

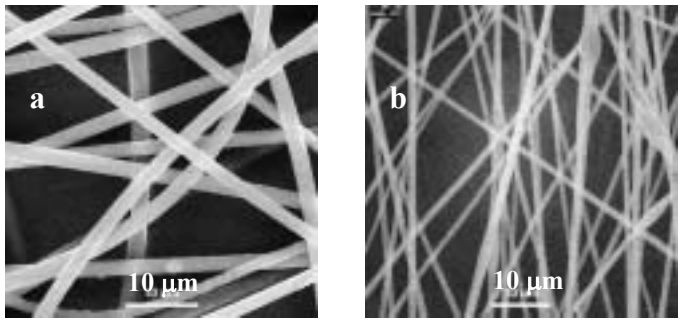

Fig. 3. 5 Effect of PF on the diameter of the PLA fibers electrospun from 5 % PLA solutions in dichloromethane. a: without PF; b: with 0.8 % PF.

Fig. 3. 6 shows clearly the redundant fiber diameter distribution and the effect of PF on the fiber diameter. The dormant diameter of the fibers from 5 % PLA solution with 0.8 % PF is between 800 - 1000 nm, while the dormant diameter of the fibers from 5 % PLA solution without PF is between 1600 - 2000 nm, 2 folds thicker than the former.

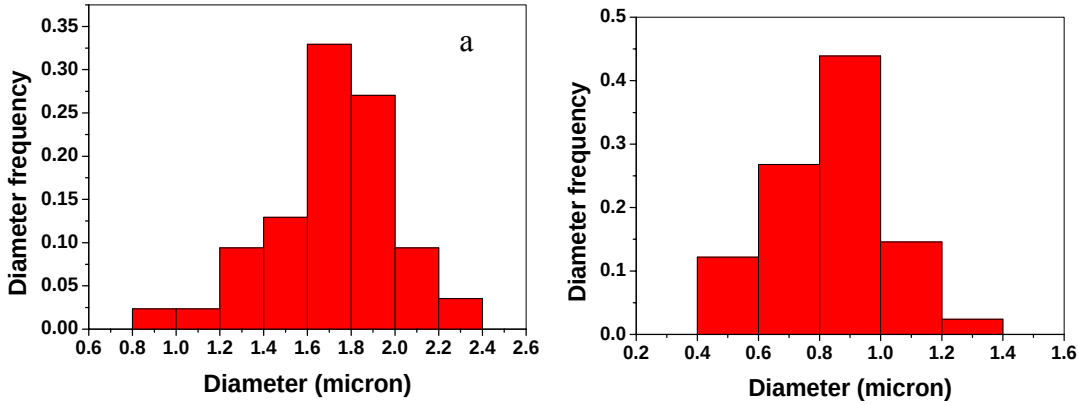

Fig. 3. 6 Effect of PF on PLA fiber diameters electrospun from 5 % PLA / dichloromethane solution. a: without PF; b: with 0.8 % PF.

Besides PF, another organic salt, tetraethylene benzylammonium chloride (TEBAC) was also an efficient additive for PLA solution and exhibited the same effect. However, the unique advantage of PF as additive is that it is a volatile salt, which vaporizes off together with solvent during electrospinning process, and thus does not remain in the as-spun PLA fibers any more. This will be very significant for retaining the original properties of PLA fibers such as excellent biocompatibility and good tensile strength.

IR-spectrum of PF proved that PF has completely vaporized after in air for 10 min (Fig. 3. 7 A). Further more, IR-spectrum of PLA fibers spun from PF-containing solution also showed no traces of PF and is completely consistent with that of PLA fibers spun from no PF solution (Fig. 3. 7 B).

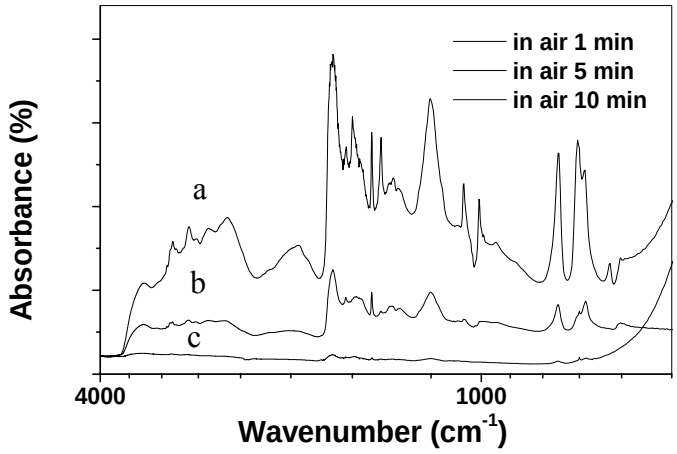

Fig. 3. 7 A IR spectra of PF. a: in air 1 min; b: in air 5 min; c: in air 10 min

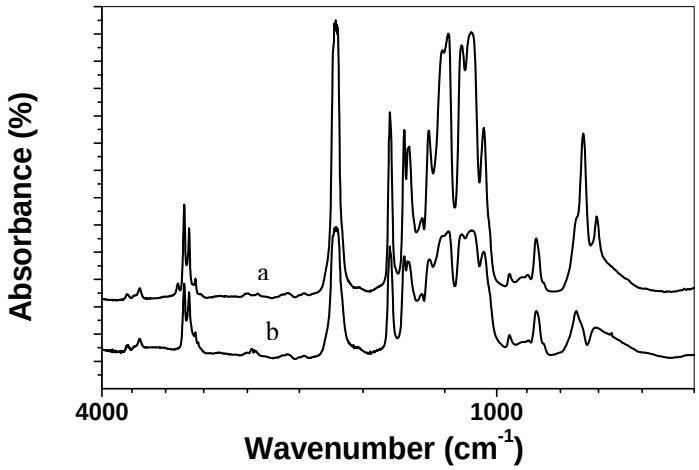

Fig. 3. 7 B IR spectra of PLA fibers electrospun from PLA solution a: without PF; b: with PF

3.1.3 Surface tension of polymer solutions

The surface tension tends to decrease the surface area per unit by changing the jets into spheres and was thought to play a very important role on the formation of "beaded" fibers. Related studies were reported for PEO/water/ethanol system by Reneker et al.[130]. However, in this system, the solution viscosity was changed simultaneously when the surface tension of the solution was varied by changing ratio of water to ethanol, and hence, it is difficult to evaluate which factor is dominant, viscosity or surface tension. In order to explore the role of the individual surface tension, PVA solution in water with addition of surfactants was investigated. Anionic and nonionic surfactants were added to the PVA aqueous solution, respectively, and a significant decrease in surface tension of the PVA solution was observed in both cases.

3.1.3.1 Effect of anionic surfactant

Fig. 3. 8 shows SEM images of PVA fibers electrospun from 7 % PVA solution in water with addition of an anionic surfactant, sodium dodecylsulfate (SDS). It was found that non-beaded and smaller fibers were obtained at lower SDS concentration (0.01 wt % and 0.04 wt % relative to solvent, corresponding to Fig. 3. 8 B - C), whereas at higher SDS concentration, beaded fibers combined with decreased fiber diameter were observed again (for 0.2 wt % SDS, Fig. 3. 8 D). There was a dramatic decrease in surface tension of the PVA solution, from 63.65 mN/m (without SDS) to 28.06 mN/m (with 0.04 %

SDS) (Table. 3. 3). However, further increase in SDS concentration to 0.2 % caused almost no further decrease in surface tension. Also, there was about 10 folds increase in conductivity, i.e. from 215 μS/cm (without SDS) to 2320 μS/cm (with 0.04 % SDS) (Table. 3. 3). There was no effect of addition of SDS on the solution viscosity. As both decrease of surface tension and increase of electrical conductivity favor formation of non-beaded fibers, the resulted thinner and smooth fibers can be attributed to combination functions of both increased conductivity and decreased surface tension. However, the reason why beaded fibers appear again with higher concentration of SDS is still not clear.

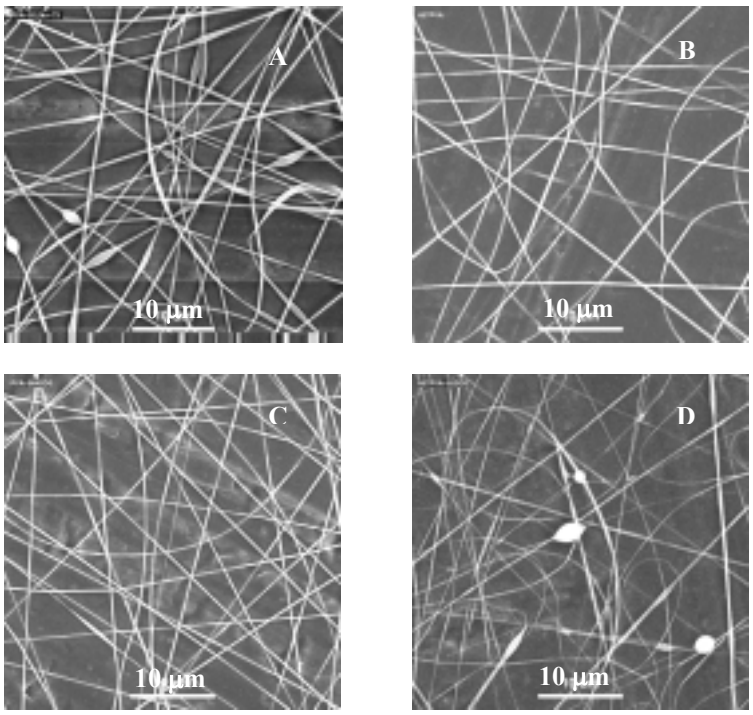

Fig. 3. 8 Influence of anionic surfactant (SDS) on fiber size and shape.A-C: PVA fibers electrospun from 7 % PVA solution in water. A: without SDS, B: 0.01 wt % SDS, C: 0.04 wt % SDS, D: 0.2 wt % SDS

Table 3. 3 Influence of anionic surfactant, SDS, on process parameters and PVA fiber diameter. Fibers were electrospun from 7 % PVA solution with different amount of SDS (concentration related to solution)

Conc. SDS [weight %]	Viscosity [mPa·s]	Electr. cond. [μS/cm]	Surface tension [mN/m]	Fiber diameter [nm]
0	219.34	215	65.67	200 - 350
0.01%	226.50	1362	48.84	20 - 250
0.04%	222.90	2320	28.06	100 - 200
0.2%	245.20	8840	26.31	80 - 250

3.1.3.2 Effect of nonionic surfactant

In order to eliminate the effect of increased electrical conductivity resulted from the anionic surfactant, three kinds of nonionic surfactants were employed, respectively. They are: Tween 85 (Polyoxyethylene(20)-sorbitantrioleate, M_n = 1839, HBL 11.0), 1-O-n-Octyl-ß-D-Glucopyranoside (OGP), and Surfynol 420 (S 420). In each case, decrease in surface tension of the solution was observed, whereas the other parameters such as solution viscosity and conductivity had almost no change.

The SEM images of the PVA fibers from the solution containing nonionic surfactant show, that the addition of the nonionic surfactants resulted in decrease in fiber diameter but an evident increase in the amount and size of beaded (Fig. 3. 9 A-F). The change of process parameters with nonionic surfactant is summarized in Table 3. 4. It demonstrates that solution viscosity and electrical conductivity remain almost the same, while the surface tension decreased to different extent, depending on the kind of the surfactant.

With OGP, the decrease in surface tension was less, i.e. from 65.67 mN/m (without additive) to 62.33 mN/m (with 0.02 % OGP). Also, a spindle-shaped beads along the fibers were observed (Fig. 3. 9A). With increase in OGP content, the beads became larger accompanied with smaller fibers (Fig. 3. 9 B-C). With Tween 85, even at an extremely low concentration, a significant decrease of surface tension was observed but heavily beaded fibers were formed (Fig. 3. 9 D-E). With S 420, decrease in surface

tension was quite significant (SFT down to 34.71 with 0.07 % S 420), but very big and round-shaped beads were produced along the small fibers (Fig. 3. 9 F).

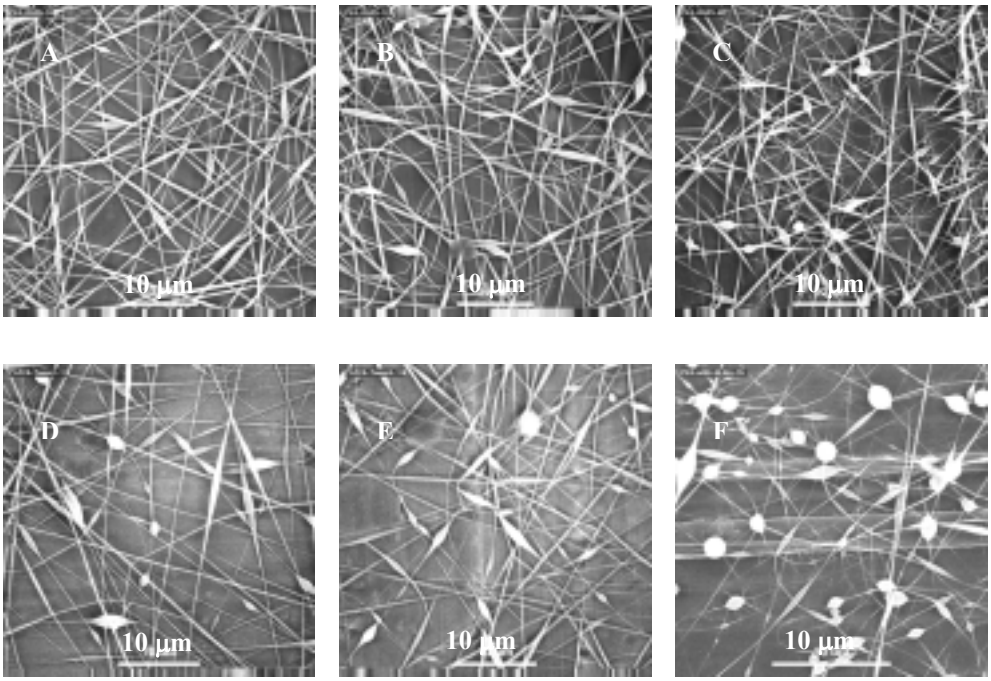

Fig. 3. 9 Influence of nonionic surfactant on fiber size and shape. A-F: PVA fibers electrospun from 7 % PVA aqueous solution with different additives. A: 0.02 % OGP, B: 0.04 % OGP, C: 0.08 % OGP, D: 0.002 % Tween 85, E: 0.005 % Tween 85, F: 0.07 % S 420.

Table 3. 4 Influence of nonionic surfactant on the diameter of the PVA fiber from 7 % PVA solution with different kinds of nonionic surfactants as additive (concentration related to solution)

Additive [weight %]	Viscosity [mPa·s]	Electr. cond. [µS/cm]	Surface tension [mN/m]	Fiber diameter [nm]
0	219.34	438	65.67	200 - 350
0.02 % OGP	218.50	505	62,33	100 - 350
0.04 % OGP	215.85	502	57.59	100 - 350
0.08 % OGP	201.53	496	52.29	50 - 350
0.002 % Tween85	-	-	52.33	100 - 250
0.005 % Tween85	-	-	48.33	80 - 150
0.07 % S420	-	-	34.71	50 - 100

3.1.4 Molecular weight and molecular weight distribution of polymers

It is well known that, under action of an electrical field, solutions of small molecular compounds exhibit the behavior of electrospraying, leading to the formation of particles, while solutions of polymers exhibit the behavior of electrospinning due to the viscoelastic properties of polymers, resulting in the formation of fibers. As the viscoelastic properties are closely related with molecular weight and molecular weight distribution of polymers, the effect of these two factors on fiber dimension and morphology was studied in this work.

3.1.4.1 Molecular weight of polymers

PVA fibers were electrospun from the PVA / water solutions with different molecular weight (M_w) of PVA. Three kinds of PVA, which are commercial available from Clariant, were employed:

PVA 56-98: M_w = 195,000 g/mol

PVA 20-98: M_w = 125,000 g/mol

PVA 10-98: M_w = 100,000 g/mol

The effect of the M_w of PVA on process parameters were summarized in Table. 3. 5.

Tab. 3. 5 Influence of PVA M_w on process parameters and PVA fiber diameter

PVA	Viscosity [mPa·s]	Electr. cond. [μS/cm]	Surface tension [mN/m]	Fiber diameter [nm]
56-98 (8%)	**973.3**	**232.0**	**51.98**	**350 - 700**
20-98 (8%)	**214.8**	**240.5**	**60.89**	**100 - 200**
10-98 (8%)	**74.0**	**247.0**	**61.71**	**50 - 150**
56-98 (6%)	**263.8**	**207.0**	**56.22**	**200 - 400**
20-98 (6%)	**67.7**	**210.0**	**60.87**	**100 - 200**
10-98 (6%)	**28.5**	**205.0**	**60.75**	**50 - 80**

Cylindrical PVA fibers with diameter ranging from 350 - 700 nm were yielded from 8 % PVA with higher M_w (56-98, Fig.3. 10 A). As compared to this, 8 % PVA with lower

M_w (10-98, Fig. 3. 10 C) gave thin fibers (50 - 150 nm) with many beads. Round and much larger beads were observed on decreasing the concentration of PVA solution with low M_w (20-98 and 10-98, Fig. 3. 10 E-F).

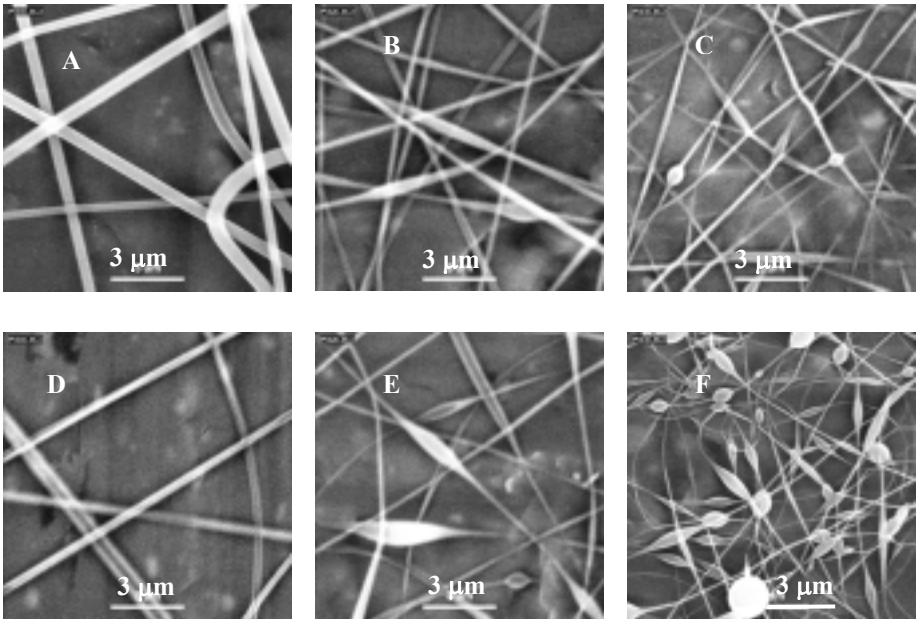

Fig. 3. 10 Variation of fiber morphology and size with Molecular weight. A-C: fibers from 8 % PVA solution in water, A: 56-98, B: 20-98, C: 10-98; D-F: fibers from 6 % PVA solution in water, D: 56-98, E: 20-98, F: 10-98

3.1.4.2 Molecular weight distribution of polymers

Molecular weight distribution (M_wD) of polymers can be varied by mixing polymers with different M_w. In this work, the M_wD of PVA was adjusted by mixing PVA 56-98 (high M_w) and PVA 10-98 (low M_w). 8 % PVA 56-98 aqueous solution was mixed with 8 % PVA 10-98 aqueous solution with the following mixing ratio: 90:10, 80:20, 75:25, 70:30, 60:40, 50:50, 45:55, 40:60. Effect of mixing ratios on processing parameters of the mixture solution is summarized in Table 3. 6.

Table 3. 6 Influence of PVA molecular weight distribution on process parameters and PVA fiber diameter

Mix. Ratio of 56-98 : 10-98	Viscosity [mPa·s]	Electr. cond. [μS/cm]	Surface tension [mN/m]	Fiber diameter [nm]
100:0	973.3	232.0	51.98	350 - 700
90:10	823.6	236.0	56.20	300 - 500
80:20	663.1	236.0	55.93	250 - 500
75:25	553.5	237.0	55.65	250 - 450
70:30	468.8	240.0	55.31	200 - 400
60:40	402.0	239.0	56.11	200 - 350
50:50	310.2	242.0	56.33	150 - 300
45:55	264.7	237.0	57.03	150 - 250
40:60	227.3	236.0	57.74	100 - 250
56-98 (6%)	263.8	207.0	56.22	200 - 400
20-98(8%)	214.8	240.5	60.89	100 - 200

It is clear that the mixing of the two PVA solutions with the same concentration did not change the solution concentration, the electrical conductivity of the solutions, and the surface tension of the solutions but changed the viscosity of the solutions. With the increase in the content of the low molecular component (PVA 10-98), the viscosity of the mixture solutions decreased dramatically (Table 3. 6), resulting in significant decrease in fiber diameters. The dependence of fiber diameters on mixing ratio was shown clearly Fig. 3. 11.

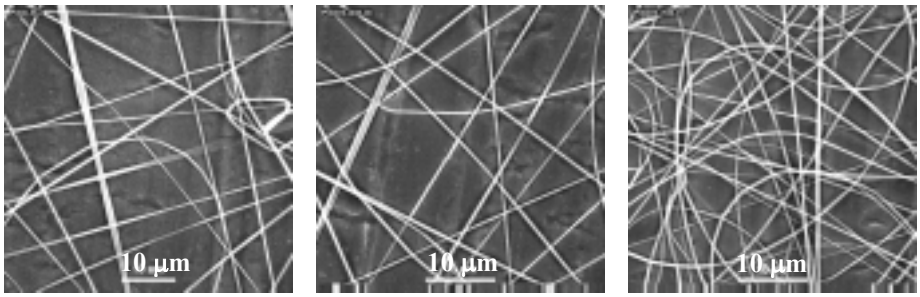

A 100:0, 350 – 700 nm **B 80:20, 250-500 nm** **C 70:30, 200-400 nm**

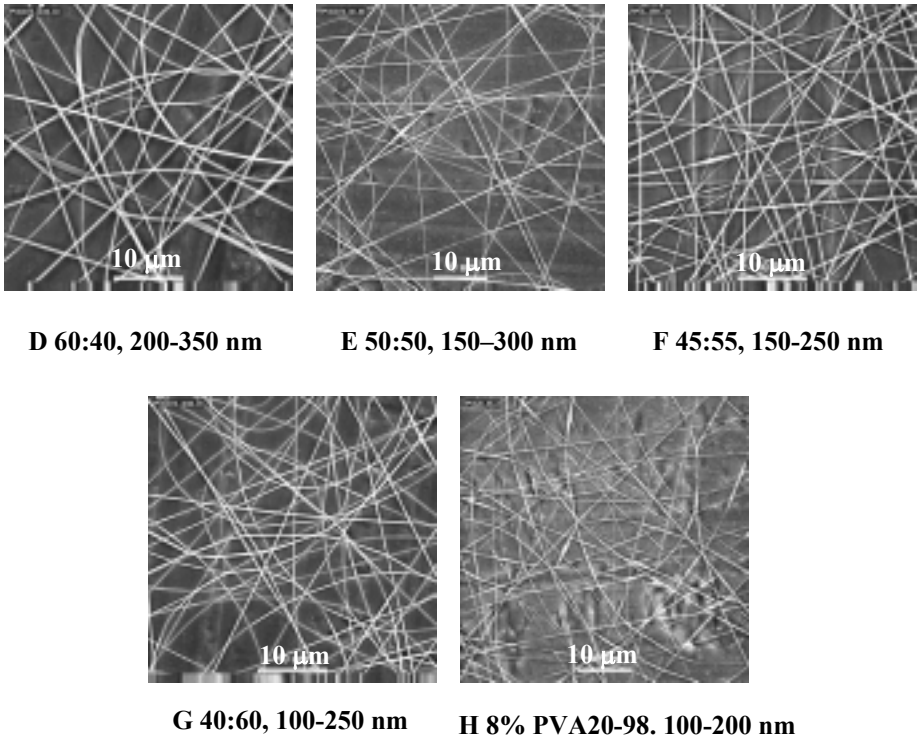

D 60:40, 200-350 nm **E 50:50, 150–300 nm** **F 45:55, 150-250 nm**

G 40:60, 100-250 nm **H 8% PVA20-98. 100-200 nm**

Fig. 3. 11 Dependence of fiber morphology and size on mixing ratio of PVA mixture. The mixing ratio of PVA 56-98 to PVA 10-98 is: A: 100:0; B: 80:10; C: 70:30; D: 60:40; E: 50:50; F: 45:55; G: 40:60; H: 8 % pure PVA 20-98 for comparison

With increase in the content of the low molecular component, fiber diameter decreased. Fibers with diameter of 350 - 700 nm were obtained from pure PVA 56-98 (Fig. 3. 11 A); while fibers with diameter of 100 - 250 nm were obtained from the PVA mixture with mixing ratio of 40:60 (Fig. 3. 11 G).

It is also found that PVA mixtures of different molecular weight components favor the formation of "non-beaded" fibers. Comparing 8 % PVA 20-98 solution and 8 % PVA 5610-4060 solution (40 parts of 8 % PVA 56-98 and 60 parts of 8 % PVA 10-98), both solutions had the same concentration, the almost same electrical conductivity, the same surface tension, and the almost same viscosity (Table 3.6). However, beaded fibers were obtained from the pure PVA 20-98 solution (Fig. 3.11 G), whereas cylindrical and smooth fibers were obtained from the PVA 5610-4060 solution. The different fiber shape could only be attributed to the difference in molecular distribution. In PVA 5610-4060 mixture solution, the high M_w component favors the formation of cylindrical and smooth fibers, while the low M_w favors the formation of smaller fibers.

3.2 Functional electrospun fibers

3.2.1 PPX-coated PEO / NaCl composite fibers

3.2.1.1 Preparation of PEO / NaCl composite fibers

10 wt % PEO (M_w = 900,000 g/mol) solution in water/isopropanol (9:1) mixture solvent was prepared. 10 % NaCl aqueous solution was added to the PEO solution. The amount of the NaCl solution was controlled so that the weight ratio of PEO to NaCl was 4:1. The final concentration of the PEO in the mixture solution was about 8 wt %. By electrospinning the 8 % PEO / NaCl solution, PEO / NaCl composite fibers were obtained with diameter ranging from 300 - 500 nm with a rough surface. The morphology of the fibers was characterized by SEM and TEM (Fig. 3. 12 A-C). The presence of NaCl in the fibers was proved by the EDX analysis (Fig. 3. 12 D).

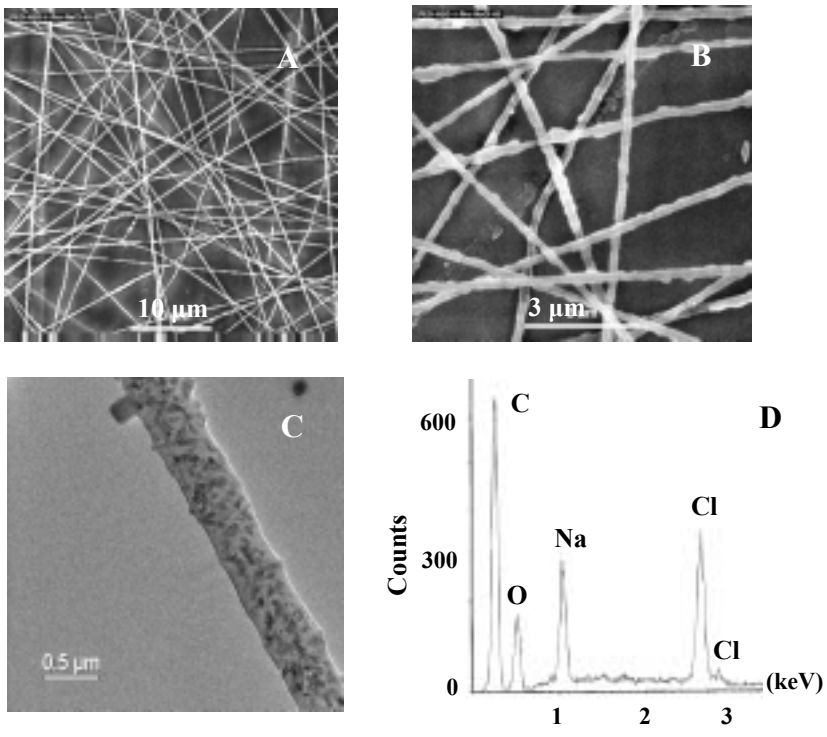

Fig. 3. 12 A-B: SEM images of PEO / NaCl fibers; C: TEM images; D: EDX microanalysis

3.2.1.2 Preparation of PPX-coated PEO / NaCl composite fibers

The PPX-coated PEO / NaCl fibers were prepared by CVD coating of the PEO / NaCl composite fibers with PPX. The morphology of the coated fibers is shown in Fig. 3. 13.

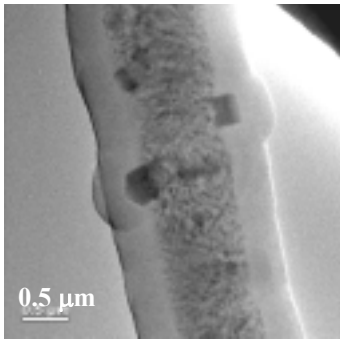

Fig. 3. 13 TEM images of PPX-coated PEO / NaCl fibers

3.2.1.3 Wide-angle X-ray diffraction of PPX-coated PEO / NaCl fibers

The WAXD pattern of PPX-coated PEO / NaCl fibers displayed four crystalline peaks at 2θ = 19º, 23º, 31º, and 45º, respectively (Fig. 3. 14 b). Compared with the WAXD diffractogram of NaCl crystal (Fig. 3.14 a), it is obvious that the peaks at 2θ = 31º and 45º are attributed to NaCl crystals, indicating the presence of NaCl in the fibers. The peak at 2θ = 19º is attributed to PPX, and the peak at 2θ = 23º is attributed to PEO.

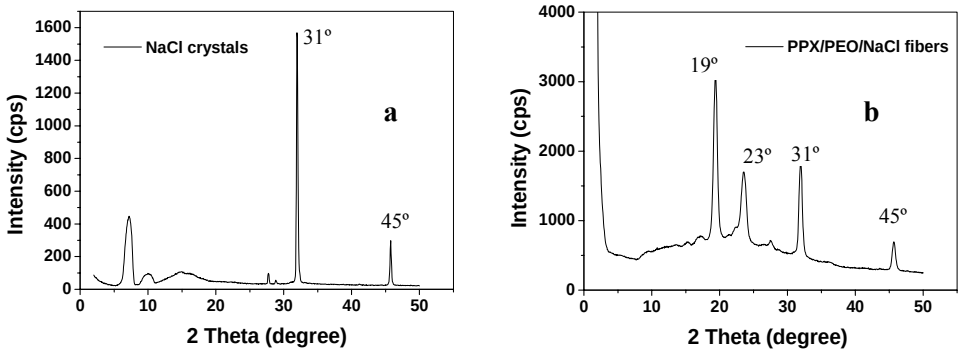

Fig. 3. 14 a: WAXD of NaCl crystal; b: WAXD of PPX-coated PEO / NaCl fibers

3.2.1.4 Controlled release of NaCl from PPX-coated PEO / NaCl fibers

Recently a great deal of interest has been paid on controlled drug delivery systems due to their improved therapeutic efficiency and safety. Some investigations on electrospun

fibers as drug-delivery matrix have been reported and patented [82, 131], where biodegradable polymers such as PLA or poly (ethylene-co-vinyl acetate) (PEVA) were electrospun from solution containing drugs such as tetracycline hydrochloride. A much higher release rate than that of film systems was observed.

In this work, PPX-coated PEO / NaCl fibers were used as model drug delivery system, where NaCl was utilized as model of small molecular drugs, PEO as drug carrier, and PPX as barrier. The release behavior of NaCl through PPX-coated PEO / NaCl fibers was investigated by immersing the fibers in water, and the release rate was characterized by measuring the change of the electrical conductivity of the water. Controlled release of NaCl was achieved by altering the thickness of the PPX coating.

Sample preparation

To study the dependency of release rate on the thickness of the PPX layers, two samples were prepared:

Sample 1 - 7PXENa: coated with 70 mg paracyclophane
Sample 2 - 14PXENa: coated with 140 mg paracyclophane

According to the TEM observation, the PPX thickness of sample 1 was 20 - 40 nm, and the PPX thickness of sample 2 was 40 - 80 nm.

Each sample with the amount of about 10 mg was immersed in 65 ml water. In order to monitor the release of NaCl, the change of the electrical conductivity of the water was measured as a function of immersion time.

Release of NaCl from PPX-coated PEO / NaCl fibers

The release of NaCl from the PPX-coated PEO / NaCl fibers in water was characterized by the electrical conductivity (Econd.) of the water. The Econd. of the water was measured as a function of immersion time, as shown in Fig. 3. 15 A.

According to the standard curve of NaCl solution ($E_{cond.}$ versus solution concentrations), $E_{cond.}$ of NaCl solution is proportional to concentration of NaCl, the curve of $E_{cond.}$ versus

immersion time can be transferred into the curve of NaCl concentration versus immersion time, that is, the release rate curve of NaCl, which is shown in Fig. 3. 15 B.

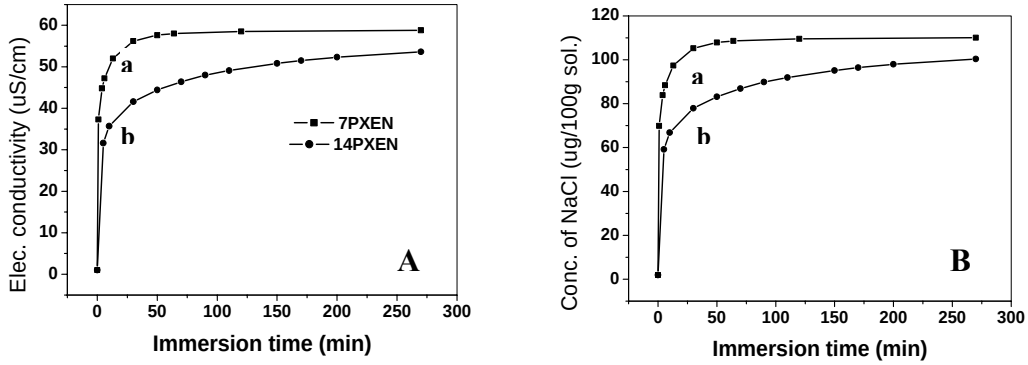

Fig. 3. 15 A: change of the electrical conductivity of the water with immersion time; B: release rate of NaCl from the PPX-coated PEO / NaCl fibers; a: 7PXENa; b: 14PXENa

A drastic increase in electrical conductivity of the water was observed within the first 10 min for sample 7PXENa (Fig. 3. 15 curve a), indicating a rapid release of NaCl at the beginning. Further in water till 30 min, a slower increase was observed, followed by an extremely slow increase. In water for 1 day, the electrical conductivity of the water reached a maximal value, indicating the complete release of NaCl. It is calculated that 87% of the NaCl was released within the first 10 min, and 95% of the NaCl was released after 30 min in water.

For sample, with sample 14PXENa, a similar release behavior was observed. However, it exhibited a slower release within the first 10 min (Fig. 3. 15 curve b). Only 63% of the NaCl was released out when in water for 10 min. In water for 30 min, 74.3% of the NaCl was released out. After 30 min, a gradual increase was observed. In water for 2 days, a maximal value was reached, indicating a complete release of NaCl.

Release of PEO from PPX-coated PEO / NaCl fibers

Accompanied by the release of NaCl, release of PEO from the PPX-coated PEO / NaCl fibers was also observed due to the water solubility of PEO. The release of PEO was qualitatively characterized by IR spectrum (Fig. 3. 16).

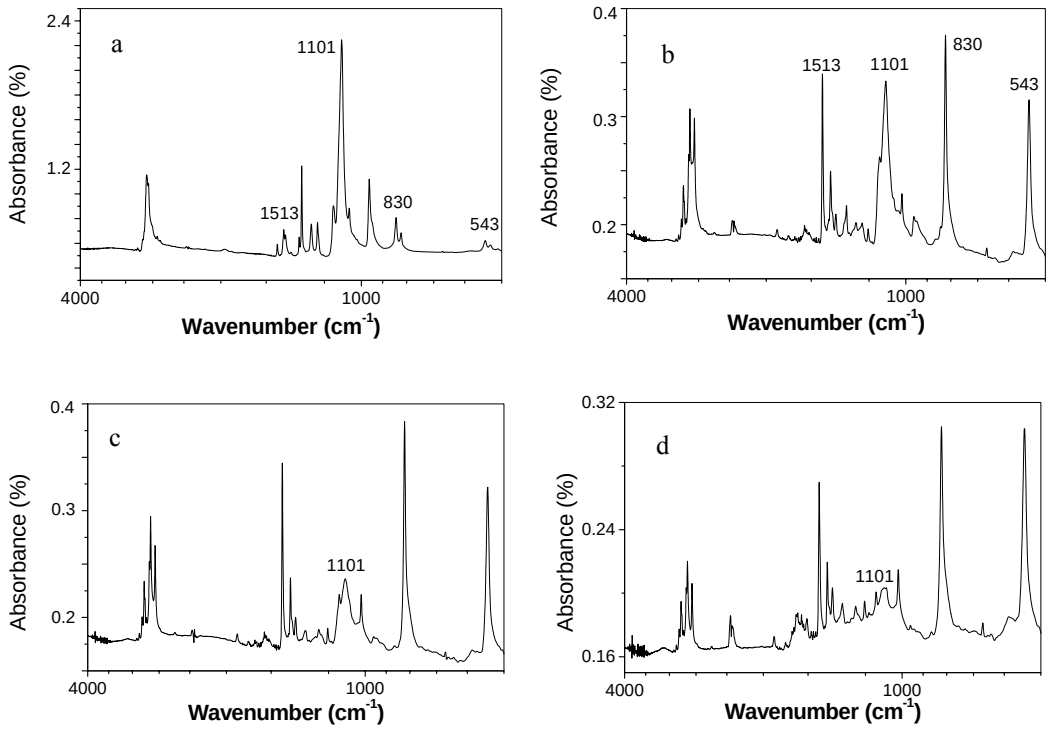

Fig. 3. 16 IR spectra of PPX-coated PEO / NaCl fibers (7PXENa), a: before immersion; b: in water for 1 hr; c: in water for 1 day; d: in water for 6 days

The IR spectrum of 7PXENa before immersion in water (Fig. 3. 16 a) exhibited a very strong PEO absorbance band (at 1101 cm^{-1}) and very weak PPX absorbance bands (at 1513 cm^{-1}, 830 cm^{-1}, 543 cm^{-1}) due to the thin PPX coating. In water for 1 hr, the PEO absorbance band at 1101 cm^{-1} decreased significantly (Fig. 3.16 b). Further immersion in water resulted in further decrease in the absorbance intensity of PEO (Fig. 3.16 c-d), indicating the gradual release of PEO from the PPX-coated PEO / NaCl fibers.

The release behavior of PEO is similar with that of NaCl, that is, a quick release within the first 1 hour was followed by a slowed down release. However, the release rate of PEO was much slower. For NaCl, most of NaCl was released after 30 min. in water, whereas for PEO, most of PEO was released after 1 day in water. It is clear that the molecular weight plays an important role. For PEO macromolecule, the diffusion rate is much slower than that of small molecular NaCl. It is also proved that the release of NaCl or PEO from the PPX-coated PEO / NaCl fibers is dependent on the diffusion rate of released substance in water.

Wide-angle X-ray diffraction

The x-ray diffraction patterns of the sample 7PXENa (Fig. 3. 17) showed, that after in water for 6 days, the peaks at 2θ = 31º and 45º, which are attributed to NaCl, disappeared completely, and the peak at 2θ = 23º, which is attributed to PEO, decreased so much that it was almost indiscernible. The strong peak at 2θ = 19º, which is attributed to PPX, remained unchanged, indicating no change in the PPX. The X-ray diffractogram further proved that all NaCl and most of the PEO have been released from the PPX-coated PEO / NaCl fibers after in water for 6 days.

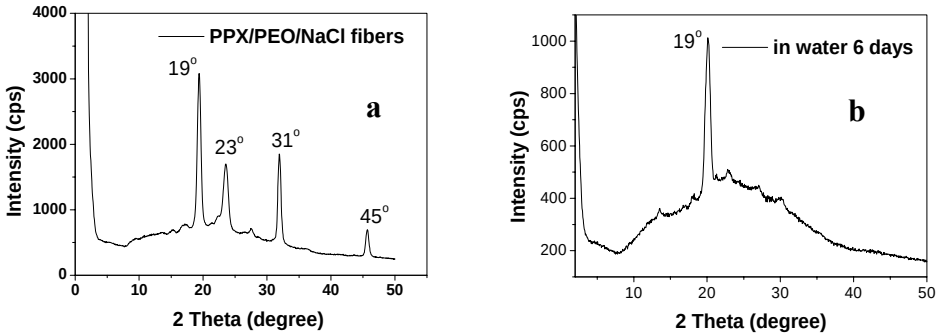

Fig. 3. 17 WAXD diffractograms of the PPX-coated PEO / NaCl fibers, a: before immersion; b: in water for 6 days.

3.2.2 PVA / protein composite fibers

Small molecular compounds represents one class of drugs, another class of drugs are represented by macromolecular peptides or proteins. As the diffusion rate of molecules is strongly dependent on the molecular weight, it is expected that the release behavior of proteins should be different from that of small molecular compounds such as NaCl. In this work, PVA / BSA fiber system was developed, where PVA as carrier, and fluorescence-tagged BSA (FTIC-BSA) as model protein. The release behavior of BSA from PVA / BSA fibers was investigated.

3.2.2.1 Preparation of PVA / BSA composite fibers

10 wt % PVA (Mowiol 56-98, M_w = 195,000 g/mol) solution in water was prepared. To this solution was added FTIC-BSA solution with the concentration of 1.03 mg/ml. The amount of BSA solution was controlled so that the weight ratio of PVA to BSA was

100:1. The final concentration of PVA in the mixture solution was about 5 wt %. Electrospinning of the PVA / BSA mixture solution was carried out at electrical field of 55.5 kV. The resulting PVA / BSA composite fibers were collected on metal frames.

The morphology of the PVA / BSA fibers was characterized by SEM. The fibers have diameter ranging from 200 - 300 nm with some beads along the fibers (Fig. 3. 18)

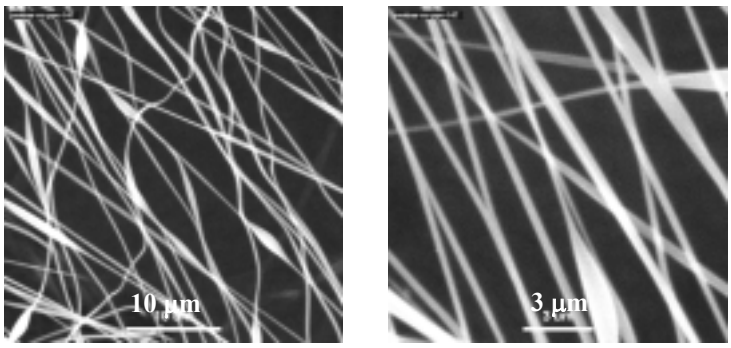

Fig.3. 18 SEM images of the PVA / BSA composite fibers

3.2.2.2 UV/Vis and IR spectrum of PVA / BSA composite fibers

UV spectrum of the fibers exhibits obvious absorbance bands between 450 - 500nm, which is attribute to BSA contained in the fibers (Fig. 3. 19).

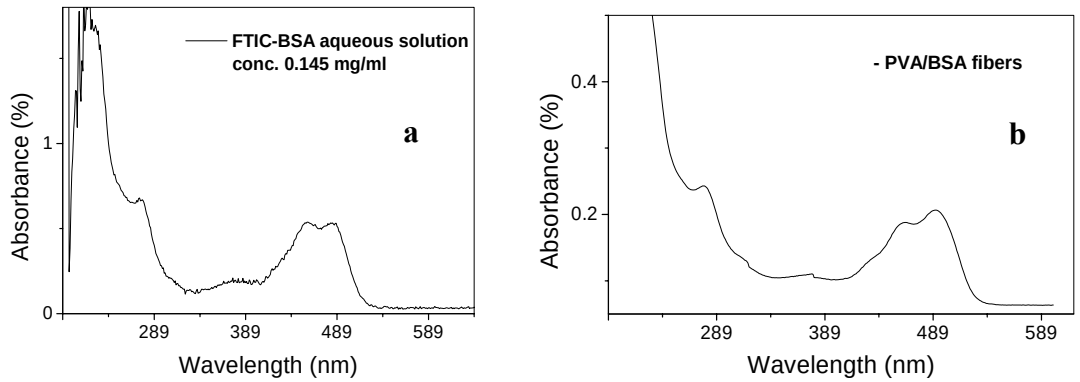

Fig.3. 19 UV/Vis spectra of a: BSA aqueous solution; b: PVA / BSA fibers

In addition, the IR spectrum of the PVA / BSA fibers shows two new absorbance bands at 1710 cm^{-1} and 1665 cm^{-1}, which are attributed to the amide bonds from BSA, indicating the presence of BSA in the PVA / BSA fibers (Fig. 3. 20).

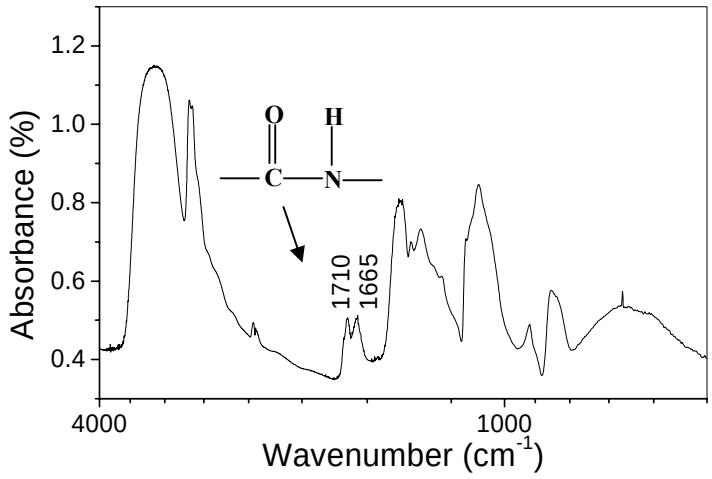

Fig. 3. 20 IR spectrum of PVA / BSA fibers

3.2.2.3 Release of BSA through PVA / BSA composite fibers

The PVA / BSA fibers were immersed in water and the change of the UV spectrum of the water solution was measured to monitor the BSA release (Fig. 3. 21).

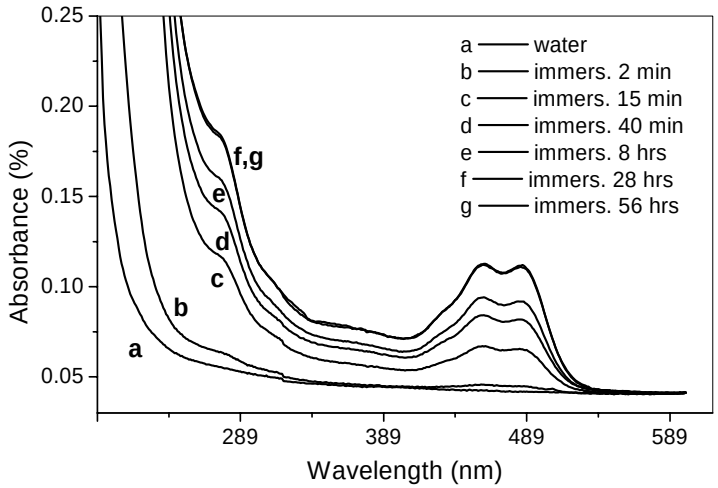

Fig. 3. 21 Change of UV/Vis spectra with immersion time of PVA / BSA fibers in water. Immersion time is a: 0 min; b: 2 min; c: 15 min; d: 40 min; e: 8hrs; f: 28 hrs; g: 56 hrs

The release curve of BSA (Fig. 3. 22) shows a very fast release of BSA within the first 2 hours, followed by a slowed down release. After in water for 2 days, the concentration of BSA in water reaches a maximal value. No further releases of BSA were observed after

2 days. By controlling the fiber morphology, porosity, and component, the release behavior of BSA from PVA / BSA fibers can be optimized to meet the clinical demands.

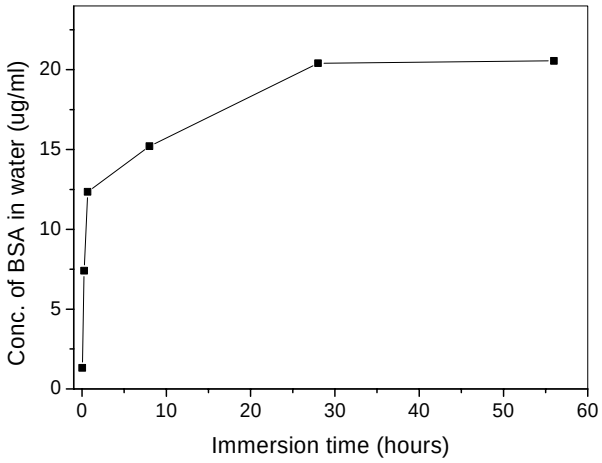

Fig. 3. 22 Release of BSA from PVA / BSA fibers

3.2.3 Water-stable PVA fibers

Although hundreds of polymers have been electrospun from the corresponding solutions, water-based polymer solution systems are always preferable in practical production considering the demands of environment protection. PVA is a water-soluble, fiber-processable and biodegradable polymer. In addition to its potential applications in biomedical field such as drug delivery, PVA electrospun fibers have also great application potential in the fields such as filtration and waste water treatment if the water-stability of the PVA fibers can be improved.

Crosslinking is one of the efficient approaches to improve the water-stability of PVA fibers. In this work, different ways for crosslinking of PVA fibers have been tried, including heat-induced crosslinking of PVA / PAA blend fibers, UV-induced crosslinking of PVA derivatives containing photo-sensitive moieties, and UV-induced crosslinking of PVA containing a photo-polymerizable and -crosslinkable monomer, tetraethyleneglycol dimethylacrylate (TEGDA) and a proper initiator. After crosslinking, the PVA fibers exhibit very good water-stability.

3.2.3.1 Crosslinked PVA / PAA fibers

Preparation of PVA / PAA blend fibers

10 wt % PVA / PAA blend solution were prepared by mixing 10 wt % PVA (Mowiol 28-99, M_w = 145,000 g/mol) aqueous solution and 10 wt % PAA (Sokalan PA 110S, M_w = 250,000 g/mol) aqueous solution with different mixing ratio. The PVA / PAA fibers were electrospun from the 7 wt % or 8 wt % PVA / PAA mixture solution which were diluted from the above 10 wt % solution.

The morphology of the fibers was characterized by SEM and TEM (Fig. 3. 23). No phase separation was observed in the SEM and TEM images, indicating that the two components in PVA / PAA blend fibers are completely compatible.

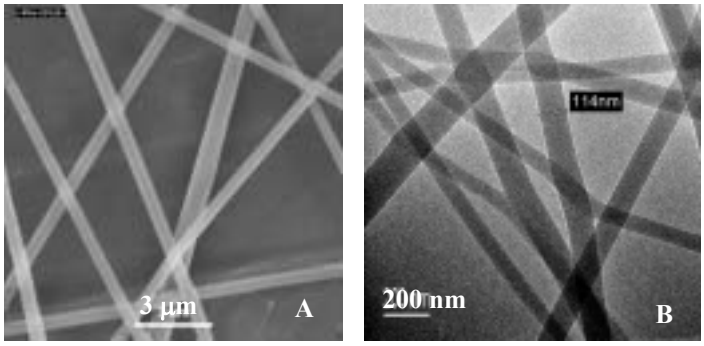

Fig. 3. 23 Morphology of the PVA / PAA blend fibers from A: 10 wt % PVA / PAA (75 : 25) solution in water, SEM images ; B: 7 wt % PVA / PAA (75 : 25) solution, TEM images

Heat-induced crosslinking of PVA / PAA fibers

The PVA / PAA fibers were crosslinked by annealing the fibers at a proper temperature in vacuum. The degree of crosslinking of the PVA / PAA fibers depends on PAA content, annealing temperature, annealing time, and the presence of acidic additives etc. The investigation on the dependence of the degree of crosslinking on these factors was conducted with PVA / PAA films as sample due to the simple operation and characterization.

Characterization of the degree of crosslinking

The degree of crosslinking of the crosslinked PVA / PAA fibers was characterized by the swelling degree (SD) of the PVA / PAA films with the same composition. The SD is defined as the increase percentage of the film weight after immersion in water for a certain time. It is calculated according to the following equation:

$$SD = (W_2 - W_1)/W_1$$

W_2 is the weight of the film after immersion in water, and W_1 is the film weight before immersion in water.

The degree of crosslinking is inversely proportional to the SD. The lower the SD is, the higher the degree of crosslinking.

The measurement of the SD of the PVA / PAA film was performed as follows: the heat-treated PVA / PAA film was immersed in water. The water was then gradually heated to boiling. After in the boiling water for 1 hr, the water was cooled down to room temperature. The film was kept in the water for another 3 hrs and then taken out. The water drops on the film surface was removed carefully by using a filter paper. The film was weighed.

Influence factors for the degree of crosslinking

In order to search for optimal crosslinking conditions, that is, a shortest annealing time at as low as possible annealing temperature for a high enough degree of crosslinking, the ratio of the PVA to PAA was varied from 90:10 to 65:35, and annealing temperature was varied from 80ºC to 140ºC. An acidic catalyst, p-toluene sulfonate (TOS), was added to the PVA / PAA solution to study the effect of the catalyst. The SD of the film treated under the different conditions is summarized in Table 3. 7.

Table 3. 7 Dependence of the SD of the PVA / PAA films on PAA concentration, annealing temperature, annealing time, and the acidic additive.

Ratio of PVA:PAA	Ann. temp.	Ann. Time 10 min	Ann. Time 30 min	Ann. Time 1 hr
90:10 without TOS	100ºC	dissolved[a]	dissolved[a]	broken gel[b]
	120ºC	broken gel[b]	broken gel[b]	7.47
90:10 5% TOS	100ºC	dissolved[a]	broken gel[b]	broken gel[b]
	120ºC	8.63	7.31	5.33
80:20 5% TOS	80ºC	broken gel[b]	broken gel[b]	8.10
	100ºC	12.52	10.68	7.70
70:30 5% TOS	80ºC	broken gel[b]	12.01	7.35
	100ºC	10.80	7.65	4.87
65:35 without TOS	140ºC	6.57	4.84	brown[c]

[a] During immersion in water, the PVA / PAA film dissolved, indicating a too low degree of crosslinking

[b] fter immersion in water, the PVA / PAA film became a broken gel due to the too much water absorption, indicating a not enough degree of crosslinking

[c] The PVA / PAA film became slightly brown, indicating decomposition to a certain extend.

It is obvious, that increase in PAA content decreased significantly the annealing time and the annealing temperature necessary for the formation of the water-stable PVA / PAA film. For the PVA / PAA film with the ratio of 90:10, good water-stability of the film could be obtained only by annealing at 120ºC for 1 hr, while for the PVA / PAA with the ratio of 70:30, low SD (i.e. high degree of crosslinking) could be achieved by annealing at 100ºC for 30 min.

The presence of the acidic additive, p-toluene sulfate (TOS), increased the crosslinking rate significantly. For the PVA / PAA (90:10) without TOS, good crosslinking was achieved only by annealing at 120ºC for 1 hr, while for the PVA / PAA (90:10) with 5 % TOS, annealing at 120ºC for 10 min was enough for a good crosslinking. However, the effect of TOS was reduced by increase in annealing temperature. At high temperature (more than 140ºC), the presence of the TOS accelerated the decomposition of PVA / PAA blend polymer.

The increase in annealing temperature reduced dramatically the annealing time. When annealed at 170ºC, 3 min was already enough for good crosslinking of the PVA / PAA (80:20) film (film thickness about 0.5 mm) (Table 3. 8).

Table 3. 8 The SD of the PVA / PAA films in water annealed at 170ºC in vacuum for different time

PVA : PAA	Annealing time	
	3 min	5 min
80:20	11.52	10.66
75:25	10.00	8.01
65:35	7.51	6.43

Hydrophilicity of the crosslinked PVA / PAA

Good hydrophilicity is the characteristics of PVA. It is not desired that the hydrophilicity of the PVA / PAA decreased too much after heat-induced crosslinking. The hydrophility of the crosslinked PVA / PAA was characterized by measuring the contact angle of the PVA / PAA film against water. Table 3.9 lists the contact angle of the PVA / PAA films after annealing at 100ºC for 30 min.

Table 3. 9 Contact angle of the crosslinked PVA / PAA against water

PVA :PAA	75:25	65:35	58:42
Contact angle	51.8	51.9	52.1

The crosslinked PVA / PAA film still exhibited a relative low contact angle (about 52º), indicating the good hydrophilicity of the crosslinked PVA / PAA.

Water-stability of the crosslinked PVA / PAA fibers

PVA / PAA (75:25) fibers were crosslinked by annealing at 100ºC for 30 min. The water-stability of the crosslinked PVA / PAA fibers were characterized by observing the change of the fiber morphology after exposure to water or steam (95ºC). The fibers were immersed in water at RT for 1 day or exposed to steam (95ºC) for 1 hr, respectively. No

change in fiber morphology was observed after 1 day in water at RT, whereas a slight swelling of the fibers was observed after exposure to steam for 1 hr, indicating the good water-stability of the crosslinked PVA / PAA fibers (Fig. 3.24).

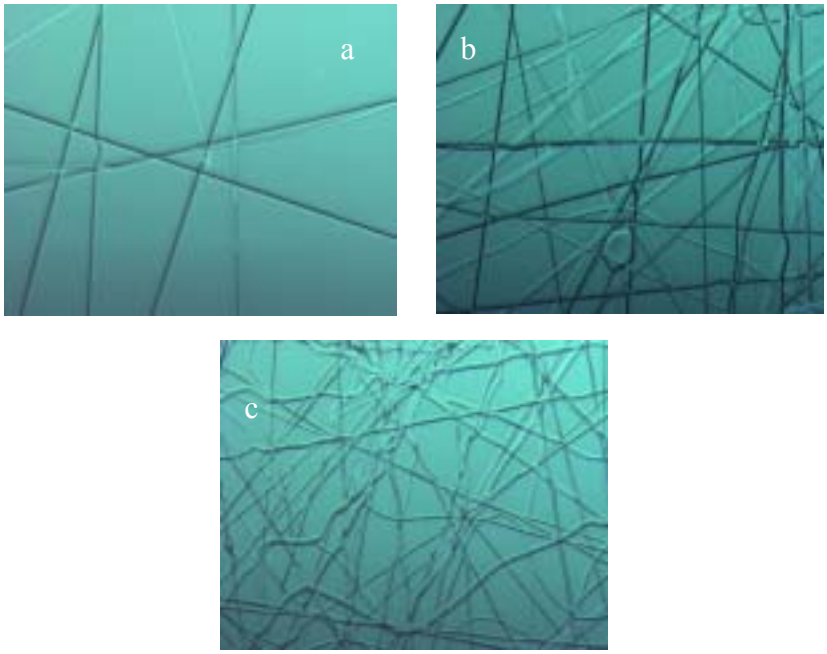

Fig. 3. 24 Optical microscopy morphology of the crosslinked PVA / PAA (75:25) fibers, a: before immersion in water; b: immersion in RT water for 1 day; c: immersion in vapor for 1 hr

IR spectrum

The IR spectrum of the crosslinked PVA / PAA (75:25) fibers exhibits a strong hydroxyl absorbance band at 3391 cm^{-1} and a middle ester absorbance band at 1710 cm^{-1}.

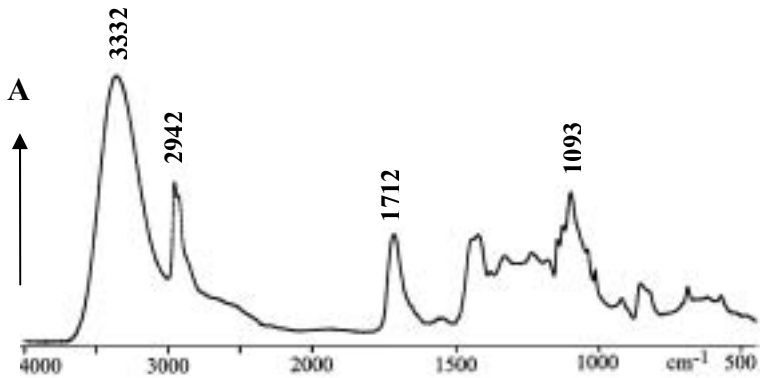

Fig. 3. 25 IR spectrum of the crosslinked PVA / PAA (75:25) fibers

3.2.3.2 Photo-curable PVA derivatives and their fibers

An alternative method for crosslinking of PVA is UV irradiation. In this work, a highly photosensitive thienyl acrylate group [132-134], was introduced onto PVA side-chain by means of analogous reaction. This generated partially esterified PVA, where hydroxyl groups were partially substituted by thienyl acrylate groups. This partially esterified PVA derivative proved to be photo-curable. Under the irradiation of a mercury lamp (Hg/10, OSMAR, emission wavelength more than 300 nm) for 10 min, the PVA fibers with very good water-resistance were obtained.

Synthesis of photo-curable PVA derivatives

The photo-curable PVA derivative was synthesized by means of the analogous reaction of PVA with thienyl acryloyl chloride, which was synthesized with thiophenealdehyde as starting material (Fig. 3. 26 a).

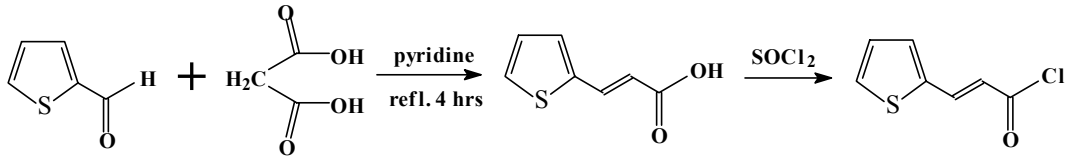

Fig. 3. 26 a Synthesis of thienyl acryloyl chloride

The analogous reaction was performed at 110ºC under argon atmosphere with dried DMF as solvent. 2g PVA (Mowiol 28-99) was dissolved in 250 ml dried DMF at 160ºC. The solution was then cooled to 110ºC. Lower temperature is not possible as the PVA solution in DMF becomes a gel at lower temperature. To the PVA solution at 110ºC was slowly added thienyl acryloyl chloride solution in dried DMF. The amount of thienyl acryloyl chloride was controlled according to the desired substitution degree. In this work, the desired substitution degree was 5 mol % and 0.4 g thienyl acryloyl chloride was used. The resulted partially esterified PVA containing thienyl acrylate groups in the side-chain (PVA-Thio) was a light-brown solid. The reaction is shown in Fig. 3. 26 b.

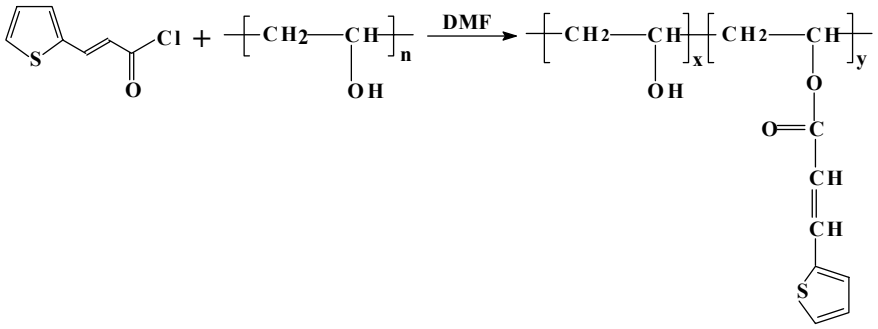

Fig. 3. 26 b Synthesis of the PVA derivative containing thienyl acrylate groups in the side chain

^{1}H-NMR spectrum

^{1}H-NMR spectrum of PVA-Thio shows the presence of the thiophene groups (δ = 7.56 ppm) (Fig. 3. 27). The integration shows there are 23.93 H from –CH_2– , 11.31 H from –CH–, and 1.58 H from the thiophene group in the PVA-Thio. The degree of esterification of the PVA derivative was thus calculated to be 4.52 mol %.

To confirm the degree of esterification, the titration method was employed. 2 g PVA – Thio solution in 70 ml water was hydrolyzed by heating together with 50 ml of 0.1 N KOH. The solution was then titrated with 0.1 N standard HCl solution. The result showed that the degree of esterification is about 4.0 mol %, well consistent with the value calculated from ^{1}H - NMR data.

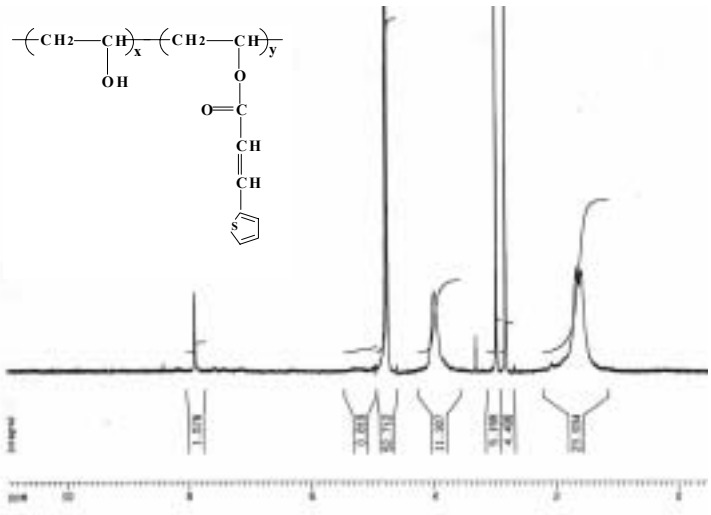

Fig. 3. 27 ^{1}H - NMR spectrum of PVA-Thio

IR spectrum

In IR spectrum of PVA-Thio three new absorbance bands (at 1710 cm^{-1}, 1659 cm^{-1} and 1623 cm^{-1} respectively) appeared, which are attributed to thienyl acrylate groups.

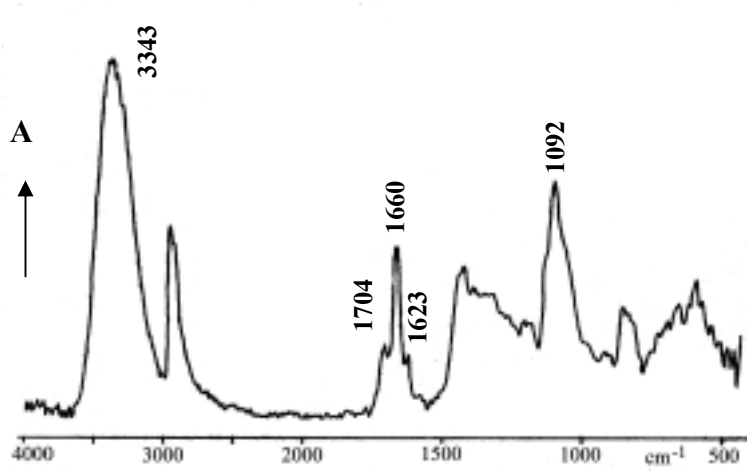

Fig. 3. 28 IR spectrum of PVA containing thiophenyl acrylate substituent

UV/Vis-spectrum

UV/Vis spectrum of PVA-Thio exhibited a maximal absorbance at 310 nm (Fig. 3. 29).

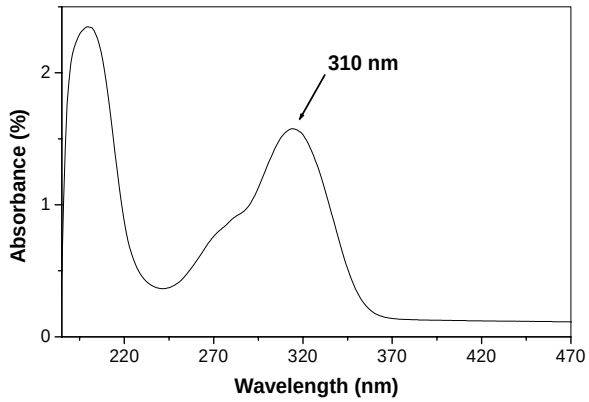

Fig. 3. 29 UV/Vis spectrum of PVA-Thio

UV-induced crosslinking of PVA-Thio film

The PVA-Thio film was prepared by means of spin-coating of the PVA-Thio solution in DMF. The produced PVA-Thio film (about 0.3 mm) was then subjected to UV radiation (emission wavelength more than 300 nm). With increase in the exposure time, the amount of the double bond in the thienyl acrylate groups decreased due to the formation of the intermolecular bonding (Fig. 3. 30).

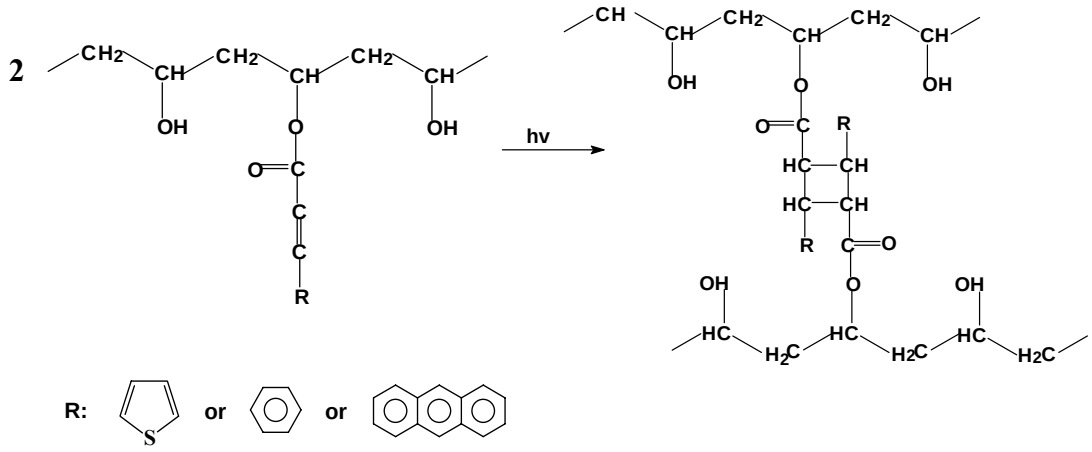

Fig. 3. 30 UV-induced crosslinking of PVA-Thio

As the absorbance band at 310 nm in the UV/Vis spectrum is attributed to the double bond in the thienyl groups, the crosslinking of the PVA-Thio could be monitored by means of the change in the absorbance intensity at 310 nm of the film (Fig. 3. 31).

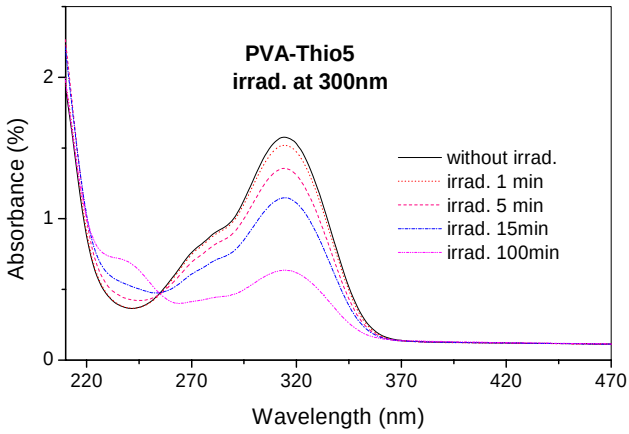

Fig. 3. 31 Variation of UV/Vis spectrum of PVA-Thio film with exposure time

The absorbance intensity (at 310 nm) of the PVA-Thio film decreased significantly with increase in irradiation time. Obvious crosslinking of the PVA-Thio film was observed after exposure to UV radiation for even 1 min. In UV irradiation for 15 min, the absorbance intensity at 310 nm decreased to half of the original value, indicating that half of the double bonds in the PVA-Thio were transferred to single bonds by means of the intermolecular crosslinking. It is proved that thienyl acrylate groups are very sensitive to UV radiation.

Water-stability of the crosslinked PVA-Thio fibers

The PVA-Thio fibers were prepared by electrospinning 10 wt % PVA-Thio solution in water. The fibers were then crosslinked by exposure to UV irradiation (using a OSRAM mercury lamp with emission wavelength more than 300 nm) for 3 min, 5 min, 10 min, respectively.

The water-stability of the crosslinked PVA-Thio fibers was characterized by the change in the morphology of the fibers after exposure to steam (95ºC) for 1 hr. The morphology of the PVA-Thio fibers was observed by SEM (Fig. 3. 32). With short time UV radiation (3 min, Fig. 3. 32 b), the PVA-Thio fibers swelled, indicating a crosslinking of the PVA-Thio to a less extend. However, when the radiation time was increased to 10 min, almost no swelling of the fibers was observed (Fig. 3. 32 c), indicating a complete crosslinking of the PVA-Thio fibers.

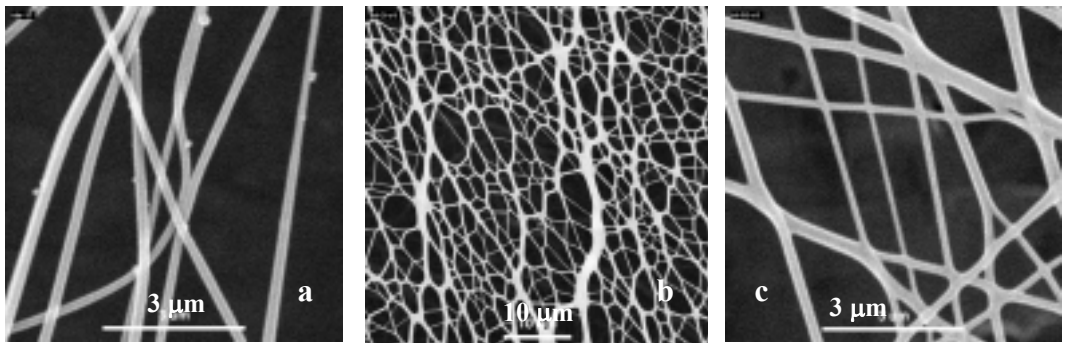

Fig. 3. 32 SEM images of PVA-Thio fibers: a: crosslinked PVA-Thio fibers before steam treatment; b: UV-radiated for 3 min, in steam for 1 hr; c: UV-radiation for 10 min, in steam for 1 hr

3.2.3.3 Crosslinking of PVA in the presence of a crosslinking agent

In addition to the UV-induced crosslinking of the PVA derivative containing photo-sensitive substituents, crosslinking of PVA fibers can also be realized by incorporating a crosslinkable and polymerizable monomer and a proper initiator into PVA fibers. Due to the formation of an interpenetrating network after polymerization and crosslinking of the monomer, water-stable PVA fibers can be produced.

In this work, tetraethylenglycol dimethacrylate (TEGDA) was used as crosslinking agent and ammonium persulfate (APS) as photoinitiator.

Structure of TEGDA

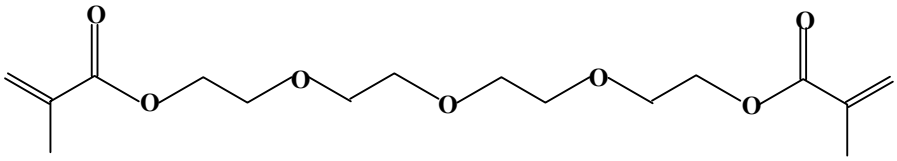

Preparation of PVA / TEGDA / APS fibers

To 7 wt % PVA solution (Mowiol 28-99) was added TEGDA and APS to prepare the PVA / TEGDA / APS mixture solution with the following compositions:

Sample 1: 7 wt % PVA, 2 wt % TEGDA, 1 wt % APS
Sample 2: 7 wt % PVA, 3.5 wt % TEGDA, 1 wt % APS
Sample 3: 7 wt % PVA, 2 wt % TEGDA, 0.5 wt % APS

The PVA / TEGDA / APS composite fibers were obtained by electrospinning the above solutions and the morphology of the fibers were characterized by SEM (Fig. 3. 33).

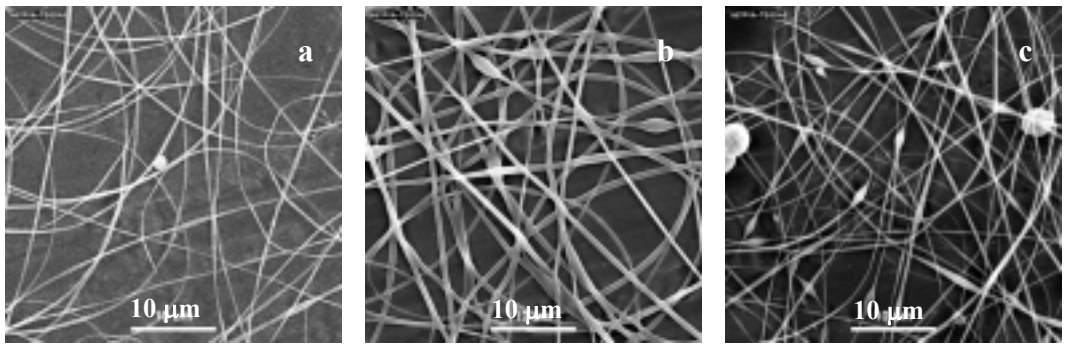

Fig. 3. 33 SEM images of PVA / TEGDA / APS fibers electrospun from a: sample 1, b: sample 2; and c: sample 3

The morphology and size of the fibers were affected by the concentration of the TEGDA and APS. When the concentration of the APS remained constant, with increase in TEGDA concentration, fiber diameter increased accompanied with formation of beads. With 2 wt% TEGDA (related to the solution), smooth fibers with diameter ranging from 150 – 350 nm were obtained (Fig. 3. 33 a). Also, the concentration of the APS has some effect on fiber shape. Decrease in concentration of ASP resulted in more beaded fibers (Fig. 3. 33 c). The optimal composition was sample 2.

UV-induced crosslinking of PVA / TEGDA / APS fibers

UV-induced crosslinking of the PVA / TEGDA / APS fibers was performed by exposure the fibers to a mercury lamp (Hg/10, OSRAM, the emission wavelength more than 300 nm) at RT in N_2 atmosphere for different time.

Water-stability of the crosslinked PVA / TEGDA / APS fibers

The water-stability of UV irradiated PVA / TEGDA / APS fibers was characterized by the change in the morphology of the fibers after exposure to the steam (95ºC) for 30min. The crosslinked PVA / TEGDA / APS fibers were exposed to steam for 30 min. It is found that, with the UV irradiation for 50 second, the fibers exhibited to a lower extent crosslinking. Much water-absorption and some damage of the fibers were observed when exposure to the steam; while with the UV irradiation for 5 min, the fibers had very good water-stability. After exposure to the steam, less fiber damage and low water-swelling of the fibers was observed (Fig. 3. 34).

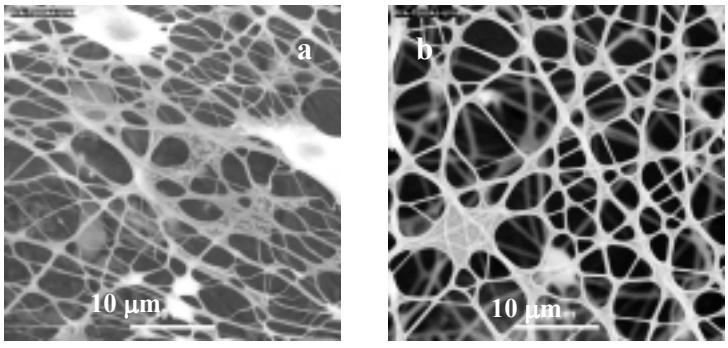

Fig. 3. 34 Water-stability of the PVA / TEGDA / APS fibers from sample 2 solution. a: UV irradiation for 50 seconds; b: UV irradiation for 5 min. After UV irradiation, fibers were exposed to steam for 30 min.

Comparing the UV-induced crosslinking of the PVA-Thio fibers and the UV-induced crosslinking of the PVA / TEGDA / APS fibers, the latter is more readily realized, because the former needs synthesis of a PVA derivative, the latter needs only a mixture of PVA / TEGDA / APS. In addition, heat-induced crosslinking of the PVA / TEGDA / APS fibers is also possible. However, due to the introduction of other compounds, the properties, such as mechanical strength, of the PVA / TEGDA / APS fibers may change.

3.2.4 Fluorescent polymer nanofibers

3.2.4.1 Fluorescent PVA nanofibers

Similarly with the synthesis of photo-sensitive PVA derivatives, fluorescent PVA can be prepared by introducing fluorescent moieties onto the PVA side-chain. Electrospinning of the fluorescent PVA derivative gives fluorescent polymer nanofibers.

Synthesis of partially esterified PVA derivative containing anthracene groups

Partially esterified PVA derivative containing anthracene groups (PVA-Anth) was synthesized by means of an analogous reaction between PVA (Mowiol 28-99, hydrolysis degree 99 %) and anthracenoyl chloride. The synthesis of anthracenoyl chloride and the analogous reaction are shown respectively in Fig. 3. 35 and Fig 3. 36.

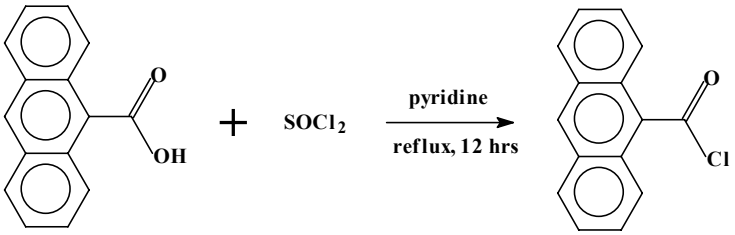

Fig. 3. 35 Synthesis of anthracenoyl chloride

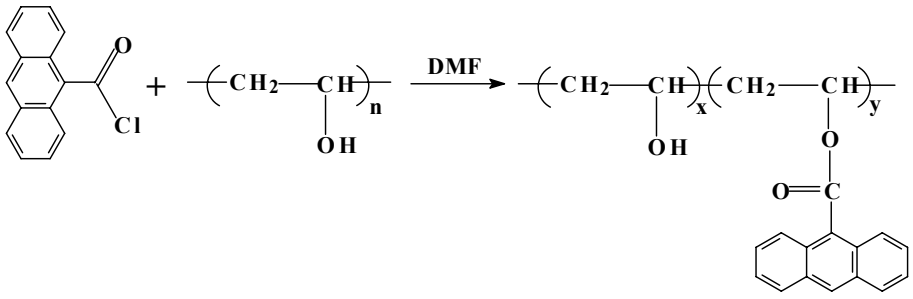

Fig. 3. 36 Synthesis of partially esterified PVA derivative containing anthracene groups

By controlling the amount of anthracenoyl chloride, PVA-Anth with 1.5 mol % esterification degree was obtained.

IR spectrum

IR spectrum of the PVA-Anth film exhibits a new weak absorbance band at 1711 cm^{-1}, which is attributed to the ester bonds in the side-chain the PVA-Anth (Fig. 3. 37). Due to the low substitution degree, the other absorbance bands from anthracene group could not be detected within the resolution of the IR spectrophotometer.

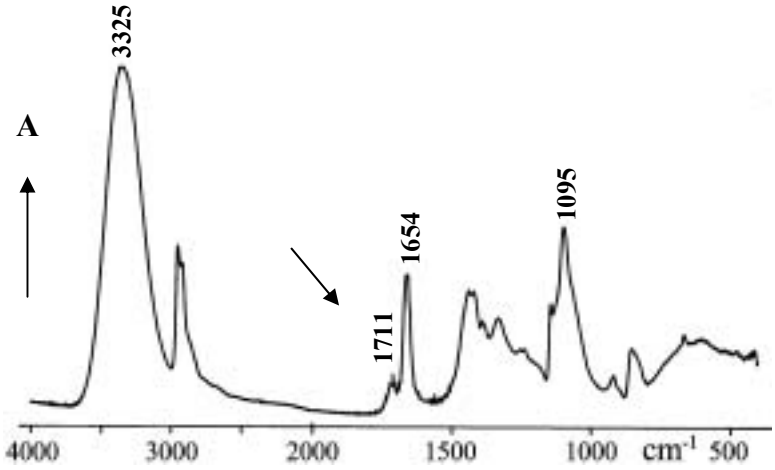

Fig. 3. 37 IR spectrum of PVA-Anth

UV/Vis spectrum

UV/Vis spectrum of the PVA-Anth film exhibits a triplete absorbance band between 280 – 350 nm, indicating the presence of anthracene groups in the film (Fig. 3. 38).

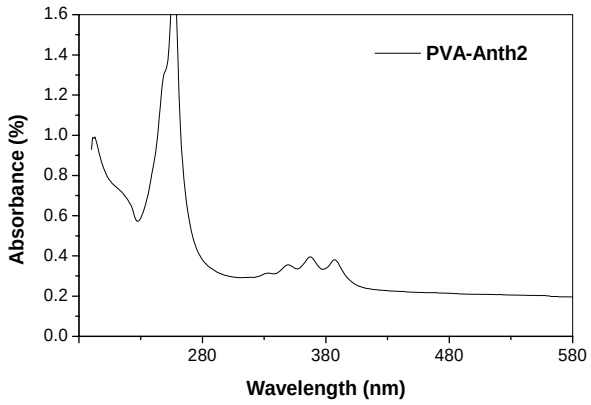

Fig. 3. 38 UV/Vis spectrum of PVA-Anth

Fluorescence spectrum

Fluorescence spectrum of PVA-Anth film was recorded with 300 nm light as excitation light. A wide fluorescence emission with a maximal emission wavelength of 448 nm was observed (Fig. 3. 39 a). The fluorescent optical microscopic image of the PVA-Anth film further confirmed the fluorescence property of the PVA-Anth film (Fig. 3. 39 b).

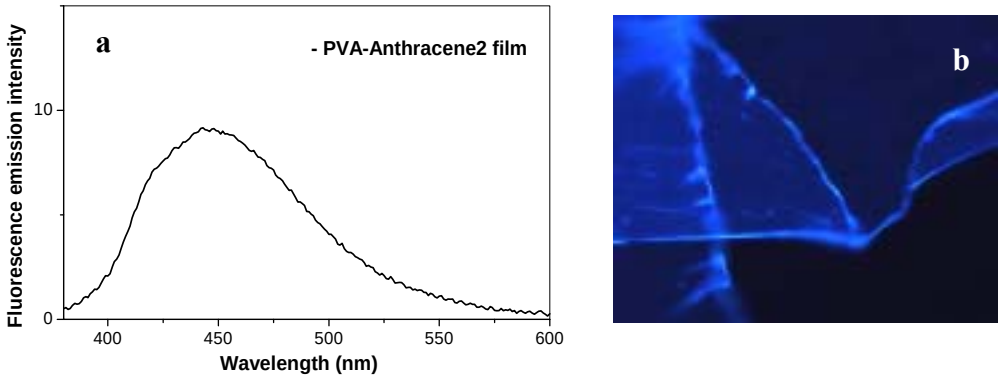

Fig. 3. 39 a: fluorescence spectrum of; b: fluorescent optical microscopic image of PVA–Anth film

Preparation of PVA-Anth nanofibers

PVA-Anth with 2.5% esterification degree is water-soluble. By electrospinning 10 wt% PVA-Anth solution in water, fluorescent PVA-Anth fibers with diameter in the range of 20 - 100 nm were obtained. The morphology of PVA-Anth fibers was characterized by using fluorescent optical microscope (Fig. 3. 40 a) and TEM (Fig. 3. 40 b).

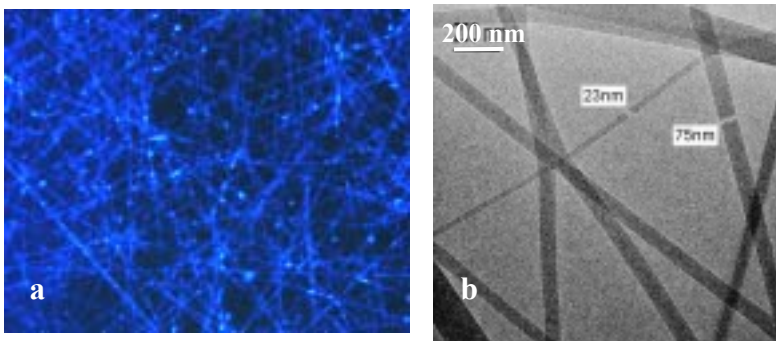

Fig. 3. 40 Morphology of the fluorescent PVA-Anth fibers. a: fluorescent optical microscopic image (400 X magnification), b: TEM image

3.2.4.2 Fluorescent PAA nanofibers

At first, a tert-amine compound containing fluorescent groups was synthesized. By mixing polyacrylic acid (PAA) and the tert-amine compound, a neutralization reaction between the acid and the base took place, resulting in a stable PAA-tert-amine salt. By electrospinning of this fluorescent PAA salt fluorescent PAA nanofibers could be obtained.

Synthesis of the tert-amine compound containing anthracene groups

N, N'-dimethylhydrazin was used as start material. By means of the reaction between N, N'-dimethylhydrazin and anthracenoyl chloride at -20ºC, a tert-amine compound containing anthracene group was obtained (Fig. 3. 41).

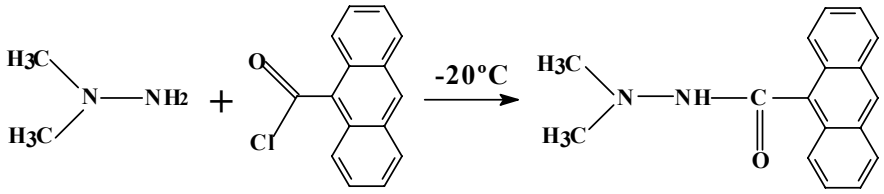

Fig. 3. 41 Synthesis of fluorescent tert-amine compound

Synthesis of PAA-tert-amine salt

To the PAA solution in water was added the anthracene-substituted amine compound. Under a slight heat (60°C) and stirring, the acidic PAA reacted with the weak basic amine compound, resulting in PAA-tert-amine salt (Fig. 3.42). By controlling the amount of the fluorescent amine compound, PAA-tert-amine with 2 % neutralization degree were obtained, which was proved to be water-soluble.

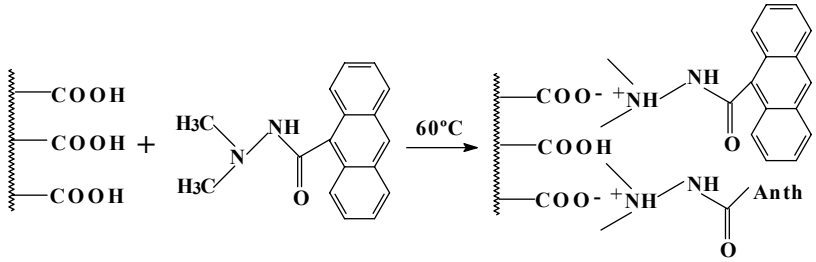

Fig. 3. 42 Synthesis of the fluorescent PAA-tert-amine

Preparation of PAA-tert-amine nanofibers

2 g PAA-tert-amine was dissolved in 18 g water / DMF (1:1) to prepared 10 wt % PAA-tert-amine solution. By electrospinning the solution under 55.5 kV of electrical field, ultra-fine PAA-tert-amine fibers were produced. The morphology of the fibers was characterized by SEM (Fig. 3. 43). The fibers have diameter ranging from 80 to 200 nm.

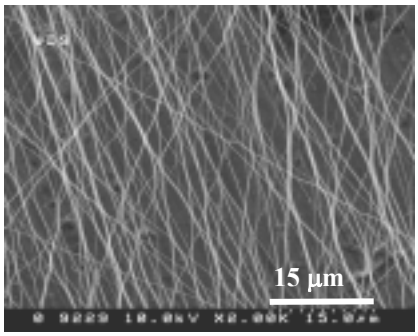

Fig. 3. 43 SEM image of the PAA-tert-amine fibers

UV/Vis spectrum of the PAA-tert-amine fibers

The UV/Vis spectrum of PAA-tert-amine fibers displays a strong absorbance band between 270 - 320 nm, which is attributed to anthracene groups in the fibers (Fig. 3. 44).

It was reported that anthracene substitutions in a polymer chain could be employed as a crosslinking sites to produce photo-crosslinked polymers. In this work, the PAA-tert-amine fibers were irradiated by a UV lamp (emission wavelength >300 nm) for different period, and the irradiated fibers were then exposed to steam (95ºC) to test their water-stability.

It was found that the UV absorbance intensity of the PAA-tert-amine decreased with irradiation time, as shown in Fig. 3. 44. However, after the irradiation, the fibers proved to be still water-soluble, indicating no enough crosslinking occurred, which might be caused by the structure of the substituted PAA or too low esterification degree of anthracene groups.

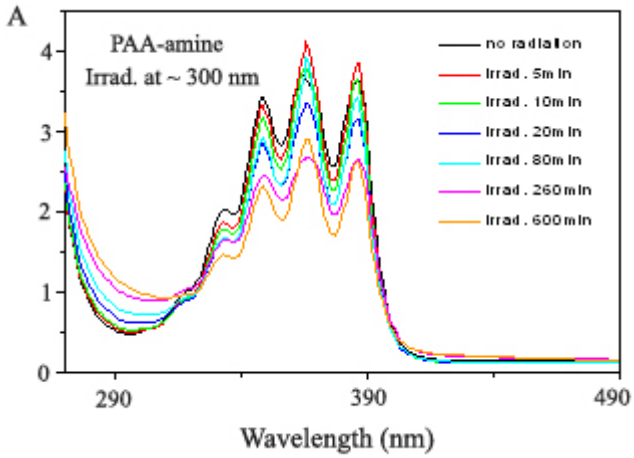

Fig. 3. 44 Change in UV/Vis spectrum of the fluorescent PAA-tert-amine film with irradiation time (emission wavelength of the UV lamp > 300 nm)

Fluorescence spectrum

A wide fluorescence emission peak with the maximal fluorescence emission at 460 nm was observed in the fluorescence spectrum of the PAA-tert-amine fibers (Fig. 3.45 a). In addition, under a fluorescent optical microscopy, very strong fluorescence of the fibers was observed (Fig. 3. 45 b).

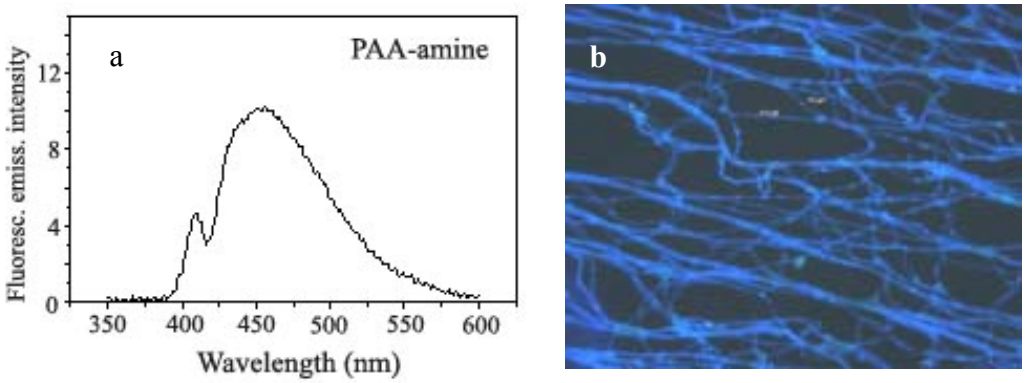

Fig. 3. 45 a: fluorescence spectrum and b: fluorescent optical microscopic image of PAA-tert-amine fibers (400x magnification)

3.2.5 Polymer / metal compound hybrid fibers

3.2.5.1 PLA / $Pd(OAc)_2$ hybrid fibers

The PLA / $Pd(OAc)_2$ hybrid fibers were prepared by electrospinning 3 wt % PLA solution in dichloromethane containing 3 wt % $Pd(OAc)_2$ (related to solution). Structured fibers with porous surface were obtained (Fig. 3. 46 a-b). The similar phenomena was observed during the electrospinning of PLA solution in dichloromethane (Fig. 3. 46 c). According to the study by Wendorff et al., the porous structure of PLA fibers resulted from the phase separation caused by the fast vaporization of the solvent during the electrospinning process.

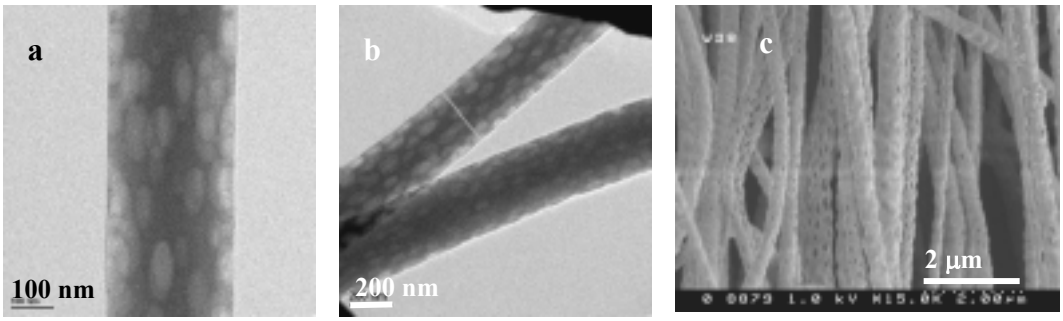

Fig. 3. 46 a-b: TEM images of PLA / $Pd(OAc)_2$ hybrid fibers, c: SEM images of porous PLA fibers

Energy – dispersive X-ray microanalysis (EDX)

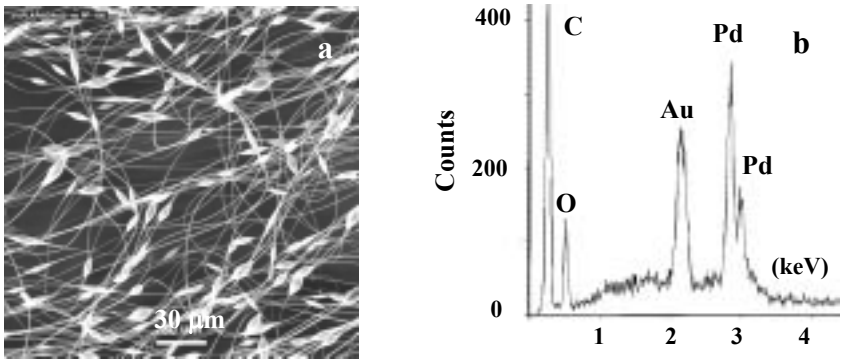

Fig. 3. 47 a: SEM image of PLA / $Pd(OAc)_2$ hybrid fibers, b: EDX of PLA / $Pd(OAc)_2$ hybrid fibers.

The PLA / $Pd(OAc)_2$ hybrid fibers electropsun from 3 wt % PLA solution in dichloromethane containing 3 wt % $Pd(OAc)_2$ (related to solution) had diameter between

200 - 400 nm with some beads in the fibers (Fig. 3. 47 a). The EDX analysis on a spot of the fiber identified the presence of palladium on the fibers (Fig. 3. 47 b).

Application of the PLA / $Pd(OAc)_2$ hybrid fibers

One of the important applications of the PLA / $Pd(OAc)_2$ hybrid fibers is to be the template for preparing the PPX / Pd hybrid tubes or PPX / Pd nanowire containing Pd nanoparticles with the size ranging from less than 1 nm to a few nanometer. The PLA / $Pd(OAc)_2$ hybrid fibers was coated with PPX by CVD technique. The resulting PPX-coated PLA / $Pd(OAc)_2$ fibers were then subjected to thermal degradation. During this process, the PLA decomposed and the $Pd(OAc)_2$ was reduced to Pd, resulting in the formation of the PPX / Pd hybrid tubes (Fig. 3.48 b) or PPX / Pd nanowire (Fig. 3.48 c). As the PPX layer constricts the move and aggregation of the Pd particle, the Pd nanoparticles were dispersed very well in the PPX matrix. The fabrication process will be discussed in **Chapter 5 – Functionalization of PPX tubes** in detail.

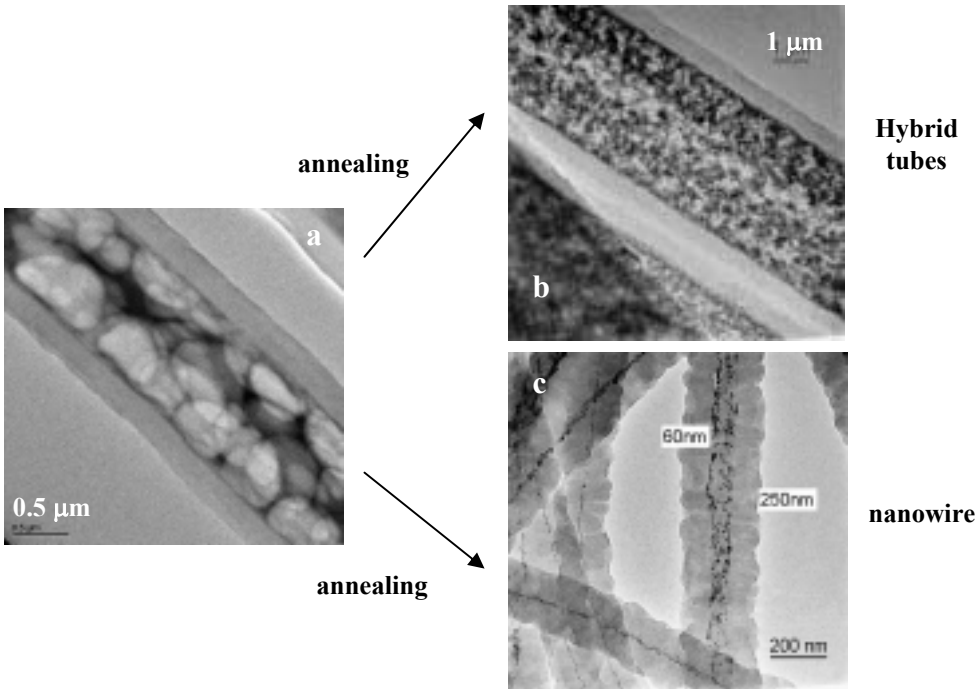

Fig. 3. 48 TEM images of a: PPX-coated PLA / $Pd(OAc)_2$ hybrid fibers; b: PPX / Pd hybrid fibers; and c: PPX / Pd nanowire

3.2.5.2 PLA / $Cu(OAc)_2$ hybrid fibers

Similarly, by electrospinning 3wt% PLA / $Cu(OAc)_2$ mixture solution in dichloromethane (the weight ratio of solid PLA to $Cu(OAc)_2$ was 1:1), the PLA / $Cu(OAc)_2$ hybrid fibers were obtained. The morphology of the fibers was characterized by TEM and SEM (Fig. 3.49), respectively. The EDX analysis on a spot of the fiber proved the presence of copper in the fibers (Fig. 3.49).

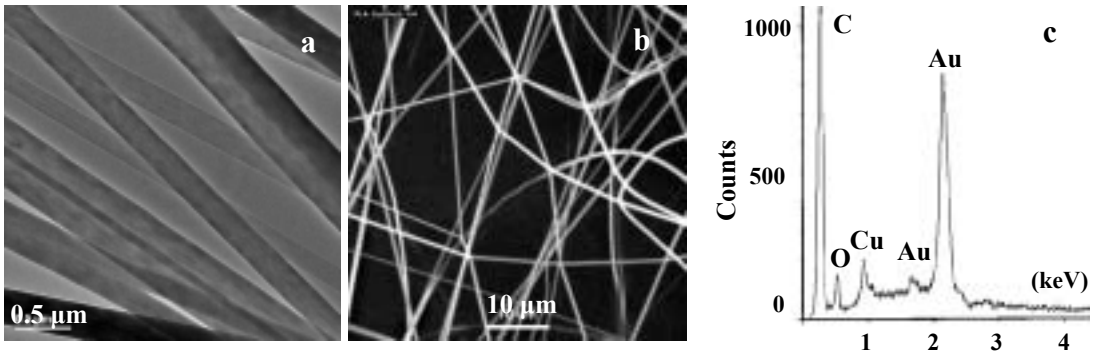

Fig. 3. 49 a: TEM image; b: SEM image; and c: EDX pattern of PLA / $Cu(OAc)_2$ hybrid fibers

3.2.5.3 PLA / Ag(OAc) hybrid fibers

The PLA / Ag(OAc) hybrid fibers were produced by electrospinning 3 wt % PLA / Ag(OAc) mixture solution in dichloromethane with 1:1 weight ratio of PLA to Ag(OAc). The morphology of the fibers is shown in Fig. 3. 50. The EDX analysis on one spot of a fiber proved the presence of silver in the fibers (Fig. 3. 50).

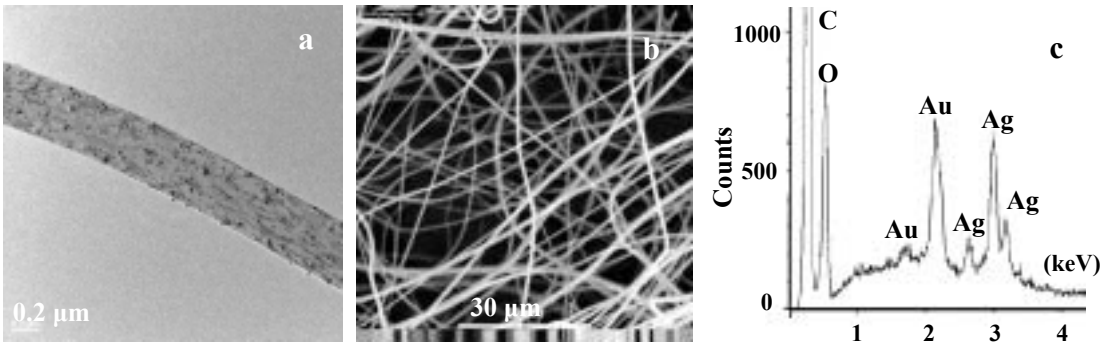

Fig. 3. 50 a: TEM image of the PLA / Ag(OAc) hybrid fibers; b: SEM images of of the PLA / Ag(OAc) hybrid fibers c: EDX pattern of PLA / Ag(OAc) hybrid fibers

Application of PLA / $Cu(OAc)_2$ hybrid fibers and PLA / Ag(OAc) hybrid fibers

Similar with the PLA / $Pd(OAc)_2$ hybrid fibers, the PLA / $Cu(OAc)_2$ hybrid fibers and PLA / Ag(OAc) hybrid fibers are also used as the template for preparing PPX / Cu hybrid tubes and PPX / Ag hybrid tubes. These tubes contain fine-dispersed Cu / Cu_2O nanoparticles (Fig. 3.51 a) and Ag nanoparticles (Fig. 3.51 b), respectively, which have great application potential in the fields of catalysis. The preparation and characterization of PPX / Cu hybrid tubes and PPX / Ag hybrid tubes will be discussed in detail in **Chapter 5 – Functionalization of PPX tubes.**

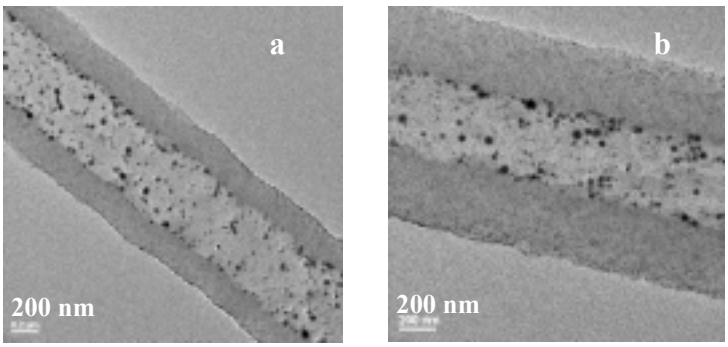

Fig. 3. 51 TEM image of a: PPX / Cu hybrid tubes; b: PPX / Ag hybrid tubes

4 PPX tubes and formation mechanism

4.1 Preparation of PPX tubes

Meso- and nano-scaled PPX or halogen-substituted PPX tubes have been successfully fabricated following the three steps of the TUFT process, i.e., 1. Preparation of the template fibers by electrospinning; 2. Coating of the template fibers with PPX or substituted PPX by CVD; 3. Removal of the template fibers by means of thermal degradation or solvent extraction.

4.1.1 Template fibers

Among various electrospun polymer fibers, PLA, PEO, nylon 4,6 or nylon 6 fiber were the most commonly used templates due to their good fiber-processability and ready removal of the fibers by means of solvent extraction or thermal degradation. The template fibers can be non-woven mats, resulting in the PPX tubes in the form of a nonwoven mats; if the template fibers were well oriented by means of a special technique, which was patented by Greiner et al., well oriented PPX tubes can be produced.

4.1.2 PPX coating by CVD

The PPX coating by CVD was carried out in the apparatus shown in Fig. 4.1. The coating conditions are as following:

Starting material: [2, 2] paracyclophane
Vacuum: <0.1 mbar
Vaporizing chamber: 140 - 150ºC
Pyrolysis furnace: 650 - 750ºC
Deposition chamber: ambient temperature

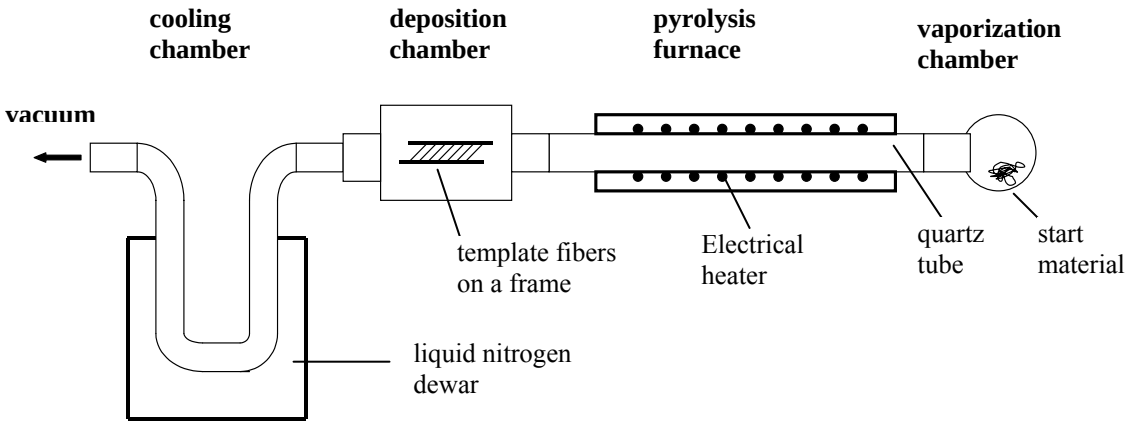

Fig. 4. 1 Apparatus for PPX coating by CVD

To produce substituted PPX coatings with the substituents in the aromatic rings, such as Parylene C and Parylene N, the procedure is the same as that for PPX coating, only that the pyrolysis temperature was 40 - 50ºC higher than that of non-substituted PPX coating.

The structures of the PPX, Parylene C, and Parylene N produced by CVD are shown in Fig. 4. 2.

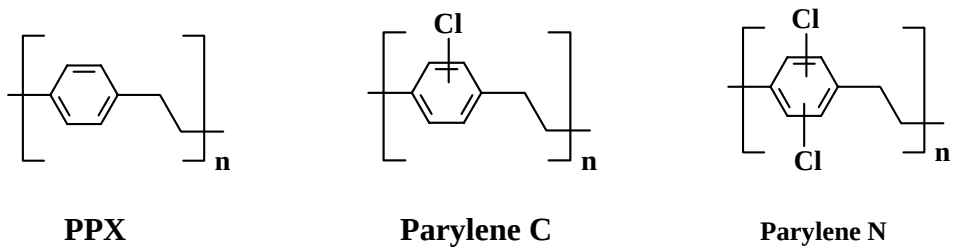

Fig. 4. 2 Structures of PPX , Parylene C, and Parylene N produced by CVD

To produce the coatings of halogen-substituted PPX with substituents in the ethylene segments, such as PPX-Cl or PPX-Br, α, α'-dichloro-xylene or α, α'-dibromo-xylene was used as starting material. The pyrolysis was performed according to the same procedures under the following conditions:

Pyrolysis temperature: 650 - 700ºC

Deposition temperature: 40 - 50ºC for PPX-Cl, 50 - 70ºC for PPX-Br

The structures of the produced PPX-X coatings are schematically shown as following:

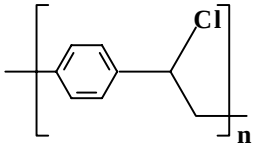

PPX-Cl

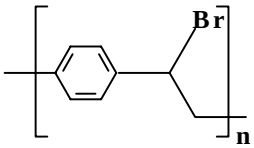

PPX-Br

4.1.3 Removal of template fibers

To remove the template fibers, either solvent extraction or thermal degradation can be employed, depending on the nature of the template fibers. For PLA or PEO fibers as template, both ways are suitable. In case of solvent extraction, chloroform or dichloromethane were usually used; while in case of the thermal degradation, annealing temperature was 365ºC for PLA and 370ºC for PEO, respectively. If nylon fibers are used as template, only solvent extraction is suitable due to the incomplete degradation of nylon under the temperature lower than 400ºC. Formic acid was used as extraction solvent.

4.2 Characterization of PPX tubes

4.2.1 Morphology

The morphology of the PPX and substituted PPX tubes were characterized by TEM and SEM. The PPX tubes produced by the TUFT process have inner diameter ranging from several nanometers to a few micron, depending on the size of the template fibers. The ultra-fine PPX tubes with inner diameter between 5 - 70 nm (Fig. 4.3 a) were produced with the corresponding ultra-fine PLA fibers as template, which were electrospun from a very dilute PLA solution (< 1 wt %) in dichloromethane containing an additive, as described in **Chapter 3 – Electrospun fibers**. Thicker PLA template fibers led to the PPX tubes with larger inner diameters (Fig. 4.3 b-c).

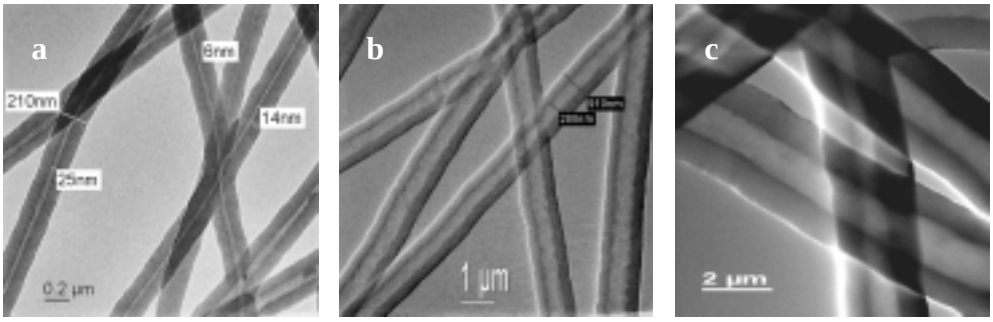

Fig. 4. 3 TEM images of PPX tubes. The inner diameter of the tubes is a: 5-70nm; b: 200-400 nm; and c: 800-1500 nm

Similarly, with ultra-fine nylon 4,6 fibers as template, ultra-fine PPX tubes with diameter ranging from 20-80 nm were also produced (Fig. 4. 4 a-b).

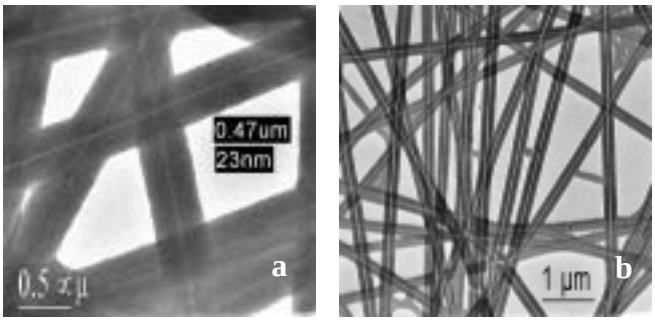

Fig. 4. 4 TEM images of PPX tubes with nylon 4,6 fibers as template. The inner diameter of the tubes is a: 20-50 nm; b: 40-80 nm

With porous PLA fibers as template, the PPX tubes with structured inner surface were produced (Fig. 4. 5). Due to the extra increased specific surface, the structured PPX tubes will be significant in the applications where large specific surface is needed.

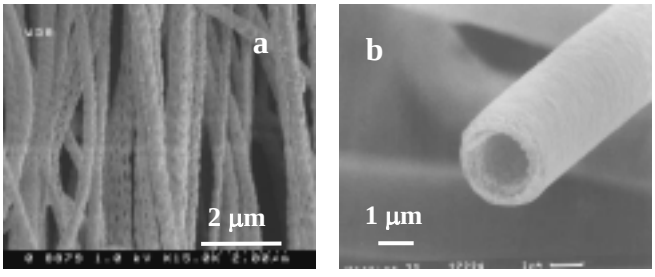

Fig. 4. 5 SEM images of a: porous PLA fibers; b: structured PPX tubes with porous PLA fibers as template

Fig. 4. 6 shows the SEM images of the PPX tubes and halogen-substituted PPX (PPX-X) tubes. Well-oriented chloro-substituted PPX tubes (Fig. 4. 6 b) were obtained with the well oriented fibers as template.

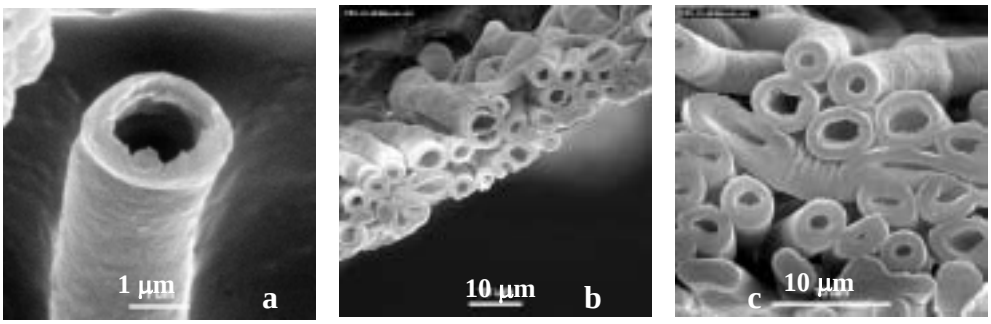

Fig. 4. 6 SEM images of a: PPX tubes; b: oriented PPX-Cl tubes; c: PPX-Br tubes;

The thickness of PPX coating depends on the amount of the starting materials. With [2, 2] paracyclophane as starting material, the thickness of the PPX coating could be almost quantitatively controlled. Generally, with 500 mg [2, 2] paracyclophane, the PPX coatings with the thickness ranging from 200 to 250 nm were produced; while with 100 mg [2, 2] paracyclophane, the resulting PPX thickness was between 40 - 80 nm. However, with α, α'-dihalogen-xylene as starting material, the thickness of the PPX-X coating is difficult to control due to the non-quantitative polymerization and the formation of byproducts.

4.2.2 IR spectrum

The IR spectrum of the PPX tubes exhibits some characteristic absorbance bands, which are summarized in Table 4. 1.

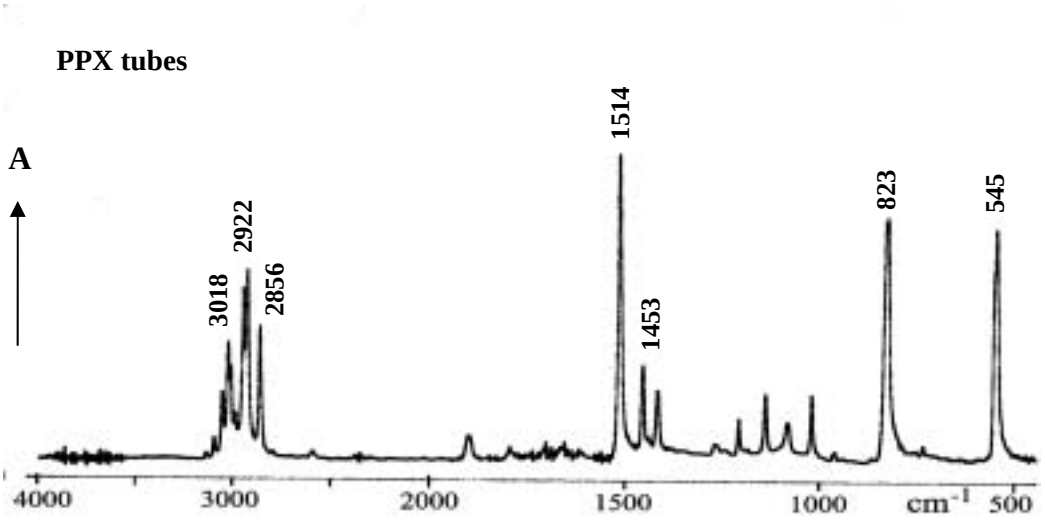

Fig. 4. 7 IR spectrum of PPX tubes

Table 4. 1 IR absorbance bands of PPX tubes

Position of absorbance bands (cm^{-1})	Attribution	Position of absorbance bands (cm^{-1})	Attribution
3018	Ar-H stretching	1514, 1453	Ar-C=C stretching
2922	$-CH_2-$ stretching	823, 545	1,4-substituted Ar-H bending
2856	$-CH_2-$ stretching		

The spectrum of the PPX-Cl tubes exhibits, in addition to the characteristic absorbance of PPX, also some absorbance bands between 600 - 750 cm^{-1}, which are attributed to C-Cl bonds (Fig. 4. 8). Due to the presence of Cl substituents, the absorbance bands between 900 - 1400 cm^{-1} are enhanced, which are attributed to C-H bonds. The IR absorbance bands and their attributions are summarized in Table 4. 2.

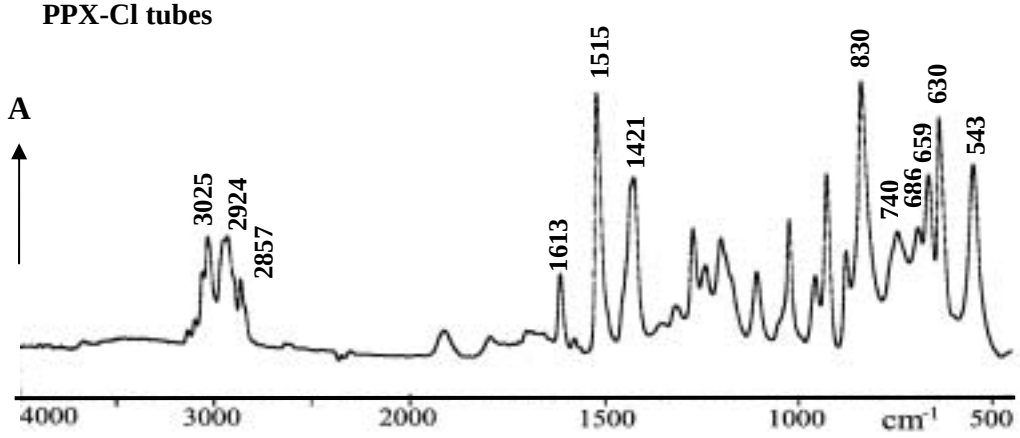

Fig. 4. 8 IR spectrum of PPX-Cl tubes

Table 4. 2 IR absorbance bands of PPX-Cl tubes

Position of absorbance bands (cm^{-1})	Attribution	Position of absorbance bands (cm^{-1})	Attribution
3025	Ar-H stretching	1421	$-CH_2-$ bending
2924	$-CH_2-$ stretching	830, 543	Ar-H bending
2857	$-CH_2-$ stretching	740, 686, 659, 630	C-Cl stretching
1613, 1515	Ar-C=C stretching		

The IR spectrum of PPX-Br tubes is very similar with that of PPX-Cl tubes. In addition to the characteristic absorbance bands of PPX at 3025 cm^{-1}, 2924 cm^{-1}, 2857 cm^{-1}, 1613 cm^{-1}, 1515 cm^{-1}, 829 cm^{-1}, and 537cm^{-1}, it also exhibits some absorbance at 757 cm^{-1}, 663 cm^{-1}, and 590 cm^{-1}, which are attributed to the C-Br bonds (Fig. 4. 9).

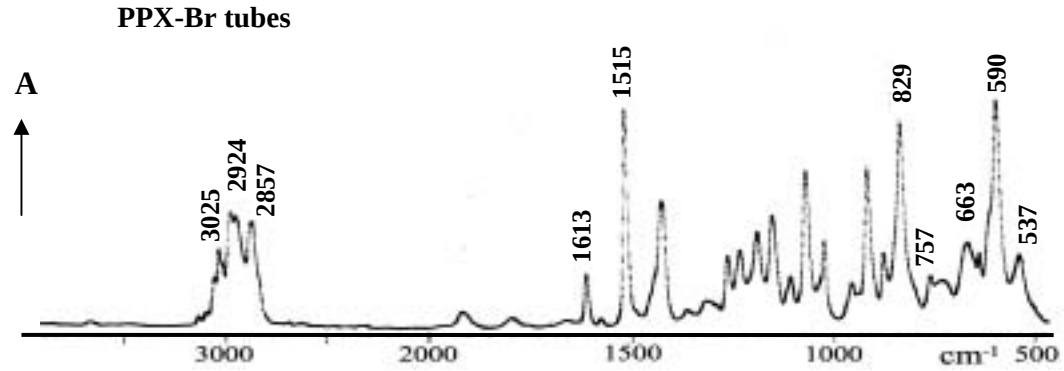

Fig. 4. 9 IR spectrum of PPX-Br tubes

4.2.3 Wide-angle X-ray diffraction

The WAXD diffractogram of the PPX tubes exhibits a sharp crystalline peak at 2θ = 19º (Fig. 4. 10), indicating that the PPX in the PPX tubes is partially crystalline.

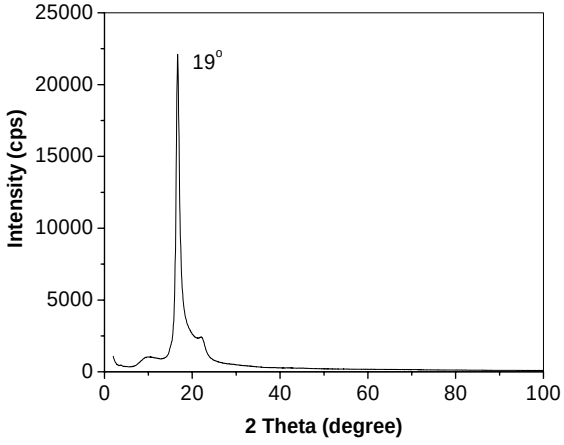

Fig. 4. 10 WAXD pattern of PPX tubes

4.3 Formation mechanism of PPX tubes

According to the TUFT process, the PPX tubes are developed by means of removal of the template fibers from PPX-coated template fibers. In this work, two methods were employed, one is thermal decomposition and the other is solvent extraction.

As previously described, PPX coating by CVD results in a conformal, partially crystalline, and pinhole-free film. In addition, template fibers by electrospinning have extremely large length-to-diameter ratio. For example, fibers with 200 nm in diameter and 2 cm in length, which were usually used as template fibers in this work, have length-to-diameter ratio as high as 100,000. How does so long a fiber move out from the PPX coating? This question motivated my investigation on the mechanism for the formation of the PPX tubes.

To study the mechanism of the formation of PPX hollow tubes, PPX-coated PLA fibers were selected as examples. Solvent extraction and thermal degradation were carried out on PPX-coated PLA fibers, respectively. IR spectra were recorded and TEM was observed to characterize the change of PLA template fibers with treatment time.

4.3.1 Removal of template fibers by solvent extraction

PPX-coated PLA fibers were immersed in chloroform for different periods. Two kinds of samples were prepared. One is uncut PPX-coated PLA fiber sample. The PLA fibers collected on a frame were coated with PPX and then directly immersed in chloroform together with the frame. In this sample, the PLA fibers were completely wrapped with the PPX coating and there were no open ends; another is the cut PPX-coated PLA fiber sample. After coated with PPX, the PPX-coated PLA fibers were cut off from the frame and further cut into small pieces so that there are many open ends along the four edges of each piece.

4.3.1.1 PPX-coated PLA fibers - uncut sample

The uncut PPX-coated PLA fiber sample was immersed in chloroform for 5 min, 15min and 80 min, respectively. The changes in the morphology of the tubes with time were observed by TEM (Fig. 4. 11).

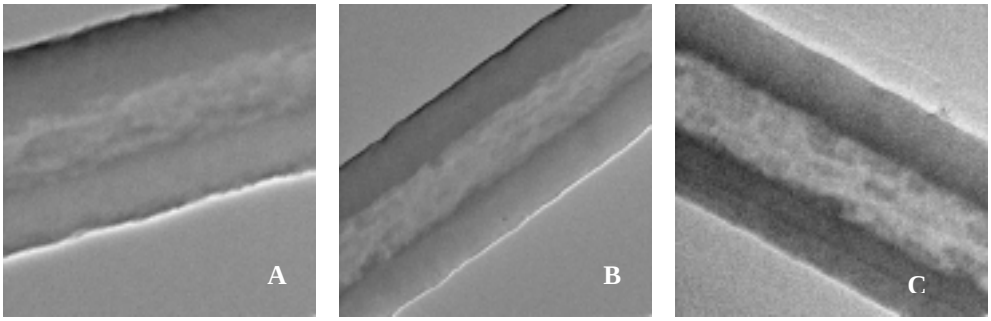

Fig. 4. 11 TEM images of uncut PPX-coated PLA fibers which were immersed in chloroform for A: 5 min; B: 15 min; C: 80 min.

In chloroform for 5 min, the "island-in-sea" morphology in the middle part was observed, indicating a partial dissolution of the PLA part in chloroform (Fig.4. 11 A). The dissolution took place uniformly along the whole length of the PPX-coated PLA fiber, showing that the solvent entered into the fibers by means of permeation through PPX layer. With increase in immersion time to 15 min, more "islands" was observed (Fig. 4. 11 B). When in chloroform for 80 min, the "island-in-sea" morphology became clearer and the "sea" part became more light-colored, indicating that most of the PLA was dissolved (Fig. 4. 11 C).

The gradual dissolution of the PLA with immersion time was further proved by the IR spectra of the fibers (Fig. 4.12). The peak at 1753 cm^{-1} is attributed to the ester bond of PLA. With increase in immersion time, this peak decreased significantly. It proved that the content of PLA in the PPX tubes decreased with increase in immersion time. As the sample is uncut PPX-coated PLA fibers, there are no open ends. In addition, the experiments were carried out at RT, no degradation of PLA took place. The only possibility for PLA to come out is to permeate out through PPX coating if there are no holes or cracks in the PPX coating. Whether there are holes or cracks in the PPX coating will be proved by the next experiment.

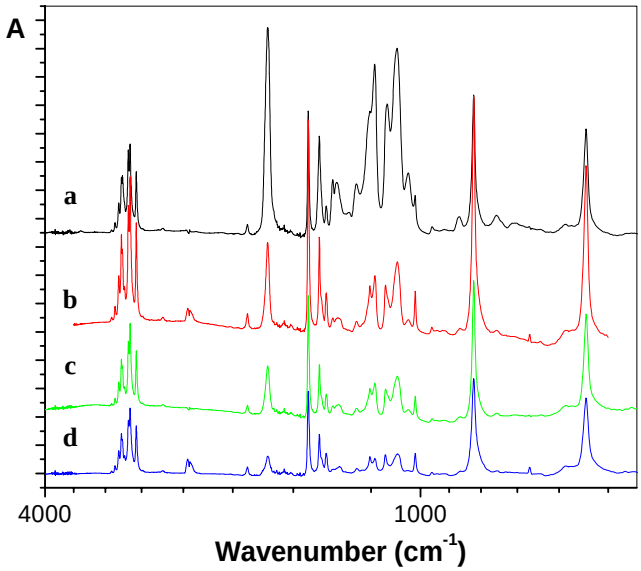

Fig. 4. 12 IR spectrum of the uncut PPX-coated PLA fiber samples immersed in $CHCl_3$ for a: 0 min; b: 5 min; c: 15 min; d: 80 min.

Above all, this experiment led to a primary conclusion, that there exist some small holes in the PPX coating, through which the solvent and even the PLA macromolecules can permeate. However, the holes are so small that they are undetectable by the ordinary SEM and TEM.

4.3.1.2 PPX-coated PLA fibers - cut sample

The cut PPX-coated PLA fiber sample was immersed in chloroform for 1 min, 15 min and 80 min, respectively. The change in the morphology of the PLA part inside the PPX coating were observed by TEM (Fig. 4.13). The similar "island-in-sea" morphology of the sample was observed after immersion in chloroform for even 1 min (Fig. 4.13 a). With increase in immersion time, the PLA part decreased (Fig. 4. 13 b-c). The gradual decrease of PLA with increase in immersion time was further proved by IR spectrum (Fig. 4. 14).

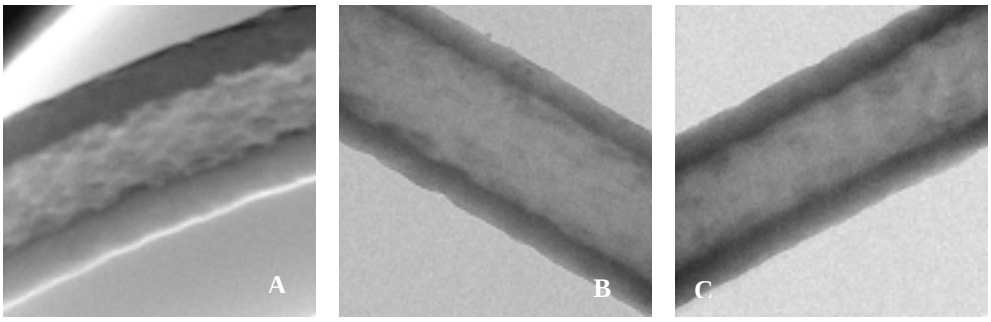

Fig. 4. 13 TEM images of the cut PPX / PLA fibers after in Chloroform for A: 1 min; B: 15 min; and C: 80 min.

It is worth noting that the IR spectrum of the cut sample demonstrates a faster removal of the PLA in the cut sample than that that in the uncut sample (Fig. 4. 14). In chloroform for 15 min, the IR spectrum of the cut sample exhibited almost no evident PLA absorbance peaks (Fig. 4. 14), whereas for the uncut sample, in chloroform even for 80 min, there were still relative strong PLA absorbance peaks (Fig. 4. 12). The faster removal of the PLA in the cut sample was caused by the presence of open ends in the sample. Through these open ends, the solvent could more quickly enter into the tubes in addition to the permeation through the PPX layer, moreover, the dissolved PLA could more quickly permeate out through these open ends. The significant effect of the presence of the open ends on the removal rate of the PLA indicates that there are no holes or cracks in the PPX coating.

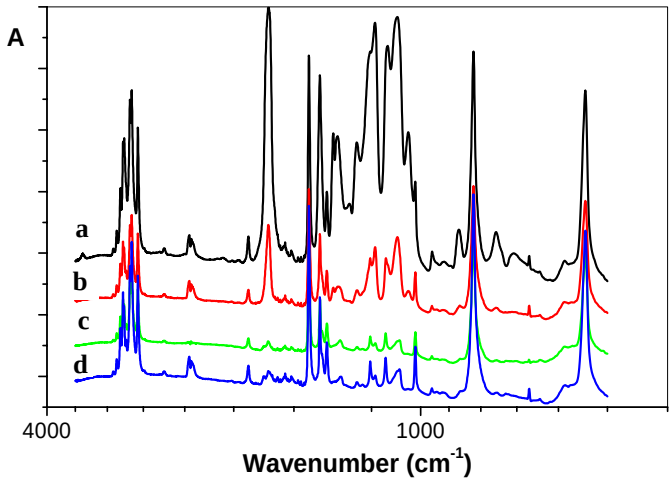

Fig. 4. 14 IR spectrum of the cut PPX / PLA fiber samples immersed in $CHCl_3$ for a: 0 min; b: 5 min; c: 15 min; d: 80 min.

It can be concluded that, during the solvent extraction process, the solvent (e.g. chloroform) can permeate through the PPX coating quickly to dissolve the PLA inside the PPX coating, and the dissolved PLA can permeate out through the PPX layer or simultaneously through the open ends if the sample is cut. A possible reason for the ready permeation of solvents and even the PLA macromolecular is that exist some very small holes. However, the presence of any big holes or cracks in the PPX coating has been excluded by the above experiments.

4.3.2 Removal of template fibers by thermal degradation

Thermal degradation is another way to remove template fibers. In this work, PPX-coated PLA fibers were subjected to annealing at 365ºC in vacuum for different periods. The change in PLA content with annealing time was characterized by the IR spectrum of the PPX-coated PLA fibers, as shown in Fig. 4. 15.

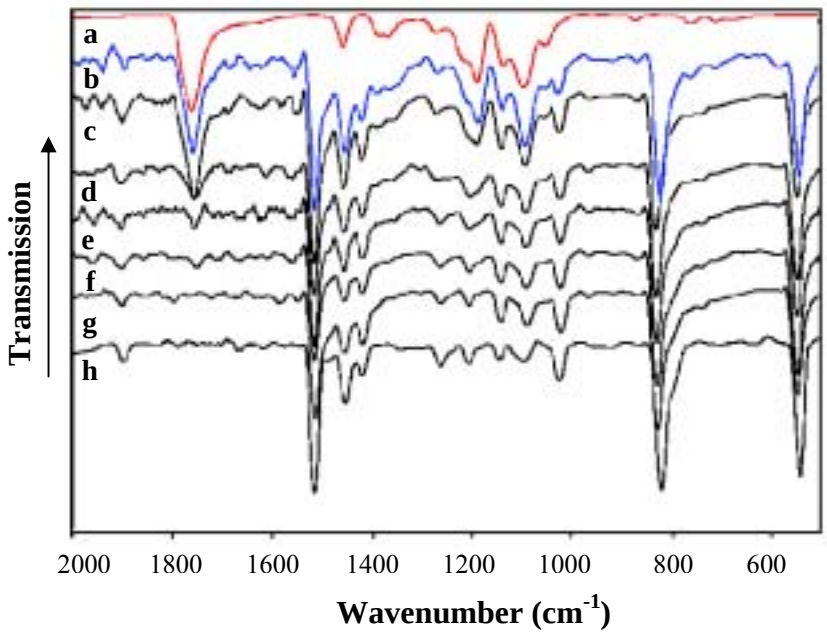

Fig. 4. 15 IR spectrum of a: pure PLA fibers; b: PPX-coated PLA fibers; c-h: PPX-coated PLA fibers after annealing at 365ºC for c: 0 min; d: 1 hr; e: 2 hrs; f: 3 hrs; g: 4 hrs; h: 5 hrs.

The IR spectra show the significant change of the PLA content with increase in annealing time. After 1 hour at 365ºC, the absorbance band of the PPX / PLA fibers at 1753 cm^{-1} decreased significantly (Fig. 4. 15 d), indicating a quick decomposition of the PLA part. With increase in annealing time, the absorbance at 1753 cm^{-1} decreased

further. After 4 hrs at 365ºC, no absorbance bands from the PLA were detected any more and the IR spectrum exhibited only the absorbance bands of the pure PPX (Fig. 4. 15 g - h), indicating that PLA was completely decomposed and only PPX left. The product was PPX tubes.

It can be concluded that during the thermal degradation process, the PLA gradually decomposed at 365ºC. 3-hour-long annealing is necessary for the complete decomposition of PLA.

5 Functionalization of PPX tubes

Due to the chemical inertness of PPX, the applications of the PPX tubes are limited. It is one of the main purposes of this work to functionalize the PPX tubes. So far, functional groups or materials have been introduced into the PPX tubes to produce functional PPX tubes, which will have extensive application potentials in the fields such as catalyst, separation, drug delivery, and sensors.

In this work, the functionalization of the PPX tubes was realized by means of the following approaches:

1. Preparation of PPX / polymer composite;
2. Preparation of PPX / metal composite tubes consisting of one layer of metal and one layer of PPX;
3. Preparation of PPX / metal hybrid tubes where the metal nanoparticles were dispersed in the PPX layer;
4. Preparation of PPX-encapsulated metal nanowires;
5. Surface modification of the PPX tubes by chemically attaching functional groups or grafting polymers on the PPX surface;
6. Hydrophilication of the PPX tubes;
7. Preparation of inorganic salts-incorporated PPX tubes;

5.1 Preparation of PPX / polymer composite tubes

PPX / polymer composite tubes were prepared by means of the modified TUFT process:

1. Preparation of electrospun fibers template
2. Coating of the second polymer solution on the template fibers by means of e.g. dip coating or sol-gel coating
3. Coating of the PPX on the resulted fibers by means of the CVD process
4. Removal of the template fibers by means of thermal degradation or solvent extraction

5.1.1 PPX / PAN composite tubes

Preparation

PLA fibers were used as template and coated with 1 wt % polyacrylonitrile (PAN) solution in DMF by means of the air-brush technique, followed by PPX coating by CVD. The resulting PPX / PAN / PLA were subjected to extraction with chloroform as solvent. As PAN is insoluble in chloroform, PPX and PAN was left after the extraction, resulting in the PPX / PAN composite tubes. The procedure is schematically shown in Fig. 5. 1.

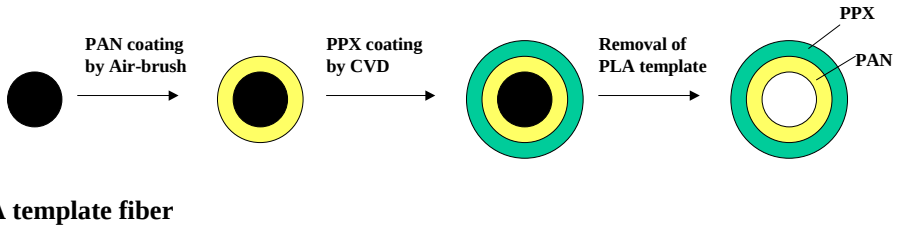

Fig. 5. 1 Procedure for preparing PPX / PAN composite tubes

Morphology of the PPX / PAN composite tubes

The morphology of the PPX / PAN tubes was characterized by SEM (Fig. 5. 2). Non-uniform surface of the tubes were observed, which was caused by the bad wetting of the PAN solution on the surface of the PLA fibers.

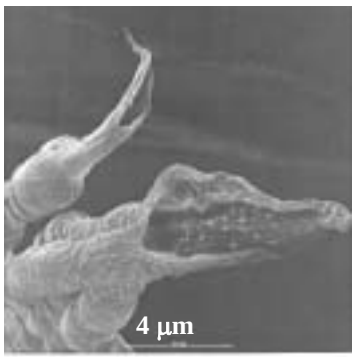

Fig. 5. 2 SEM image of PPX / PAN composite tubes

IR spectrum

Before removal of the PLA template fibers, the IR spectrum of the PPX / PAN / PLA fibers (Fig. 5. 3) demonstrates clearly the presence of the three components. The

absorbance band at 2244 cm^{-1} is attributed to PAN, and the absorbance bands at 1774 cm^{-1}, 1184 cm^{-1} and 1093 cm^{-1} are attributed to PLA, while the absorbance bands at 1513 cm^{-1}, 822 cm^{-1} and 543 cm^{-1} are three typical absorbance bands of PPX.

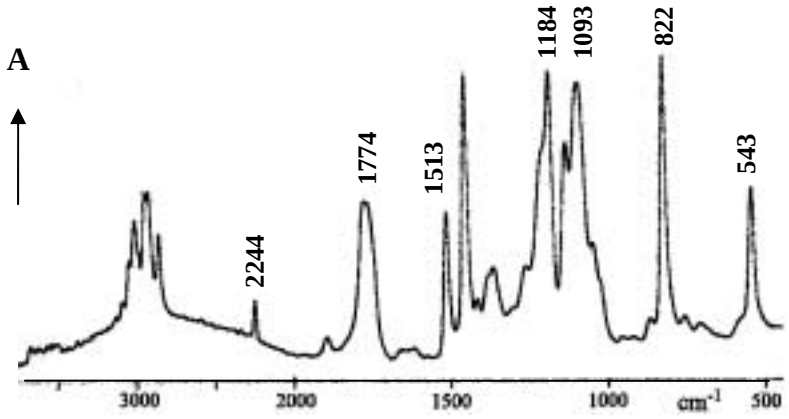

Fig. 5. 3 IR spectrum of PPX / PAN coated PLA fibers before removal of PLA

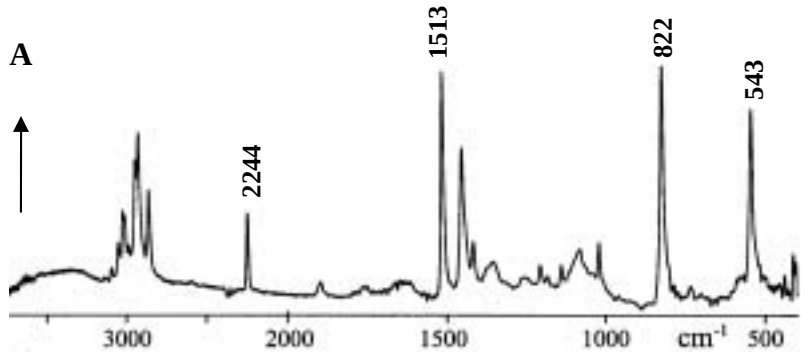

Fig. 5. 4 IR spectrum of PPX / PAN tubes after removal of PLA

After removal of the PLA template fibers by means of extraction with chloroform, the IR spectrum (Fig. 5. 4) shows no absorbance bands of PLA any more (the peaks at 1774 cm^{-1}, 1184 cm^{-1} and 1093 cm^{-1} disappeared), but the absorbance band at 2244 cm^{-1} and the three typical absorbance bands of PPX remained, indicating the presence of the two components: PAN and PPX. It is proved that the products were PPX / PAN composite tubes.

Element analysis

The element analysis proved that the PPX / PAN composite tubes contain 87.14 % C, 7.93 % H and 2.42 % N. According to the content of N, the content of PAN in the PPX / PAN composite tubes was calculated to be 9.92 %.

5.1.2 PPX / PVA / PAA composite tubes

Preparation

The second polymer used here is the PVA / PAA blend polymer with 75:25 weight ratio. 1 wt % PVA / PAA solution in water was used as coating solution for the air-brush coating. The purpose of using PVA / PAA blend polymer is to produce a stable second polymer coating. As described in **Chapter 3**, the PVA / PAA blend polymer with the weight ratio of 75:25 can be crosslinked by annealing at 120ºC for 30 min. The weight ratio of 75:25 enables the presence of plenty of hydroxyl groups after crosslinking.

The preparation procedure for the PPX / PVA / PAA composite tubes is similar as that for the PPX / PAN composite tubes. Only that the PPX / PVA / PAA coated PLA fibers were subjected to annealing at 120 ºC for 30 min before removal of the PLA template by solvent extraction.

Morphology of PPX / PVA / PAA composite fibers

The morphology of PPX / PVA / PAA composite tubes was characterized by SEM, as shown in Fig. 5. 5.

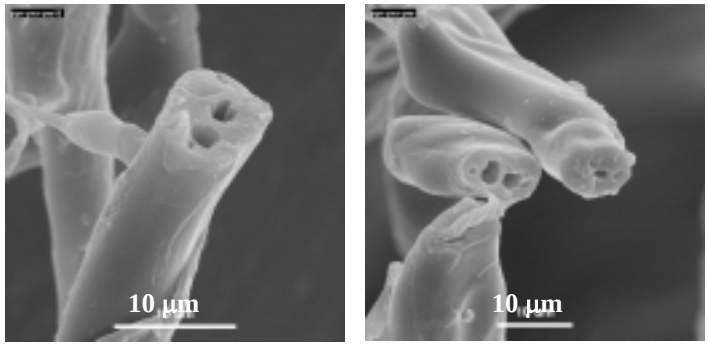

Fig. 5. 5 SEM images of PPX / PVA / PAA tubes

IR spectrum

The IR spectrum of the PPX / PVA / PAA composite tubes clearly the presence of PPX and PVA / PAA blend (Fig. 5. 6). It exhibits a wide absorbance band at about 3400 cm^{-1}, which is attributed to PVA, and an weak wide absorbance band at 1711 cm^{-1}, which is attributed to the rest PAA and the newly produced ester bonds by crosslinking of PVA and PAA. The absorbance bands at 1514 cm^{-1}, 823 cm^{-1} and 543 cm^{-1} are from PPX.

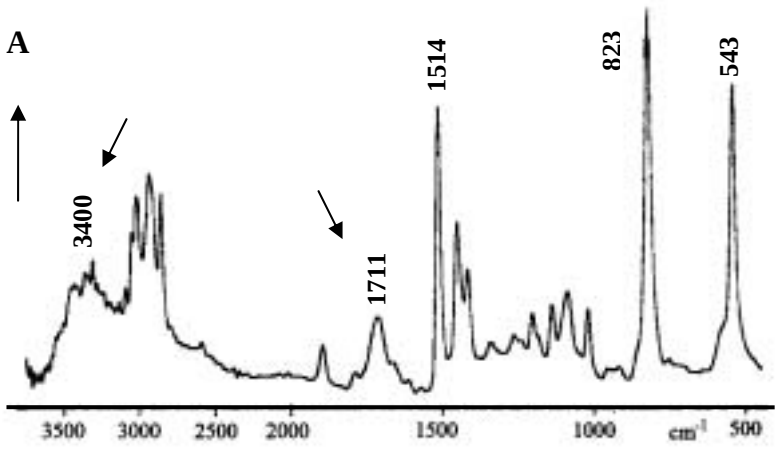

Fig. 5. 6 IR spectrum of PPX / PVA / PAA composite tubes

Chemical reactivity of PPX / PVA / PAA composite tubes

Due to the presence of active hydroxyl groups, it should be possible that some chemical reactions take place inside PPX / PVA / PAA composite tubes. To prove the reactivity of the PPX / PVA / PAA composite tubes, the following reactions were performed.

Reaction I – introduction of pyridine groups

The PPX / PVA / PAA composite tubes were immersed in 2g isonicotinoyl chloride solution in 20 ml dried THF. With addition of 40 ml pyridine, the mixture was heated at 60ºC for 4 hrs. The reaction is schematically shown in Fig. 5. 7.

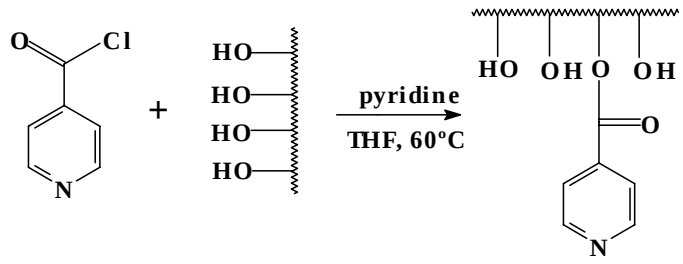

Fig. 5. 7 Reaction between the PPX / PVA / PAA tubes and isonicotinoyl chloride

IR spectrum

The IR spectrum of the PPX / PVA / PAA tubes after reacted with isonicotinoyl chloride is shown in Fig. 5. 8. Some changes in absorbance bands were observed. The absorbance band of hydroxyl groups at 3400 cm^{-1} decreased to indiscernible, and a multiple absorbance band at 1730 - 1722 cm^{-1} replaced the previous single peak at 1711 cm^{-1}, indicating the increase in the ester bonds. Moreover, some new absorbance bands between 543 cm^{-1} and 822 cm^{-1} were observed. It is proved that the reaction between the PPX / PVA / PAA composite tubes and the isonicotinoyl chloride took place inside the tubes.

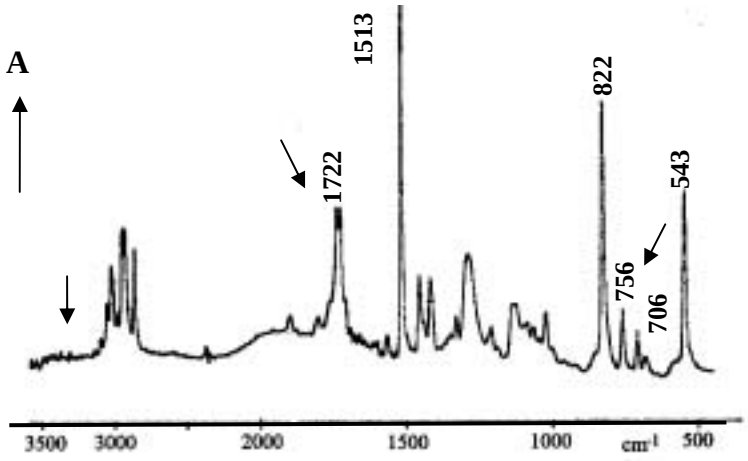

Fig. 5. 8 IR spectrum of the PPX / PVA / PAA tubes after reacted with isonicotinoyl chloride.

Reaction II - formation of fluorescent PPX tubes

According to the same procedure as that in reaction 1, the reaction between anthracenoyl chloride and the PPX / PVA / PAA composite tubes was carried out with dried DMF as

solvent. After reaction, anthracene groups were introduced into the PPX tubes, resulting in the fluorescent PPX / PVA / PAA tubes. The reaction is shown in Fig. 5. 9.

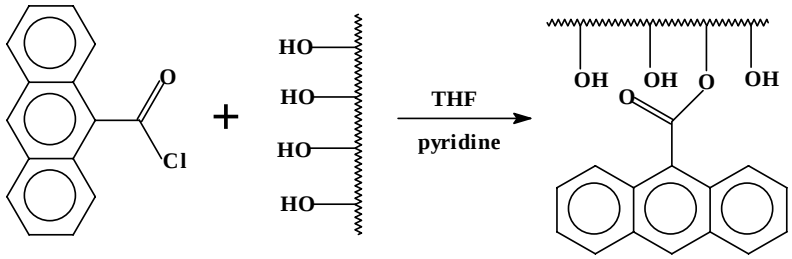

Fig. 5. 9 Reaction between anthracenoyl chloride and PPX / PVA / PAA composite tubes

Morphology of the fluorescent PPX / PVA / PAA tubes

The morphology of the reacted PPX / PVA / PAA composite tubes was characterized by fluorescence optical microscopy. Strongly fluorescent tubes were observed (Fig. 5. 10).

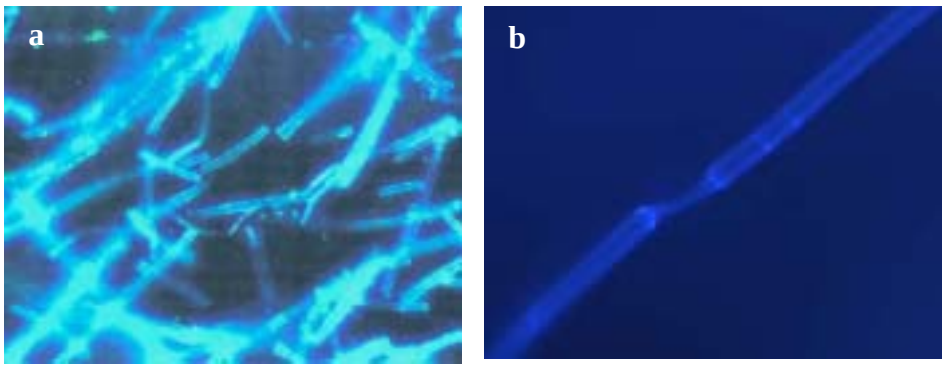

Fig. 5. 10 Fluorescent optical microscopic morphology of the PPX / PVA / PAA tubes reacted with anthracenoyl chloride

5.2 Preparation of PPX / metal composite tubes

Similarly, PPX / metal composite tubes were prepared according to the following procedure:

1. Preparation of electrospun fibers as template
2. Coating of the metal on the template fibers by means of physical vapor deposition (PVD)
3. Coating of the PPX on the resulted fibers by means of the CVD process
4. Removal of the template fibers by means of thermal degradation

The metal coating by PVD was performed in a sputter coater under high vacuum. In this work, PPX / Al and PPX / Au composite tubes were successfully fabricated.

5.2.1 PPX / Al composite tubes

PLA fibers, as template, were coated with Al by means of physical vapor deposition (PVD) in a Edward Type Auto 306 sputter coater under high vacuum (< $5x10^{-5}$ bar). The thickness of the Al coating was between 50 - 100 nm. The Al-coated PLA fibers were then coated with PPX by CVD. After that, the PPX / Al – coated PLA fibers were subjected to annealing at 370ºC in vacuum for 3 hrs, resulting in the PPX / Al composite tubes. The morphology of the PPX / Al composite tubes was characterized by SEM and TEM, respectively (Fig. 5. 10 b-c).

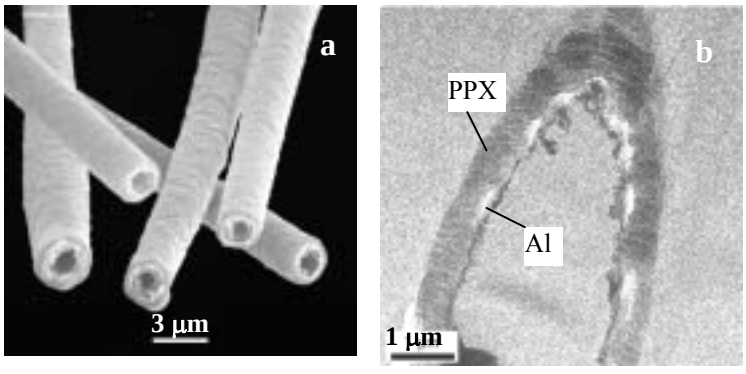

Fig. 5. 11 Morphology of PPX / Al composite tubes. a: SEM images; b: TEM image of the cross-section of PPX / Al tubes

The TEM image of the cross section of the PPX / Al tubes shows clearly the two layer coating. Outside is the PPX coating and the inside is the Al coating.

5.2.2 PPX / Au composite tubes

The PPX / Au composite tubes were prepared by means of the same process. The morphology of the PPX / Au composite tubes was characterized by SEM (Fig. 5. 12).

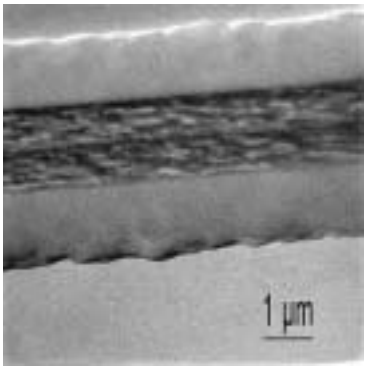

Fig. 5. 12 TEM images of PPX / Au composite tubes

5.3 PPX / metal hybrid tubes

As described in **Chapter 3**, PLA / metal compound composite fibers can be prepared by means of electrospinning the PLA solution containing the corresponding metal organic compounds. With these composite tubes as template, PPX / metal hybrid tubes can be produced by means of the TUFT process.

Various organic metal compounds, such as palladium acetate, platinum acetate, silver acetate, and copper acetate, are good candidates for preparing the PPX / metal hybrid tubes as due to the ready reduction of the metal compounds into metal under heating.

In this work, PPX / Pd , PPX / Ag, and PPX / Cu hybrid tubes were fabricated with PLA / $Pd(OAc)_2$, PLA / Ag(OAc) and PLA / $Cu(OAc)_2$ as template fibers, respectively.

5.3.1 PPX / Pd hybrid tubes

Preparation

The PLA / $Pd(OAc)_2$ composite fibers, electrospun from 3 wt % PLA / $Pd(OAc)_2$ solution in dichloromethane with 1:1 weight ratio of PLA to $Pd(OAc)_2$, was coated with PPX. The PPX-coated PLA / $Pd(OAc)_2$ composite fibers were then subjected to annealing, resulting in the formation of the PPX / Pd hybrid tubes where the Pd nanoparticles dispersed on the inner surface or/and through the PPX layer.

Morphology

Depending on the thermal decomposition condition, the PPX / Pd hybrid tubes could exhibit different morphology. When long PPX / PLA / $Pd(OAc)_2$ fibers were subjected to annealing at 365ºC in vacuum or under nitrogen for 3 hrs, the resulted PPX / Pd tubes exhibited the morphology like Fig. 5. 13 c, i.e., almost all the Pd nanoparticles were wrapped inside PPX coating, only very less amount of the Pd nanoparticles were observed in the PPX coating.

If the PPX / PLA / $Pd(OAc)_2$ were firstly cut into very small pieces (length along the fiber axis smaller than 1 mm) and then subjected to annealing at 385ºC in vacuum for more than 5 hrs, the resulted PPX / Pd tubes exhibited the morphology like Fig. 5.13 a-b, i.e., the Pd nanoparticles were dispersed through the whole PPX coating. Most of the Pd particles were still inside the PPX tubes, but some larger Pd particles (about 50 nm) were observed on the surface. At the same time, much smaller Pd particles (smaller than 1 nm) were distributed uniformly through the PPX coating.

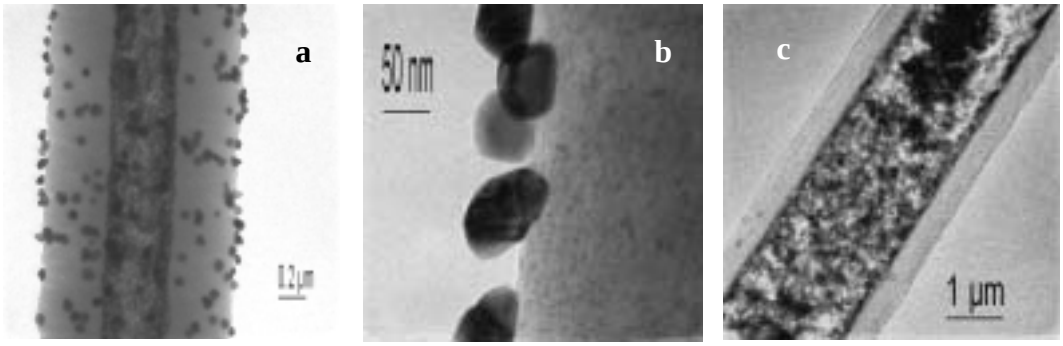

Fig. 5. 13 TEM images of PPX / Pd hybrid tubes. a - b: cut fibers annealing at 385ºC for 5 hrs; and c: long fibers annealed at 365ºC in vacuum for 3 hrs

The PPX / Pd hybrid tubes with the structure like Fig. 5. 13 a & b are significant for applications in catalysis due to the highly dispersed, ultra-small Pd nanoparticles.

The EDX microanalysis on a spot of one PPX / Pd tube proved the presence of palladium element in the PPX / Pd tubes (Fig. 5. 14).

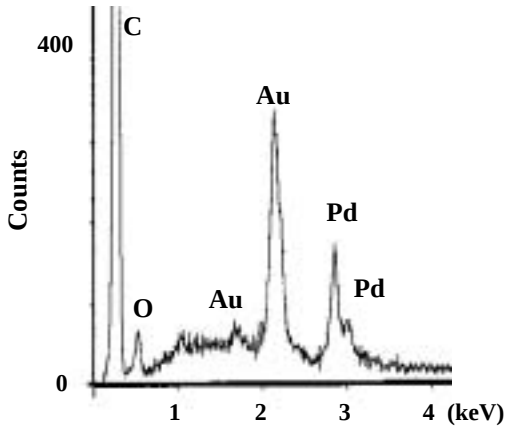

Fig. 5. 14 EDX pattern of PPX / Pd hybrid tubes

Wide-angle X-ray diffraction

The WAXD pattern of the PPX / Pd tubes shows some obvious crystal peaks at 2θ = 39º, 43º, 46º, 64º, 66º, 77º, 79º in addition to the peak at 2θ = 20º which is attributed to the crystalline peak of the PPX (Fig. 5. 15 a). Compared with the standard WAXD pattern of Pd powder (Fig. 5. 15 b), the peaks of the PPX / Pd tubes are well consistent with the Pd powder, indicating that the Pd in the tubes exists in the form of metal Pd with the cubic crystal type.

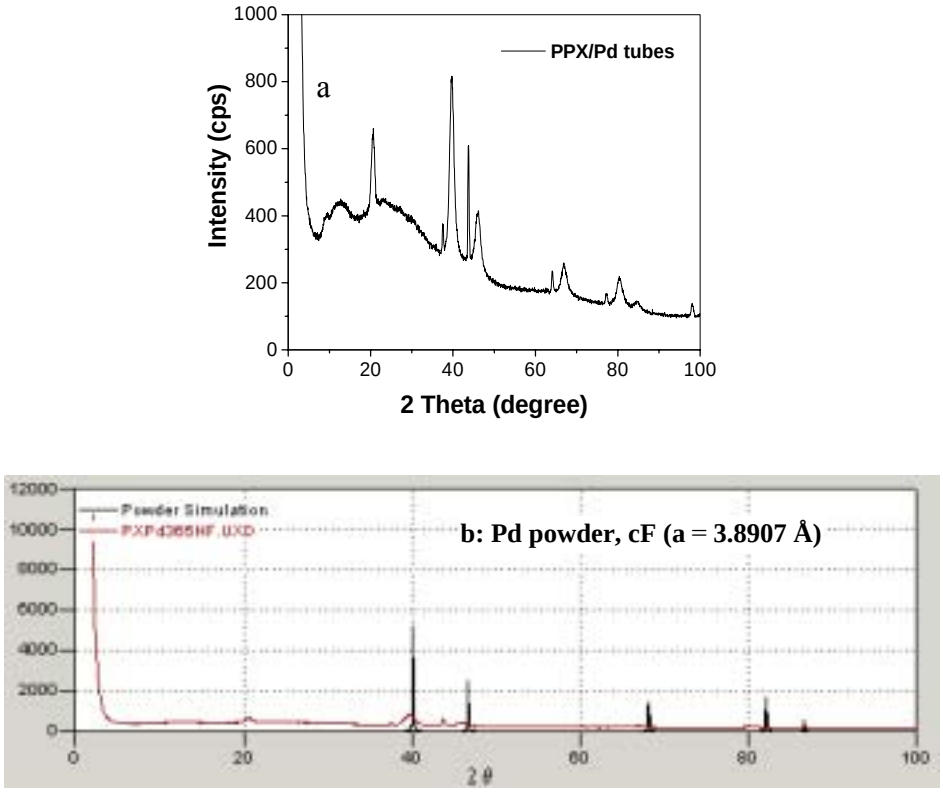

Fig. 5. 15 a: WAXD pattern of PPX / Pd tubes b: comparison with standard diffractogram of Pd powders

5.3.2 PPX / Cu hybrid tubes

Preparation

Similarly, with the PPX / $Cu(OAc)_2$ fibers as template, the PPX / Cu hybrid tubes were produced according to the same procedures. The morphologies of the tubes were characterized by TEM (Fig. 5. 16 a). Most of the nanoparticles with the size in the scale of a few nanometer were dispersed inside the PPX tubes, some of the smaller particles

(<1 nm) were dispersed through the PPX layer. The EDX microanalysis proved the presence of element Cu in the produced PPX / Cu hybrid tubes (Fig. 5. 16 b).

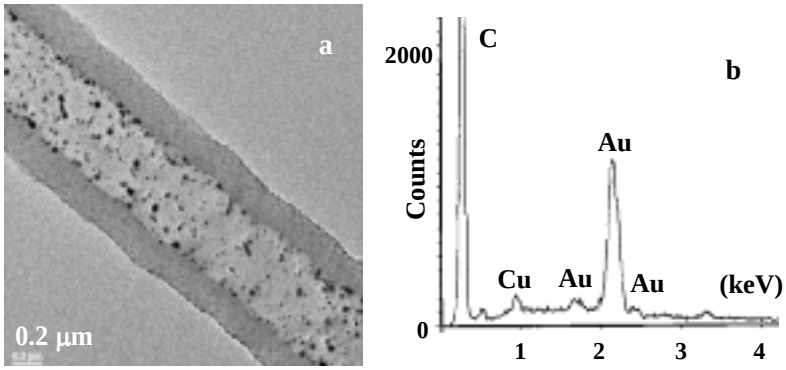

Fig. 5. 16 a: TEM images of PPX / Cu hybrid tubes; b: EDX pattern of PPX / Cu hybrid tubes

Wide-angle X-ray diffraction

The WAXD pattern of PPX / Cu hybrid tubes is shown in Fig. 5. 17. In addition to the crystalline peak of PPX (2θ = 19º), it exhibits some other peaks at 2θ = 39º, 43º, 50º, 64º, 74º, 77º, 81º, 89º, 95º, respectively.

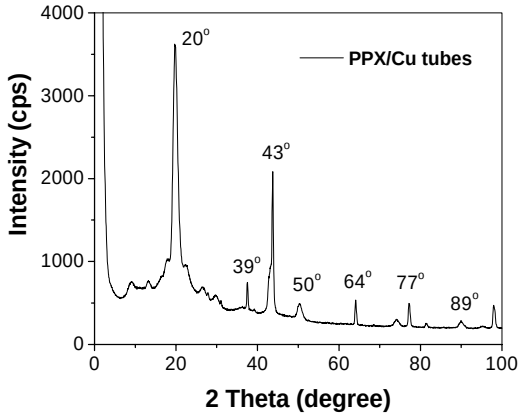

Fig. 5. 17 WAXD pattern of PPX / Cu hybrid tubes

Compared with the standard diffractogram of CuO (Fig. 5. 18 c), it is obvious that Cu in the PPX / Cu tubes is not in the form of CuO. Compared with the standard diffractogram of Cu (Fig. 5. 18 a), some peaks of the PPX / Cu tubes are well consistent with the standard peaks, but there are some more peaks in the tubes. Further compared with standard diffractogram of Cu_2O (Fig. 5. 18 b), the number of the peaks are well consistent but a uniform shift to lower diffraction angle was observed. The shift was properly caused by the improper height of the sample. Therefore, it is still difficult to confirm what kind of form Cu in the PPX / Cu tubes is, metal Cu or Cu_2O?

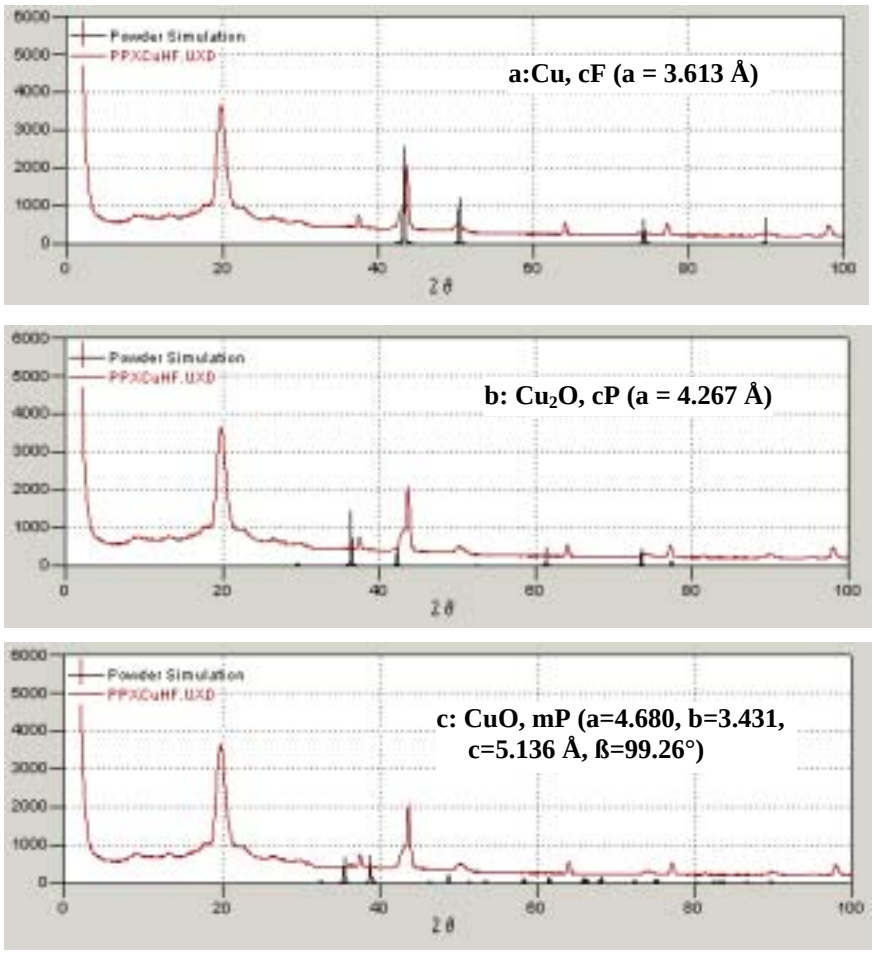

Fig. 5. 18 Comparison of the WAXD pattern of PPX / Cu hybrid tubes with standard diffractogram of a: metal Cu, b: Cu_2O, c: CuO

5.3.3 PPX / Ag hybrid tubes

PPX / Ag hybrid tubes were produced according to the same procedures as described above. The morphologies of the tubes was shown in Fig. 5. 19 a.

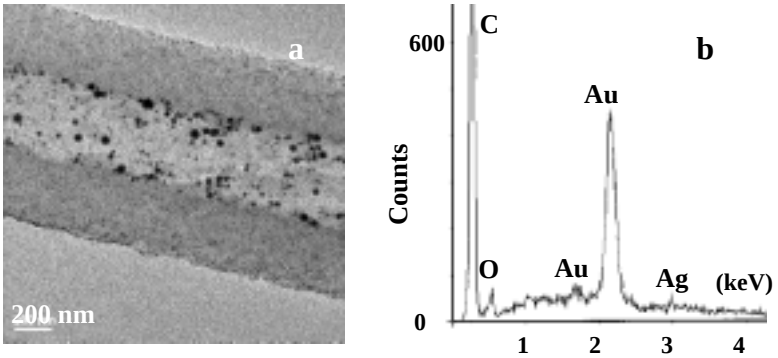

Fig. 5. 19 a: TEM images of PPX / Ag hybrid tubes; b: EDX pattern of PPX / Ag hybrid tubes

Similar with the PPX / Cu hybrid tubes, some of the larger nanoparticles were dispersed inside the PPX tubes, and the much smaller nanoparticles were dispersed through the PPX layer. The EDX analysis on one spot of a tube proved the presence of Ag element in the tubes (Fig. 5. 19 b).

Wide-angle X-ray diffraction

The WAXD pattern of the PPX / Ag hybrid tubes exhibits some crystal peaks at 2θ = 38º, 43º, 44º, 64º, 77º, 81º in addition to the PPX peak at 2θ = 20º (Fig. 5. 20).

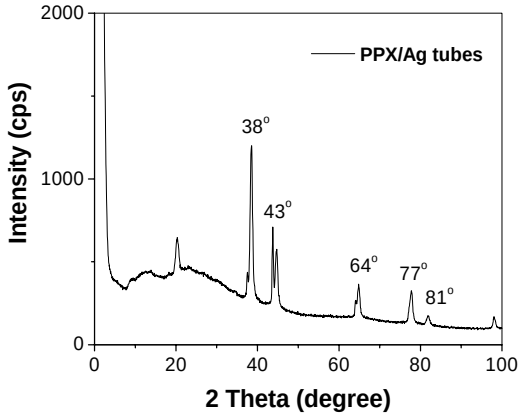

Fig. 5. 20 WAXD pattern of the PPX / Ag hybrid tubes

Compared with the standard diffractogram of metal Ag powder (Fig. 5. 21), good consistence of the two graphs was observed, indicating that the Ag in the PPX / Ag hybrid tubes exists in the form of metal Ag nanoparticles.

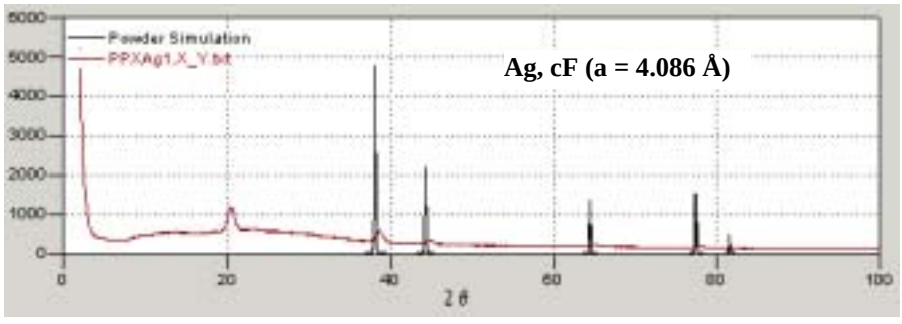

Fig. 5. 21 Comparison of the WAXD pattern of PPX / Ag hybrid tubes with standard diffractogram of Ag powder

5.4 PPX / Pd nanowires

PPX / Pd nanowires were prepared according to the same procedures as that for PPX / Pd hybrid tubes. What is different is that the template fibers for the PPX / Pd nanowires were the ultra-fine PLA/ $Pd(OAc)_2$ fibers with diameters between 5 - 70 nm, whereas for the PPX / Pd hybrid tubes, the fibers with diameter ranging from several hundred nanometer to a few micron were usually employed.

In this work, the ultra-fine PLA / $Pd(OAc)_2$ fibers with diameter between 5 - 70 nm were electrospun from 0.4 wt % - 1.5 wt % PLA / $Pd(OAc)_2$ solutions in dichloromethane with the weight ratio of PLA to $Pd(OAc)_2$ 1:1.5. The produced ultra-fine PLA / $Pd(OAc)_2$ fibers were coated with 250 mg PPX, followed by annealing at 370 ºC for 3 hrs, resulting in the PPX / Pd nanowires. The morphology of the nanowires was characterized by TEM (Fig. 5. 22). Continuous Pd threads wrapped with PPX were observed. It is found that, when the template fibers were electrospun from a solution with lower concentration (e.g. 0.7 wt %), thinner and continuous Pd wires were obtained (Fig. 5. 22 a); when the template fibers were electrospun from a solution with increased concentration (e.g. 1.5 wt %), thicker Pd wires consisting of Pd particles were obtained (Fig. 5. 22 b)

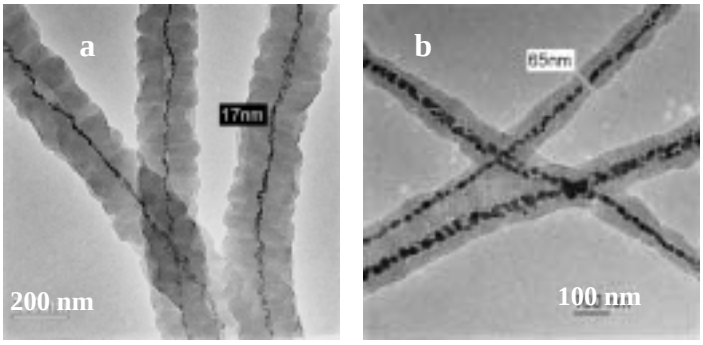

Fig. 5. 22 TEM images of PPX / Pd nanowire. The PLA / $Pd(OAc)_2$ template fibers were electrospun from a: 0.7% PLA / $Pd(OAc)_2$ solution; b: 1.5% PLA / $Pd(OAc)_2$ solution.

5.5 Surface modification of PPX tubes by chemical reactions

Principle

Compared with the chemical inertness of PPX, halogen-substituted PPX with the substituents in the ethylene segment is relative reactive due to the presence of reactive C-X bonds. In this work, various functional groups, such as -COOH, -OH, -CN, and crown ether group, were introduced onto the surface of the PPX-X tubes based on a reaction between PPX-X and amine compounds. The reaction is schematically shown in Fig. 5. 23.

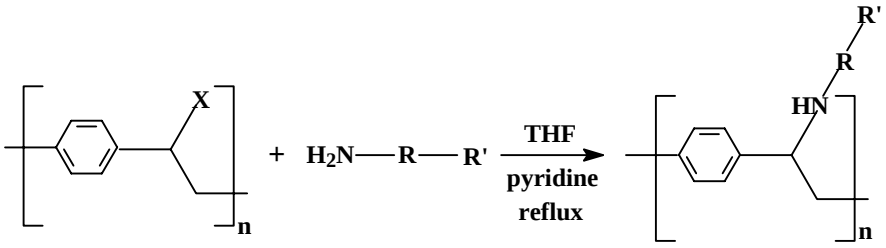

X: Cl or Br R: aromatic ring or alphatic chain

R': functional groups such as –COOH, -OH, -CN, -crown ether etc.

Fig. 5. 23 Reaction between the PPX-X tubes and amine compound

The above functionalization approach could be performed on both the inner surface and outer surface if the pure PPX-X tubes were used (Scheme. 5. 1 a). It could also be constrained only on the inner surface of the tubes if the PPX / PPX-X composite tubes were employed (Scheme 5. 1 b).

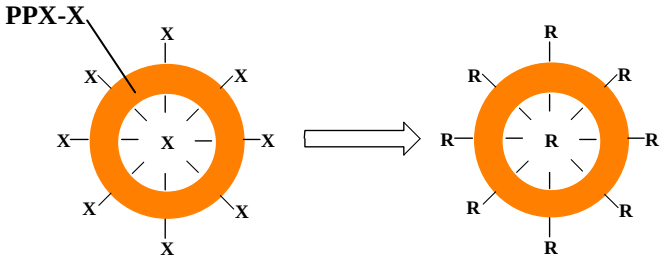

Scheme 5. 1 a Surface modification of PPX tubes (both surfaces)

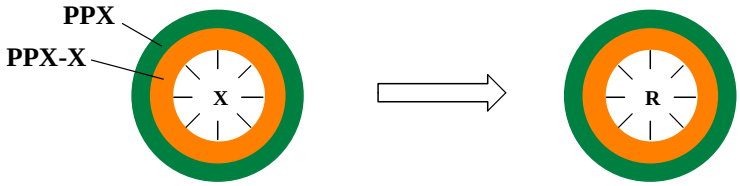

Scheme 5. 1 b Surface modification of PPX tubes (inner surface only).

The PPX / PPX-X composite tubes were prepared according to the same procedures for PPX tubes, only that the template fibers were coated two time, firstly coated with PPX-X by CVD with dihalogen-xylene as starting material, followed by PPX coating with paracyclophane as starting material.

5.5.1 Chemical attachment of carboxyl groups onto PPX tubes

The PPX-Cl tubes were immersed into 1g 4-aminobenzoic acid solution in 20 ml dried THF solution. With addition of 5 ml dried pyridine, the mixture was refluxed for 1 day under slight agitation. The treated PPX-Cl tubes were then washed with chloroform and THF for several times, resulting in the PPX-Cl tubes with some carboxyl groups chemically attached on the surface. The reaction is schematically shown in Fig. 5. 24.

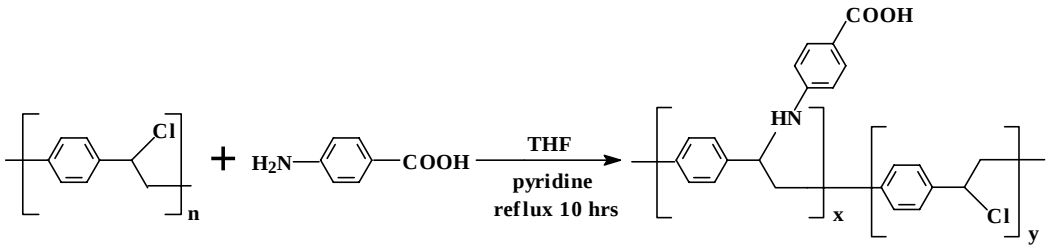

Fig. 5. 24 Reaction of the PPX-Cl tubes and 4-aminobenzoic acid

IR spectrum

After the modification by 4-aminobenzoic acid, the IR spectrum of the PPX-Cl tubes exhibited two new absorbance bands. One is a wide peak at 3406 cm^{-1}, which is attributed to –NH; the other is at 1694 cm^{-1}, which is attributed to Ar-COOH introduced by 4-aminobenzoic acid (Fig. 5. 25 b). The IR spectrum proved the presence of aminobenzoic acid group on the PPX-Cl tubes.

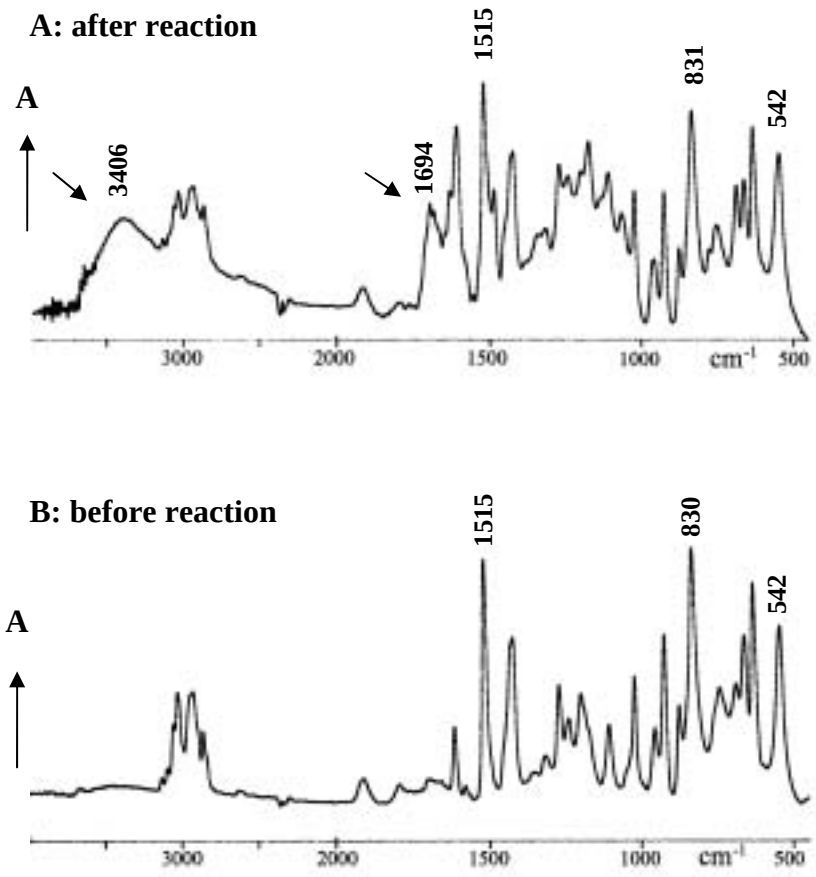

Fig. 5. 25 IR spectrum of PPX tubes. a: after reaction with 4-aminobenzoic acid; b: before reaction

5.5.2 Chemical attachment of cyano groups onto PPX tubes

By means of the reaction of the PPX-Cl tubes and 4-cyanoaniline, -CN groups were introduced onto the surface of the PPX-Cl tubes. The reaction was performed according to the same procedures as in 5.5.1 (Fig. 2. 26).

4-cyanoaniline: 1 g; THF: 20 ml, dried; pyridine: 5 ml, dried, reflux time 10 hrs.

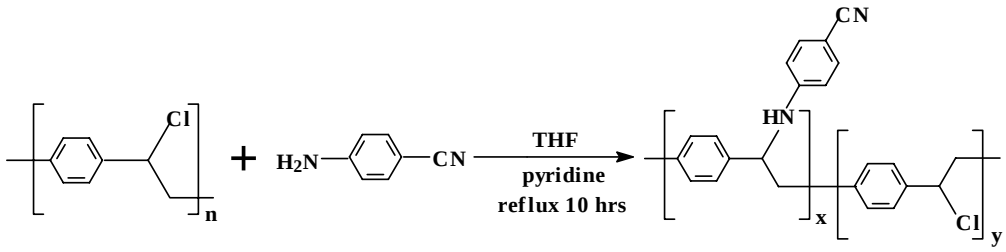

Fig. 5. 26 Reaction of the PPX-Cl tubes and 4-cyanoaniline

IR spectrum

The IR spectrum of the PPX-Cl tubes modified with 4-cyanoaniline exhibited also two new peaks, one at 3397 cm^{-1} which is attributed to –NH, and the other at 2212 cm^{-1} which is a characteristic absorbance band of Ar-cyan compounds (Fig. 5. 27).

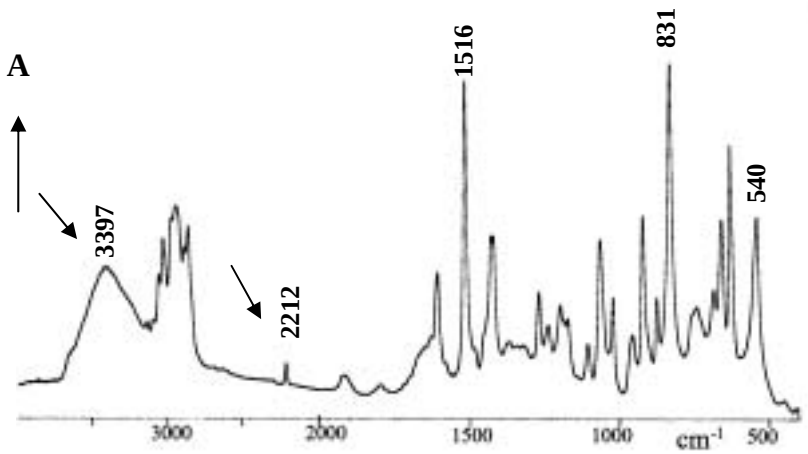

Fig. 5. 27 IR spectrum of the PPX-Cl tubes after reacted with 4-cyanoaniline

5.5.3 Chemical attachment of hydroxyl groups onto PPX tubes

Similarly, hydroxyl-modified PPX-Cl tubes were prepared by means of the reaction of the PPX-Cl with 2-aminoethanol. The reaction was performed according to the same procedure as in 5.5.1.

2-aminoethanol: 1 g; THF: 20 ml, dried; pyridine: 5 ml, dried, reflux time 10 hrs.
The structure of the modified PPX-Cl tubes was shown in Fig. 5. 28.

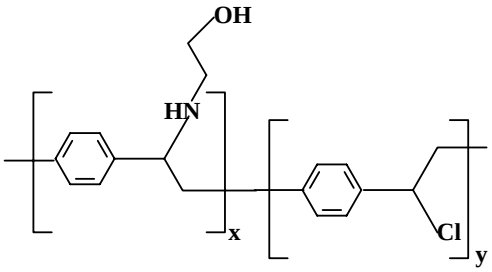

Fig. 5. 28 Structure of the PPX-Cl tubes after reacting with 2-aminoethanol

IR spectrum

After modification by 2-aminethanol, the IR spectrum of the PPX-Cl tubes exhibited some new peaks, one at 3406 cm^{-1} which is attributed to the hydroxyl group, one at 3334

cm^{-1} which is attributed to –NH, and the other at 1059 cm^{-1} which is attributed to the newly introduced C-O bond (Fig. 5. 29).

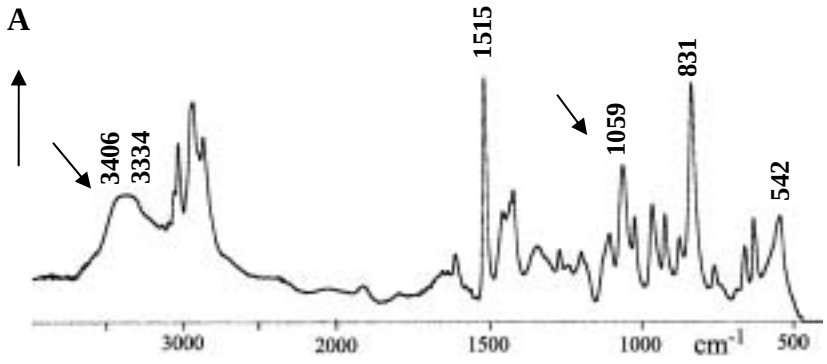

Fig. 5. 29 IR spectrum of the PPX-Cl tubes after reacted with 2-aminethanol

5.5.4 Chemical attachment of crown ether groups onto PPX tubes

The PPX-Cl tubes with crown ether groups on the surface were prepared by means of the reaction of the PPX-Cl tubes with 4-aminobenzyl-15-crown-5.
4-aminobenzyl-15-crown-5: 1 g; THF: 20 ml, dried; pyridine: 5 ml, dried; reflux 10 hrs.
The structure of the modified PPX-Cl was schematically shown in Fig. 5. 30.

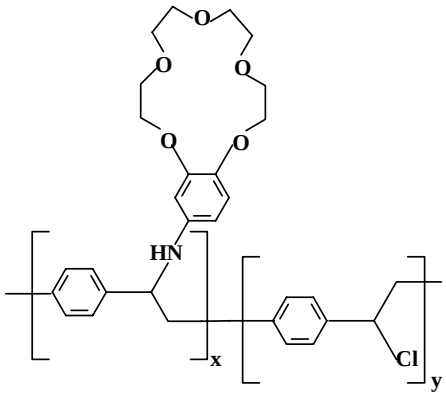

Fig. 5. 30 Structure of the crownether-modified PPX-Cl tubes

IR spectrum

The IR spectrum of the crown ether-modified PPX-Cl tubes exhibits three new peaks, one at 3391 cm^{-1} which is attributed to –NH, the other at 1134 $cm^{-1}$and 1063 cm^{-1}, which comes from the crown ether bonds (Fig. 5. 31).

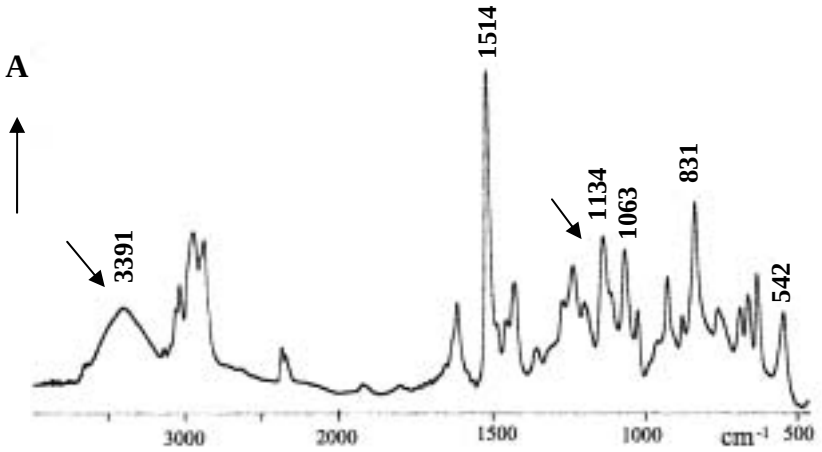

Fig. 5. 31 IR spectrum of the PPX-Cl tubes after reaction with 4-aminobenzyl-15-crown-5

5.5.5 Hydrophilicity of modified PPX-Cl tubes

By introducing hydrophilic groups on PPX-Cl surface, the hydrophilicity of PPX-Cl can be improved. The hydrophilicity of PPX-Cl was characterized by contact angle of PPX-Cl film against water. As comparison, a contrary sample of PPX-Cl film was prepared as follows: PPX-Cl film was immersed in a solution of THF and pyridine without the amine compound. The film was then treated under the same conditions as that for the modified PPX-Cl film. Contact angle of the treated PPX-Cl film against water is summarized in Table. 5. 1.

Table 5.1 Contact angle of PPX-Cl film and modified PPX-Cl film by 4-aminbenzoic acid

Sample	PPX-Cl film	Modified PPX-Cl film
Contact angle	92.3º	74.6º

PPX-Cl is highly hydrophobic and characterized by a high contact angle of 92.3º against water. After modified with 4-aminobenzoic acid, the contact angle of PPX-Cl film decreased significantly to 74.6º, exhibiting somewhat hydrophilicity. This evident improvement in hydrophilicity indicates the presence of the hydrophilic carboxyl groups on the surface. The change of the surface structure is schematically shown in Fig. 5. 32.

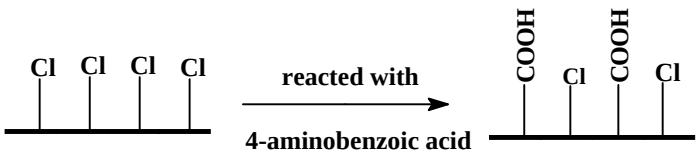

Fig. 5. 32 Surface modification of PPX-Cl by carboxyl groups

5.6 Surface grafting of PPX tubes by ATRP

Preparation

According to the principle described in Chapter 2, it is possible to perform atom transfer radical polymerization (ATRP) on the surface of the PPX-X tubes. In this work, methyl methacrylate (MMA) was used as model monomer. The PPX-X surface-mediated ATRP of MMA was performed with CuBr as catalyst and 2, 2'-bipyridin as ligand.

The PPX-Br tubes were immersed in the MMA solution in THF or CH_3CN containing CuBr and 2, 2'-bipyridin. The mixture was slightly agitated at 40ºC for 2 days, resulting in PMMA-grafted PPX-Br tubes. The polymerization reaction is schematically shown in Fig. 5. 33.

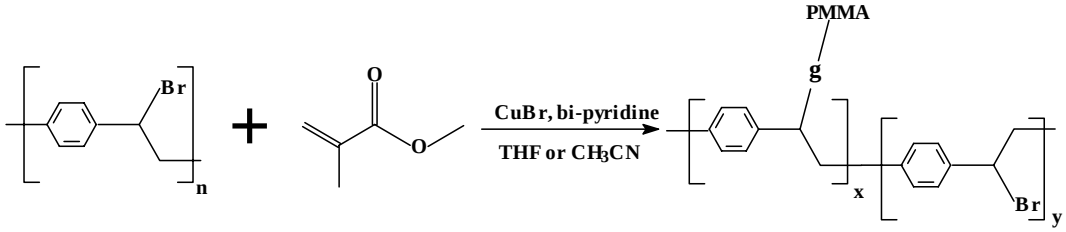

Fig. 5. 33 ATRP of MMA on the surface of PPX-X tubes. X: Cl or Br

MMA: newly destilled, 36.13 ml (336 mmol).
THF: dried, 20 ml
CuBr: 0.16 g (1.12 mmol),
2, 2'-bipyridin: 0.58 g (3.71 mmol)

The ATRP of MMA could also carried out on the surface of the PPX-Cl tubes. The reaction was performed at 70ºC for 1 day, other conditions were the same as that for the PPX-Br tubes. The PMMA-grafted PPX-Cl tubes were produced.

IR spectrum

The IR spectra of the PMMA-grafted PPX-Br tubes and the PMMA-grafted PPX-Cl tubes exhibit a new and strong absorbance band at 1731 cm^{-1} which is attributed to the carbonyl group, indicating the presence of PMMA (Fig. 5. 34).

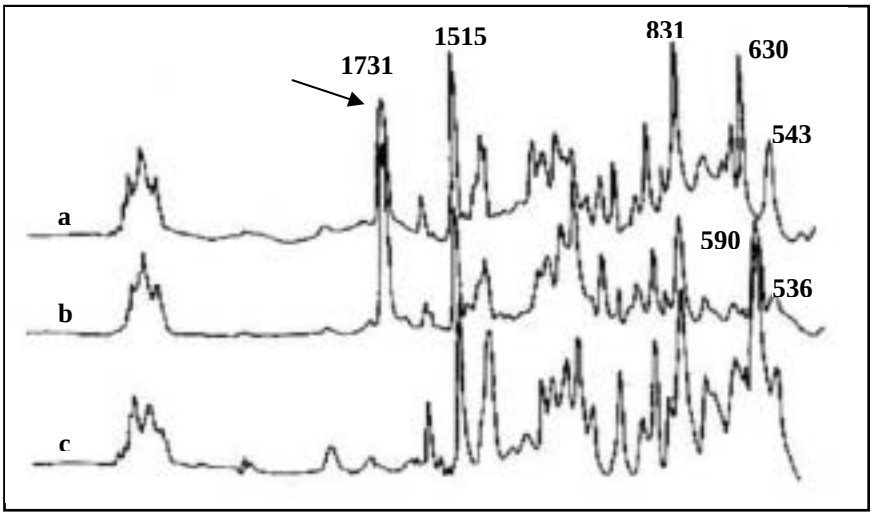

Fig. 5. 34 IR spectra of PPX-X tubes grafted with PMMA. a: PPX-Cl grafted with PMMA; b: PPX-Br grafted with PMMA; C: PPX-Br tubes without grafting

Element analysis

Element analysis shows that, after grafted with PMMA, the C and H content increased, whileas Br content decreased. It also proved that PMMA was grafted on the surface of PPX-Br tubes.

Table 5. 2 Change in element content of PPX-Br tubes after grafted with PMMA

Element	PPX-Br tube	PPX-Br-g-PMMA	Chang of element content
C	54.39	61.35	Increase
H	4.06	5.09	Increase
Br	36.44	23.32	decrease

Thermal gravimetrical analysis (TGA)

The TGA curve of the PPX-Br films shows clearly the decomposition process of PPX-Br (Fig. 5. 35 a). It consists of two stages. In the first stage, a weight loss of 36.67 % took place at the temperature between 120ºC - 200ºC, corresponding to the elimination of HBr. In the second stage, a weight loss of 17.02 % took place at the temperature between 500 - 600ºC, corresponding to the complete decomposition of the polymer.

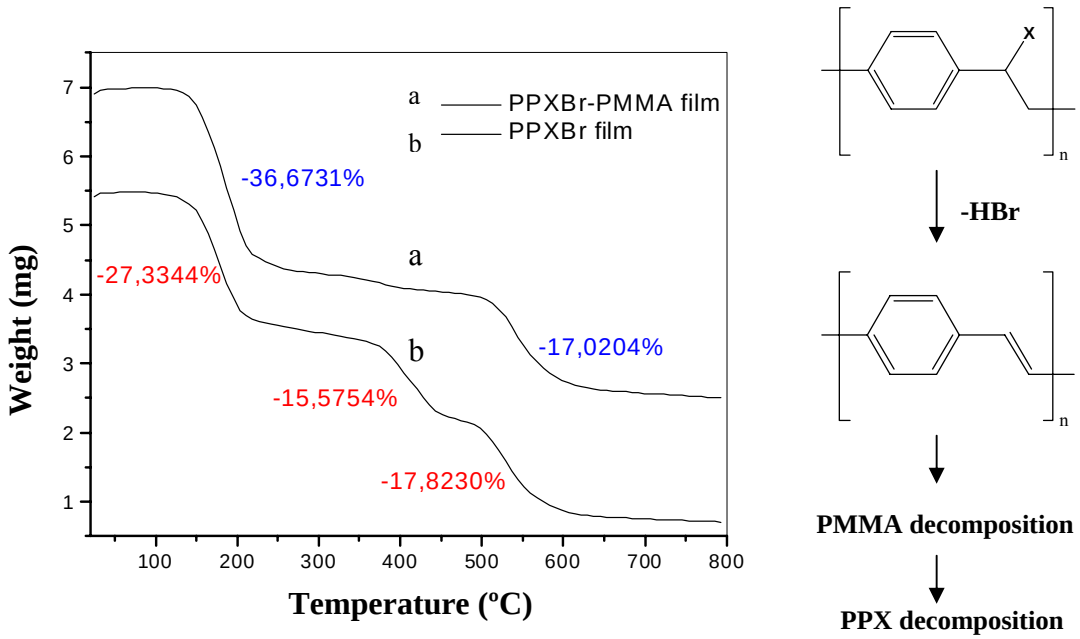

Fig. 5. 35 TGA graphs of a: PPX-Br films and b: PMMA-grafted PPX-Br films

Comparably, the TGA curve of the PMMA-grafted PPX-Br films exhibited three stages. The first stage and the third stage appeared in the same temperature ranges as in case of PPX-Br, corresponding to the HBr elimination process and the complete decomposition of the polymer, respectively. However, less weight loss (27.33%) at the first stage was observed due to the replacement of some Br substituents by PMMA, whereas the same weight loss was observed at the third stage. In addition to these two stages, a second stage with 15.58% of the weight loss was observed at the temperature between 350ºC to 420ºC. This stage is attributed to the decomposition of the surface grafted PMMA as the bulk PMMA decomposes just at this temperature range.

5.7 Hydrophilication of PPX films and PPX tubes

As mentioned before, the unique CVD method produces solvent-free, pinhole-free and highly conformal PPX and Parylene C (PPX-C, with one chloride substituent in the aromatic ring) film, which has been extensively applied as a barrier for biomedical devices. However, due to the strong hydrophobicity of PPX films, there occurs a problem, that is, the bad biocompatibility of PPX coating in human body. A solution for this problem is to improve its hydrophilicity.

In this work, improved hydrophilicity of the PPX-C (with one chloride substituent in the aromatic ring) films or tubes was achieved by incorporating hydrophilic component into the PPX-C bulk film.

Principle

PPX-C is a partially crystalline polymer. Some solvent molecules, such as chloroform, THF, have good interaction with PPX-C macromolecular chains, and can hence penetrate into the amorphous area of PPX-C films, resulting in swelling of the PPX-C films.

If a solution of a monomer is employed, the monomer can penetrate together with the solvent into the amorphous area of the PPX-C film. By means of a quick removal of the solvent, the monomer is left in the PPX-C. A sequential annealing results in the polymerization of the monomer and the formation of an interpenetrating network of PPX-C and the newly produced polymer.

According to this principle, a hydrophilic monomer, tetraethylglycol dimethylacrylate (TEGDA), was incorporated into the PPX-C film. After polymerization of TEGDA, an interpenetrating network of PPX-C and the hydrophilic poly(TEGDA) were obtained. The treated PPX-C proved to have improved hydrophilicity.

The structure of TEGDA is schematically shown in Fig.5. 36.

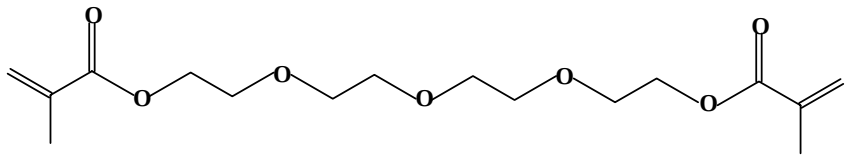

Fig. 5. 36 Structure of Tetraethylglycol dimethylacrylate (TEGDA)

Procedure

TEGDA is a crosslinkable monomer due to the two double bonds in the chain ends. The four ethylene oxide units between acrylate groups render TEGDA good hydrophilicity and medium water-solubility.

A PPX-C film was immersed into 10 % (w/w) TEGDA solution in chloroform or THF containing AIBN (1 %, related to TEGDA) for one week. After that, the PPX-C film was taken out and dried in vacuum at RT to remove the solvent quickly. The film was sequentially subjected to annealing at 80ºC for 2 hrs under N_2 atmosphere. The resulted film was immersed in chloroform to remove the physically attached TEGDA or poly (TEGDA), followed by rinsing with chloroform for several time, and washing with hot water to further remove the water-soluble parts.

Contact angle

The hydrophilicity of the PPX-C film was characterized by the contact angle of the films against water. The results are summarized in Table 5. 3.

Table. 5.3 Contact angle of TEGDA-treated PPX-C film

Sample	Untreated PPX-C film	CHCl3 immersed PPX-C film	THF immersed PPX-C film	10% TEGDA/$CHCl_3$ treated PPX-C	10% TEGDA/THF treated PPX-C	10% TEGDA /methanol treated PPX-C
Contact angle (º)	**99.2**	**97.4**	**97.9**	**65.0**	**62.1**	**95.8**

Contact angle of PPX-C film against water dropped from about 100° for untreated PPX-C films to about 66° for TEGDA treated films (Table 5. 3). The presence of TEGDA on

the surface of the treated PPX-C films was proved by the IR spectrum (Fig. 5. 37 a). Annealing of the untreated PPX-C films did not show any significant effect on the contact angle against water (Table.5. 3). Therefore, the observed increase in hydrophilicity is attributed to the treatment with TEGDA / chloroform solution.

Similar with the TEGDA / chloroform treated PPX-C, the surface of PPX-C films treated by TEGDA / THF had contact angle of 62.1°, exhibiting also good hydrophilicity.

However, the surface of PPX-C films treated by TEGDA / methanol displayed no increase in hydrophilicity (Table 5. 3)

IR spectrum

Both the IR spectra of the PPX-C film treated by TEGDA / $CHCl_3$ and by TEGDA / THF solution exhibited a new absorbance band at 1734 cm^{-1}, which is attributed to the carbonyl groups of the produced poly(TEGDA) (Fig. 5. 37 a-b), whereas the IR spectrum of the PPX-C film treated by TEGDA / methanol solution displayed no any new absorbance band (Fig. 5. 37 c). It is proved that only TEGDA / $CHCl_3$ or TEGDA / THF solution could improve the hydrophilicity of the PPX-C film.

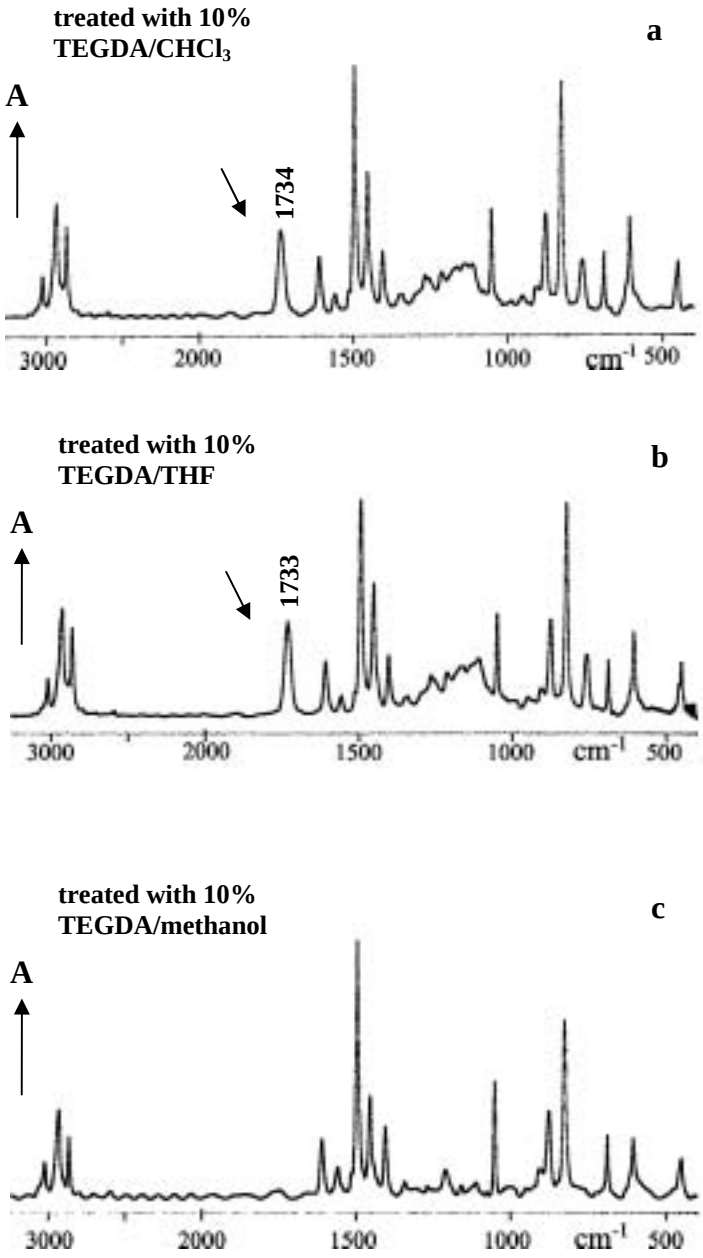

Fig. 5. 37 IR spectra of the TEGDA treated PPX-C films

Clearly, the choice of the solvent plays an important role. This is due to the different interaction between PPX-C and different solvents. Chloroform and THF have good interaction with PPX-C and can permeate into the amorphous areas of PPX-C easily. In the contrary, methanol is a strong polar solvent and has a bad interaction with PPX-C, therefore, methanol can not permeate into the PPX-C film.

Hydrophilicity of TEGDA modified PPC-C film

In addition, the increased hydrophilicity of the PPX-C film treated by the TEGDA solutions was clearly demonstrated by the shape of a drop of water on the film surface (Fig. 5. 38). The round-shaped water droplet on the surface of the untreated PPX-C film indicates that the untreated PPX-C film is highly hydrophobic; while the flat-shaped water droplet on the surface of the TEGDA-treated PPX-C film indicates that the treated film is to some extent hydrophilic.

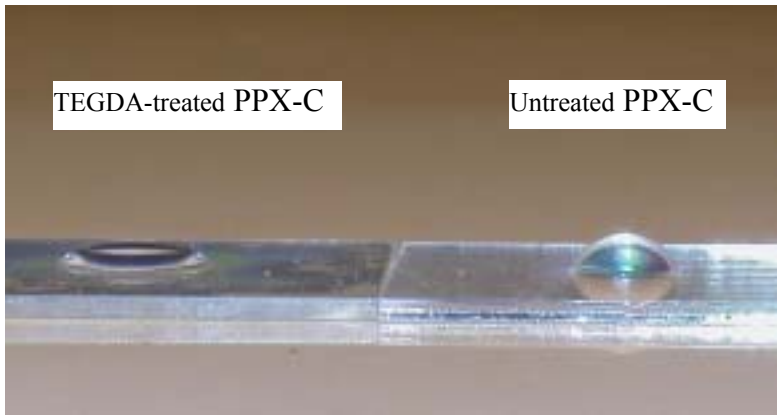

Fig. 5. 38 Change in hydrophilicity of the PPX-C film after treated with TEGDA / $CHCl_3$

6 Application of functionalized PPX tubes

6.1 Release of BSA from PPX-coated PVA / BSA fibers

The release of protein BSA from PVA / BSA electrospun fibers has been in detail discussed in **Chapter 3 – Functional electrospun fibers**. It is found that the release of BSA from PVA / BSA fibers is relative fast. Within 2 hours, 50% of BSA has been released out. In two days, more than 95% BSA has been released out. In practical applications, long-term sustained drug delivery systems are sometimes demanded. This can be achieved by coating the drug-containing fibers with PPX with regard to the good barrier property of PPX. Depending on the thickness of PPX coating, the drug release rate can be controlled at different levels.

In this work, fluorescence-labeled BSA (FITC-BSA) was used as model protein, PVA electrospun fibers as drug carrier and PPX as release barrier. The PPX-coated PVA / BSA fibers were immersed into water at 37ºC. The release of BSA from PPX-coated PVA / BSA was characterized by UV/Vis spectrum.

6.1.1 Preparation of samples

PVA / BSA composite fibers were prepared according to the method described in **Chapter 3 – functional electrospun fibers**. After PPX coating by CVD, the PPX-coated PVA / BSA fibers were obtained. Two samples with different PPX thickness were prepared.

Sample 1 - **100PXVB**: coated with 100 mg paracyclophane
Sample 2 - **500PXVB**, coated with 500 mg paracyclophane

The SEM observation (Fig. 6. 1 a-b) shows that the PPX thickness for sample 100PXVB ranges from 80 to100 nm and for sample 500PXVB ranges from 250 to 300 nm.

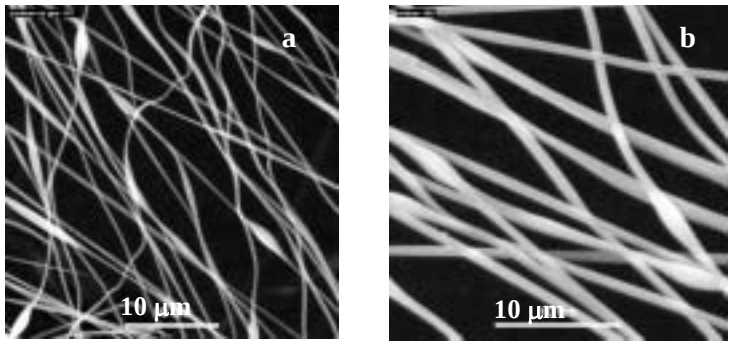

Fig. 6. 1 SEM images of a: PVA / BSA fibers before PPX coating; b: PPX-coated PVA / BSA fibers

6.1.2 Release of BSA from PPX-coated PVA / BSA fibers

The PPX-coated PVA / BSA fibers were cut into small pieces with the size of 5 mm x 5 mm prior to immersion. 10 mg of the samples were immersed into 10 ml water in a sealed glass. For each measurement of UV/Vis spectrum, 2.8 ml water was taken out from the glass, and then placed into a quartz cuvette. After measurement, the 2.8 ml water was return back to the glass.

The release rate of BSA from the PPX-coated PVA / BSA fibers was characterized by the UV/Vis spectra of the water. The change of the UV/Vis spectrum of the water with immersion time is shown in Fig. 6. 2 and Fig. 6. 3.

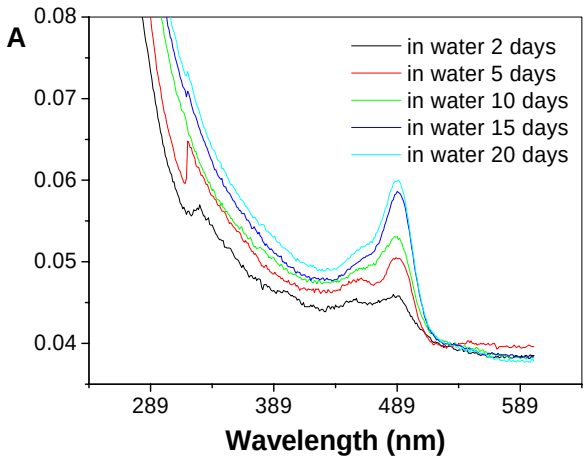

Fig. 6. 2 Change of UV/Vis spectrum of the water immersed with 100PXVB

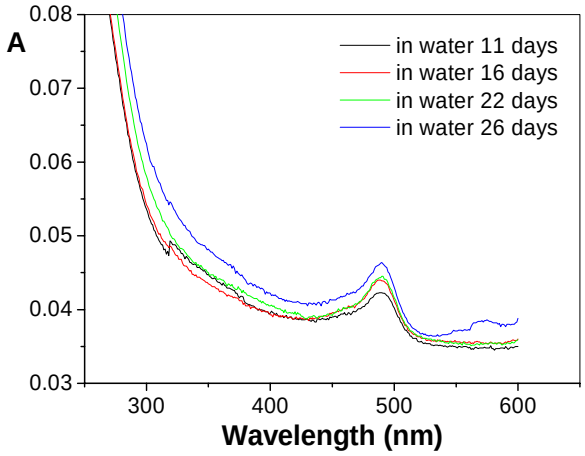

Fig. 6. 3 Change of UV/Vis spectrum of the water immersed with 500PXVB

For both samples, the maximal intensity of UV absorbance bands (A_{max}) appeared at 489 nm, which is attributed to FITC-BSA. Obviously, the A_{max} increased slowly with immersion time, indicating a very slow release of BSA. However, a faster release was observed for sample 100PXVB (Fig. 6. 2) compared with sample 500PXVB (Fig. 6. 3). It is clear that the thickness of the PPX coating plays an important role on the release rate. Thin PPX coating results in a fast release and thick PPX coating results in a slow release. Therefore, controlled release can be achieved by controlling the thickness of the PPX coating.

Compared with the release behavior of BSA from PVA / BSA composite fibers (see **Chapter 3 – Functional electrospun fibers**), the PPX-coated PVA / BSA fibers have much slower release rate. For the former system, most of BSA was released out within about 2 days, while for the latter system, it is expected that complete release of the BSA can be achieved after several months or even up to more than one year. The PPX-coated PVA / BSA fiber system proved to be a good long-term sustain release system.

6.2 Release of NaCl from PPX / NaCl tubes

6.2.1 Preparation of PPX / NaCl tubes

The NaCl-incorporated PPX tubes were prepared with the PEO / NaCl (4:1) composite fibers as template (the preparation of the PEO / NaCl composite fibers see **Chapter 3 – Functional electrospun fibers)**. The template fibers were coated with 1.5 g paracyclophane, resulting in the PPX-coated PEO / NaCl composite fibers with the PPX thickness of about 1 micrometer. After that, the fibers were subjected to annealing at 370ºC in vacuum for 2 hrs. Due to thermal degradation of PEO, NaCl-incorporated PPX tubes were formed. The morphology of the tubes was characterized by TEM (Fig. 6. 4).

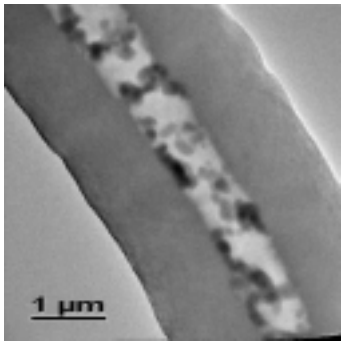

Fig. 6. 4 TEM images of NaCl-incorporated PPX tubes

6.2.2 Release of NaCl from PPX / NaCl tubes

The release of NaCl through PPX tubes were performed by immersing PPX / NaCl tubes into water. Measurement of electrical conductivity of the water was used to characterize the release of NaCl. X-ray diffraction patterns of the PPX / NaCl tubes presented the proof for the presence of NaCl in the tubes.

Electrical conductivity

The release rate of the NaCl from the PPX / NaCl tubes was characterized by change in the electrical conductivity of the water with water. With increase in the content of NaCl in water, the electrical conductivity of the water increased. The change of the conductivity of the water with immersion time was summarized in Table 6. 1.

A very fast increase in the conductivity of the water was observed within the first 30 min, followed by a slower increase. After about 5-day-long immersion, the conductivity of the water reached a maximal value, indicating all the NaCl in the tubes has been released. Comparing the release rate of cut and uncut PPX / NaCl tubes, the cut PPX / NaCl tubes exhibited a slightly faster release rate due to the presence of more open ends.

Table 6. 1 Change in electrical conductivity of the water immersed with PPX-coated PEO / NaCl fibers, PPX / NaCl tubes, and PPX-coated PEO, respectively.

Immers. time / Sample	0 min	5 min	30 min	2 hrs	1 day	3 days	5 days	8 days	10 days
PPX-coated PEO/NaCl Fiber [a)]	3.0	120.0	151.0	158.5	168.0	170.5	180.5	192.3	187.2
PPX/NaCl Tubes-1 [b)]	3.0	67.0	198.6	224.0	237.0	202.0	202.0	202.0	202.0
PPX/NaCl Tubes-2 [b)]	3.0	35.0	175.9	190.6	194.4	195.6	196.4	195.0	195.0
PPX-coated PEO fibers [c)]	3.0	10.3	25.5	35.0	50.0	71.3	70.8	72.3	74.0
Water [d)]	3.0	7.1	10.9	18.3	40.2	40.8	43.5	49.7	54.0

[a)] PPX-coated PEO / NaCl fibers were not cut and 4.45 mg sample was used.

[b)] PPX / NaCl tubes-1 were cut tubes and PPX / NaCl tubes-2 were uncut tubes.
For both sample 4.21 mg sample was used.

[c)] PPX-coated PEO fibers were not cut.

[d)] Blank experiment at the same conditions with other samples. The change in conductivity of pure water with time resulted from the dissolution of CO_2 in water.

Also, the conductivity of the water showed some increase on immersing PPX-coated PEO fibers (without NaCl). This can be attributed to the release of PEO. The IR spectrum of PPX-coated PEO fibers proved, that after in water for 10 days, PEO in the fibers was completely removed and PPX-tubes were formed. It indicated that PEO can also diffuse out through PPX layer.

Release of NaCl through PPX / NaCl tubes

According to Table 6. 1, curves of the electrical conductivity ($E_{cond.}$) of the water versus immersion time were obtained (Fig. 6. 5 a). According to the standard curve of NaCl solution, the $E_{cond.}$ is proportional to the concentration of NaCl solution, the release curve can be hence obtained (Fig. 6. 5 b).

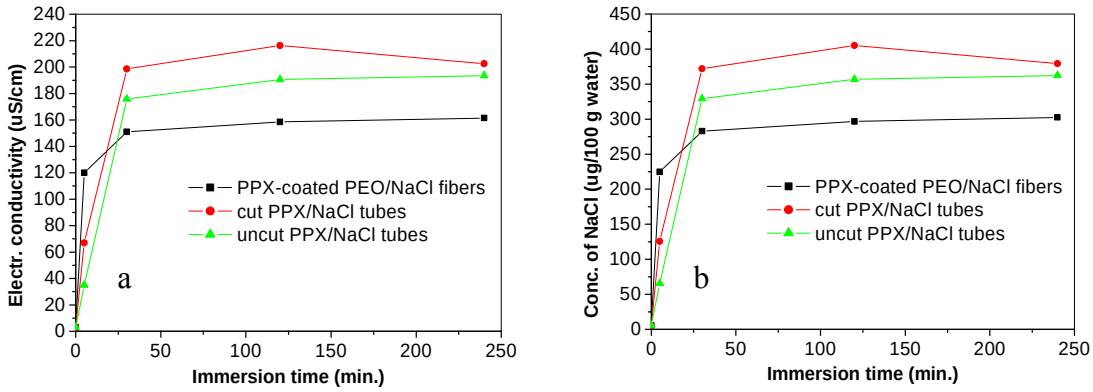

Fig. 6. 5 a: Change of the electrical conductivity of water with immersion time; b: release curve of NaCl from PPX / NaCl tubes

Change in morphology of PPX / NaCl tubes after release of NaCl

The morphology of PPX / NaCl tubes changed with immersion time. Before immersion in water, the tubes was full of NaCl crystals (Fig. 6. 6 a). After 5 min in water, the amount of NaCl inside the tubes decreased significantly (Fig. 6. 6 b), indicating that water permeated into the tubes and dissolved some of NaCl crystals. After 6 days in water, no NaCl crystals were observed any more inside the tubes (Fig. 6. 6 c), indicating that all NaCl was dissolved and released out.

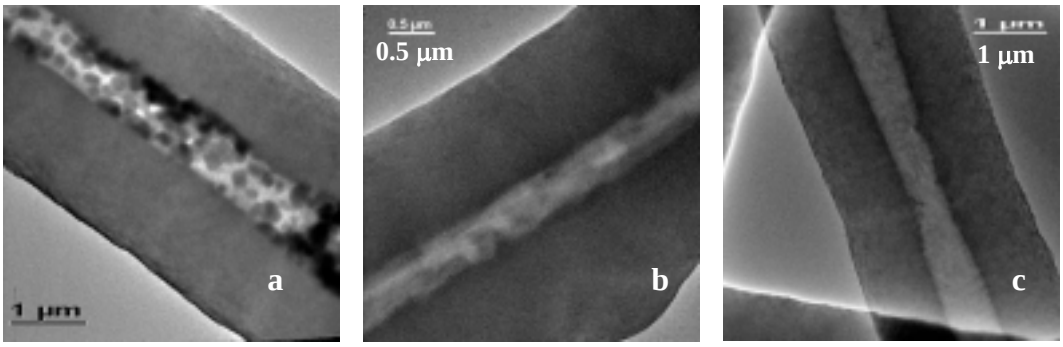

Fig. 6. 6 TEM images of PPX / NaCl tubes. a: before immersion in water; b: in water 5 min; c: in water 6 days.

Wide-angle X-ray diffraction of PPX / NaCl tubes

The results of wide-angle x-ray diffraction also proved the release of NaCl from PPX / NaCl tubes. Before immersion in water, the WAXD of the tubes (Fig. 6. 7 a) displayed three crystal peaks, one at 2θ = 19º which is attributed to PPX, the other two is at 2θ = 31º and 45º, respectively, which are attributed to NaCl crystals. After 6 days in water, the two peaks at 2θ = 31º and 45º disappeared, indicating no presence of NaCl in the tubes (Fig. 6. 7 b).

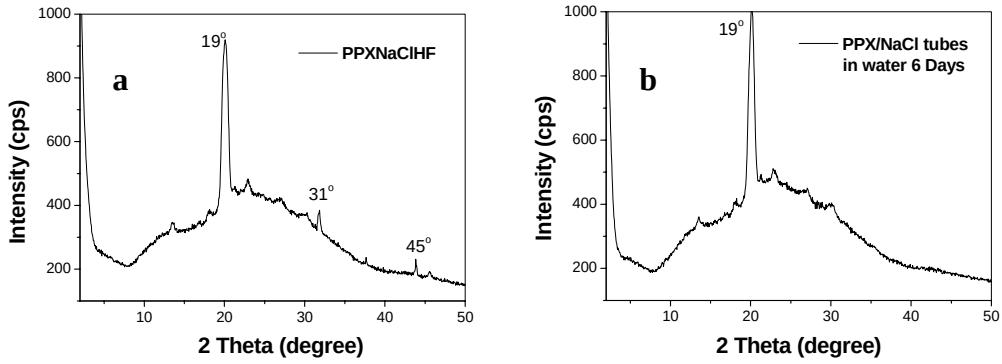

Fig. 6. 7 WAXS patterns of PPX / NaCl tubes. a: before immersion in water; b: after immersion in water for 6 days.

7 Experimental part

7.1 Reagents and solvents

Aceton	BASF, used as received
Ammonium persulfate	Aldrich, used as received
4-aminobenzoic acid	Acros, used as received
4-aminobenzonitrile 98%,	Acros, used as received
Anthracene carboxylic acid	Aldrich, used as received
Azobisisobutylenenitrile (AIBN)	Aldrich, recrystallized over methanol prior to use.
4-aminobenzyl-15-crown-5	Aldrich, used as received
2, 2'-bipyridin 99+%	Aldrich, used as received
Chloroform	Riedel-de Häen, destilled, b.p. 61ºC
Chloroform-d_1	Riedel-de Haen, used as received
Copper (II) acetate 98%	Aldrich, used as received
Copper (I) bromide 98%	Acros, used as received
α, α'-Dibromo-1, 4-xylene	Acros, used as received
α, α'-Dichloro-1, 4-xylene	Acros, used as received
Dichloromethane	Riedel-de Haen, distilled, b.p. 40ºC
N, N-Dimethylformamide (DMF)	Bayer, purified by vacuum distillation over Bis-(4-isoxyanatophenyl) methane and catalyst
Ethanol	Lenz-chemie, absolute, distilled, b.p. 78ºC
Formic acid 98%	Merck, used as received
Isopropanol	Bayer, distilled prior to use
Isonicotinyl chloride	Aldrich, used as received
Methanol	BASF, >98%, used as received
Methylmethacrylate (MMA)	Acros, distilled in vacuum prior to use
Nylon 4/6	Aldrich, used as received
1-O-n-Octyl-β-D-glucopyranoside 98%	Acros, used as received
Palladium (II) acetate	Degussa, used as received
[2, 2] paracyclophane	Aldrich, 97%, used as received

Parylene N	SCS (Speedline Technologies company), used as received
Parylene C	SCS, used as received
Parylene D	SCS, used as received
Platinum acetate	Aldrich, used as received
Polyacrylic acid	
Sokalan PA 13PN, M_w = 1000 g/mol	BASF, used as received
Sokalan PA 110S, M_w = 125,000 g/mol	BASF, used as received
Polyacrylonitrile (PAN) M_w = 150,000 g/mol	Polyscience, used as received
Poly (ethylene oxide) M_w = 300,000 g/mol	Aldrich, used as received
Poly (ethylene oxide) M_w = 900,000 g/mol	Aldrich, used as received
Poly (L-Lactide), M_w = 670,000 g/mol	Boehringer Ingelheim, used as received
Polyvinyl alcohol	
Mowiol 28-99, M_w = 145,000 g/mol	Clariant, used as received
Mowiol 56-98, M_w = 195,000 g/mol	Clariant, used as received
Mowiol 20-98, M_w = 125,000 g/mol	Clariant, used as received
Mowiol 10-98, M_w =100,000 g/mol	Clariant, used as received
Pyridine	Bayer, used as received
Silver acetate 99%	ABCR, used as received
Sodium	Merck, 99%, used as received
Sodium chloride	Acros, used as received
Sodium dodecylsulfate (SDS)	Fluka, used as received
Tetrahydrofurane (THF)	BASF; purified by drying and distillation over sodium, b.p. 66ºC
Tetraethyleneglycol dimethacrylate	Aldrich, used as received
Thionyl chloride	BASF, used as received
2-Thiophene-carboxyaldehyde 98%	Aldrich, used as received
Toluene	BASF, distilled over potassium
p-Toluene sulfonic acid	Acros, used as received
Tween 85	Aldrich, used as received
Water	Deionized water

7.2 Characterization methods

7.2.1 Contact angle

Contact angle of films against water was measured by means of dynamic measurement mode using kruess contact angle system G10 equipped with a digital camera. The contact angle was calculated by means of software SCA20 (Version 1.2.1 Building 56).

The sample was prepared on a glass slide substrate by means of spin coating or CVD coating so that the film surface is smooth and in the same horizon level. At least three different points were measured for each sample and the average value was used.

7.2.2 Differential scanning calorimetry (DSC)

Glass transition temperature (T_g) and melting point (T_m) were measured by DSC using a Mettler Toledo DSC 821^e under nitrogen atmosphere. The sample was placed in a standard aluminum pan. The sample amount is in the range of 5-15 mg. The cycle of heating and cooling at a rate of 10 K/min was carried out two times. The second heating curve was used to calculate T_g and Tm. Temperature and enthalpy was calibrated with ultra-pure zinc- and indium sample.

7.2.3 SEM and TEM

The morphology of meso- and nano-scaled fibers or tubes were characterized by scanning electron microscopy (SEM) using a CamScan 4 at 15 kV accelerating voltage and a Hitachi S-4100 at 1 kV accelerating voltage as well as by transmission electron microscopy (TEM) using a JEM 3010 operated at 300 KV.

For SEM observation, the samples were firstly fixed on an aluminum sample holder by means of a double-side adhesive graphite film, and then coated with a thin layer (about 5 nm) of gold by means of vacuum sputtering coating with a Edward Auto 306 coater under a vacuum degree $< 5 \times 10^{-5}$ mbar.

For TEM observation, the fiber or tube samples were directly placed on a copper grid and covered with another cupper grid to fix them.

7.2.4 Elemental analysis

The elemental analysis was performed in the routine analysis center of the Chemistry Department in Philipps-University Marburg.

7.2.5 Electrical conductivity

The electrical conductivity of polymer solutions was measured at 25°C by using a conductometer inoLab® Cond Level 3 equipped with a detector (Wissenschaftlich-Technische Werkstaetten GmbH). For samples with electrical conductivity in the range of 0.000 – 2.000 µs/cm, the LR 325/001 detector was used, whereas for samples with electrical conductivity in the range of 50 µs/cm – 500 ms/cm, the TetraCon 325 detector was used; for samples with electrical conductivity in the range of 2.00 µs/cm – 50.00 µs/cm, the LR 325/01 detector was used.

The amount of the solution sample was in the range of 20 – 50 ml so that the sensor part of the detector was completely immersed into the solution.

7.2.6 Energy-dispersive X-ray microanalysis (EDX)

EDX element analysis was performed on a CamScan 4 scanning electronic microscopy equipped with a Voyager EDX microanalysis system from Thermo Noran Company. The operation was carried out at 15 kV accelerating voltage.

7.2.7 Fluorescence spectrophotometer

Fluorescence spectra of the samples were recorded on a Shimadzu RF1502 Fluorescence Spectrophotometer. For film samples, the sample was fixed on a quartz slide; for a liquid sample, it was contained in a quartz cell. The sample was firstly scanned by a mix light with wavelength ranging from 250 nm to 600 nm to obtain its maximal absorbance

wavelength. The sample was then excited by the light with a wavelength slightly lower than the maximal absorbance wavelength.

7.2.8 Gas chromatography (GC)

The GC measurement was performed using a Hewlett Packard GC-HP 5890. A quartz capillary column (length 30m, inner diameter 0.32mm, film thickness 0.25 um) was used with nitrogen as carrier gas.

Injector: 300ºC
Detector (FID): 300ºC
Start temperature: 50ºC
Heating rate: 10 K/min
End temperature: 280ºC

7.2.9 Gel permeation chromatography (GPC)

GPC measurements were performed versus polystyrene standards with a set of three columns with chloroform as solvent (300 × 8 mm, type SDV, 10 μm from PSS) using a differential refractometer as detector at 25°C.

7.2.10 Infrared spectroscopy (IR)

IR-spectra were recorded by using a Perkin Elmer FT-IR 1600. For measurement of liquid samples, the sample was spread on a sodium chloride plate; for powder samples, KBr pellets were prepared; Fiber, for film or tube samples, the sample were pressed into a smooth film prior to measurement.

7.2.11 Mass spectroscopy (MS)

The mass spectroscopy analysis was performed in the routine analysis center of the Chemistry Department in Philipps-University Marburg.

7.2.12 NMR-spectroscopy

^{1}H-NMR and ^{13}C-NMR spectra were recorded on a Bruker AC300. The frequency for measurement is 300 MHz (^{1}H-NMR) and 75 MHz (^{13}C-NMR). Polymer samples were measured on a Bruker WH400. For PLA sample, chloroform-d_1 was used as solvent; for PVA sample, D_2O was used as solvent.

7.2.13 Optical microscopic morphology

The optical microscopic morphologies of the fiber or tube samples were observed on a Leica DMRX microscopy equipped with a Leica DC 200 digital camera.

The Leica DMRX microscopy was connected with a fluorescence emission device so that fluorescent morphology of the samples could be observed under the fluorescence incident.

7.2.14 Surface Tension

Surface tension of polymer solutions was measured at 20°C by using a Dataphysics DCAT 11 dynamic contact angle meter and tensiometer equipped an extremely accurate balance. The amount of the solution sample was in the range between 10 ml to 30 ml. The sample was placed in a 50 ml quartz container, which should be completely cleaned and dried every time prior to use. To measure the surface tension, a palladium plate with a rectangular form and standard size was immersed into the solution with a programmed velocity and then pulled up. The weight change of the palladium plate during the down and up process was measured by a very accurate balance. The process was repeated 50 times. The surface tension of the tested solution sample was automatically calculated by software SCAT 12.

7.2.15 Thermogravimetric analysis (TGA)

The thermal decomposition behavior of polymer samples was measured by using a Mettler Toledo TGA / SDTA 851e instruments under nitrogen atmosphere. 5 – 10 mg

sample was placed in an alumina tiegel. The sample was heated from room temperature to 800ºC at a 20 K/min rate.

7.2.16 UV/Vis spectroscopy

The UV/Vis spectra were recorded on a Perkin Elmer Lambda 9 UV/Vis Spectrophotometer. Film samples were measured by sticking the sample on the sample holder; liquid samples were measured in a quartz cell.

7.2.17 Viscosity

The viscosity of polymer solutions was measured at 20°C using a Hoeppler Viskosimeter B984 (Haake, Karlsruhe). The amount of the solution sample was about 40 ml. A round ball, steel or glass, freely falls down through the solution under its gravity, and the time interval needed for the ball to travel from the above line to the underneath line was recorded. The viscosity of the sample was calculated according to the following formula:

$$\eta = \kappa \times t \times (D_b - D_s)$$

κ is a ball constance, depending on the material and size of the ball. For the steel ball, κ is **1.257**; for the glass ball, κ is **0.0069886**. t (unit is second) is the time interval for the ball to travel from the above line to the underneath line. D is density (g/cm^3), D_b is the density of the ball, and D_s is the density of the tested solution. The unit of η is mPa•s.

For solutions with low viscosity, the glass ball was used, and the D_b is 2.401; for solution with high viscosity, the steel ball was used and the D_b is 8.1082.

7.2.18 Wide angle X-ray diffraction (WAXD)

The WAXD pattern of the samples was measured using a Siemens D-5000 Diffractometer with a Nickel-filtered Cu-Kα- radiation (λ = 0.15406 nm).

For pure polymer fibers or tubes, a 2θ scanning range from 0 to 50 was used; for fiber or tubes samples containing metal, a 2θ scanning range from 0 to 100 was used.

7.3 General experiment process (GEP)

7.3.1 GEP 1 – Electrospinning

Set up

The electrospinning of polymer fibers was carried out on the self-made device (Fig. 7. 1). The device includes a syringe where polymer solutions were loaded, a stainless steel capillary connected with the syringe, a piston over the syringe, which is driven by a motor, a high intensity of electrical field and a glass plate as collect substrate. The anode of the electrical field is connected with the capillary and grounded, the cathode is connected with a metal plate installed about 30 cm away underneath the capillary.

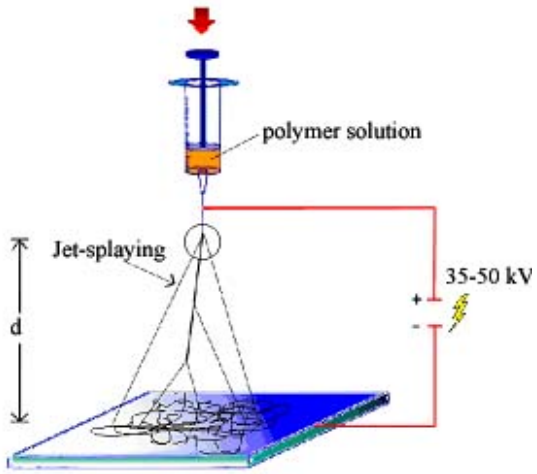

Fig. 7. 1 Electrospinning set up

In this work, three kinds of capillaries with different diameter were used: 0.1 mm, 0.3 mm, 0.5 mm. Different collecting substrates were employed, including glass plate, aluminum foil, aluminum frame, stainless steel frame, and paper. The distance between the capillary to the collect substrate varied from 10 cm to 14 cm. The intensity of the electrical voltage was in the range between 20 kV to 55.5 kV. The feed rate of the solution ranged from 0.5 ml/hr to 1.3 ml/hr.

Procedure

The polymer solution to be electrospun was placed in a 20 ml syringe. The amount of the solution was usually in the range of 2 – 5 ml. At first, the piston was pressed down with

the lowest velocity driven by a motor until a droplet of the solution appeared on the tip of the stainless steel capillary. The intensity of the electrical field was then adjusted until the droplet on the tip was split into many jets. The resulting fibers were collected on the substrate. If the substrate was glass plate or aluminum foil, the collected fibers were in the form of non – woven mats; if the substrate was metal frame, the collected fibers were in the form of half oriented mats.

7.3.2 GEP 2 – PPX coating by CVD

CVD apparatus

The CVD coating of Parylene N, Parylene C or Parylene D was performed in an automatic coating machine (Specialty Coating Systems) made by Speedline Technologies company. The machine consists of a vaporizing chamber, a pyrolysis furnace, a deposition chamber, a cooling dewar and a vacuum pump. With Parylene N as start material, the pyrolysis temperature was set up at 650ºC and the maximal temperature in the vaporizing chamber was set at 175ºC. The vacuum degree was set up lower than 55 mTorr. With Parylene C as start material, the pyrolysis temperature was set up at 690ºC, the other parameters were the same as that in case of Parylene N.

To produce halogen-substituted PPX films with substituents on the ethylene segments, α, α'-dichloro-1, 4-xylene or α, α'-dibromo-1, 4-xylene was used as start materials. The coating process was performed in a self-made CVD apparatus (Fig. 7. 2).

The vacuum degree of the whole system is lower than 0.1 mbar. The vaporizing temperature for sublimation of the monomer was about 140ºC, the pyrolysis temperature was in the range of 650 - 700ºC, and the deposition temperature was 40 - 50ºC for chloro-substituted PPX and 50 - 80ºC for bromo-substituted PPX.

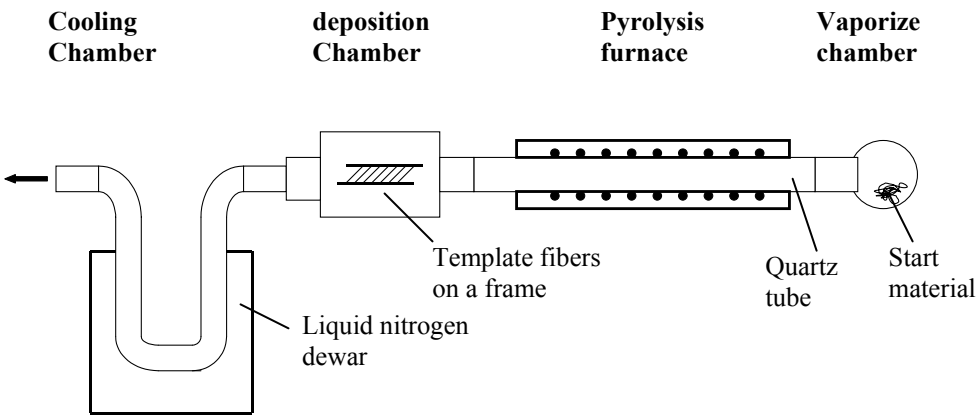

Fig. 7. 2 Pyrolysis device for PPX coating by CVD

CVD process I – with SCS automatic coating machine

The machine was switched on and the pyrolysis furnace was automatically heated. When the temperature of the pyrolysis furnace reached the set value, the starting material, dimmer Parylene N or Parylene C, was placed in the vaporization chamber and the fiber samples on a frame were placed on the deposition chamber. The vacuum pump was then switched on and liquid nitrogen was added into the cooling Dewar. After the vacuum reached lower than 8 mTorr, the temperature of the vaporization chamber elevated automatically and the vapor pressure of the start material was hence increased gradually. The coating began automatically. The coating was finished when the vapor pressure decreased again below 20 mTorr.

CVD process II – with the self-made CVD apparatus

The fiber sample on a frame was placed in the deposition chamber. The vacuum pump and the furnace were switched on. After the vacuum reached about 0.1 mbar and the temperature of the pyrolysis furnace reached about 650 - 700ºC, the start materials was heated manually by using a heating gun. The sublimation rate of the starting material was controlled so that the vacuum was always kept lower than 0.15 mbar. For PPX coating, the deposition chamber was kept at ambient temperature, for halogen-substituted PPX coating, the deposition chamber was heated by a heating gun to the desired temperature. When all the starting material sublimed off, the coating finished.

7.3.3 GEP 3 – Removal of template fibers

Method I – removal of template fibers by solvent extraction

To remove the template fibers, the PPX-coated template fibers were placed in a Sohxlet extractor and extracted for 24 hours with suitable solvents. In case of PLA or PEO fibers as template, chloroform was used as extracting solvent; in case of Nylon fibers as template, formic acid was used as extracting solvent.

Method II – removal of template fibers by thermal degradation

The PPX-coated template fibers were placed in a pyrolysis furnace. Under vacuum (< 0.3 mbar) the PPX-coated template fibers were annealed at a proper temperature (lower than 390ºC) for 3 hours, the annealing temperature depended on the template materials. For PLA template fibers, the annealing temperature was usually at 365ºC; for PEO template fibers, the annealing temperature was at 370ºC. Alternatively, the thermal degradation of the template fibers could be carried out under argon atmosphere, the required annealing time should be prolonged to about 5 hours.

7.3.4 GEP 4 – Preparation of PPX tubes

PLA fibers electrospun from a PLA solution in dichloromethane with a proper concentration were used as template. The concentration of the PLA solution depended on the desired inner diameter of the PPX tubes. The PLA fibers were then coated with PPX according to GEP 2 in the SCS automatic coating machine. After that, the PPX-coated PLA fibers were subjected to extraction with chloroform for 24 hrs, resulting in PPX tubes. Alternatively, PPX tubes could also be produced by annealing the PPX-coated PLA fibers at 365ºC in vacuum for 3 hrs.

7.3.5 GEP 5 – Preparation of substituted PPX-X tubes

PPX-Cl tubes

PLA electrospun fibers were used as template. α, α'-dichloro-1, 4-xylene was used as starting material for coating. The PLA fibers were then coated with PPX-Cl according to

GEP 2 in the self-made pyrolysis machine. After that, the PPX-Cl-coated PLA fibers were subjected to extraction with dichloromethane for 24 hrs, resulting in PPX-Cl tubes.

It is worthy of noting that the formation of PPX-Cl tubes was possible only by means of solvent extraction. Annealing of the PPX-Cl-coated PLA fibers at more than 200ºC for more than 1 hr resulted in elimination of HCl and formation of PPV-tubes.

PPX-Br tubes

The procedures to prepare PPX-Br tubes were the same with that of PPX-Cl tubes, only that α, α'-dibromo-1, 4-xylene was used as start material for coating. The formation of PPX-Br tubes was possible only by means of extraction with dichloromethane due to the ready elimination of HBr under heat.

7.3.6 GEP 6 – Functionalization of PPX tubes by surface chemical reactions

Reaction:

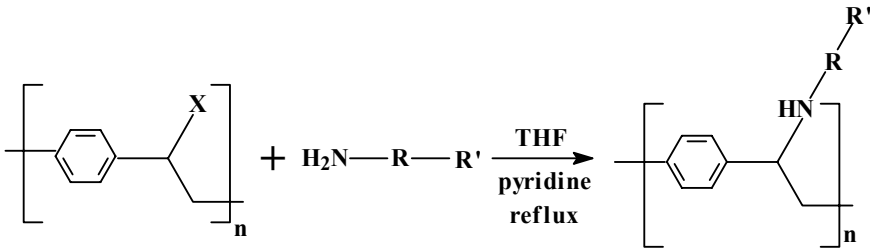

R: aromatic ring or aliphatic chain
R': -COOH, -CN, -OH, -crown ether

Method I – Surface modification of PPX-Cl tubes on both inner and outer surfaces

PPX-Cl tubes were placed in a 50 ml round-bottom flask. To the flask was added 1 g amine compound in 20 ml dried THF and 2 ml dried pyridine as catalyst. The mixture was then refluxed for 1 day. After cooling down, the PPX-Cl tubes were taken out, washed with THF three times and immersed in chloroform for 2 hrs. After washed with THF for another two times, the PPX-Cl tubes were dried in air and subjected to test and analysis.

Method II – Surface modification of PPX-Cl tubes only on the inner surface

At first, the template fibers were coated with PPX-Cl according to GEP 5, and then coated with PPX according to GEP 2. The resulting PPX tubes possessed two layers of coating, inner coating was PPX-Cl and outer coating was PPX. The PPX / PPX-Cl composite tubes were subjected to reactions with amine compounds according to the same procedure as described in **Method I**.

7.3.7 GEP 7 – Metal coating by physical vapor deposition

The coating of metal, such as Au, Al etc., on the surface of the fibers was performed by means of physical vapor deposition using an Edward Type Auto 306 sputter coater. The demanded vacuum degree is up to $< 5 \times 10^{-5}$.

7.4 Preparation of electrospun polymer fibers

7.4.1 Preparation of PLA fibers

Procedure:

Step 1 Preparation of PLA solution

PLA (M_n = 420,000 g/mol, M_w = 670,000, g/mol, M_w/M_n = 1.60) was dissolved in dichloromethane at room temperature. Solution concentration varied from 0.8 % to 5 % (w/w). For PLA solution containing additives, pyridinium formiate (PF), as an organic soluble additive, was added into the PLA solution (PF was formed by mixing equal molar of pyridine and formic acid). The amount of PF varied from 0.2 wt % to 0.8 wt % (related to solution).

Step 2 Electrospinning of the PLA solution

The electrospinning of the PLA solutions was carried out according to GEP 1 under the following electrospinning conditions:

Electrical voltage: 40 kV
Distance between the capillary to the substrate: 14 cm

Diameter of the capillary (Φ):

For solution concentration lower than 2 wt %, Φ = 0.1 mm

For solution concentration more than 2 wt %, Φ = 0.3 mm

Flow rate: 1.3 ml/hr

Temperature: room temperature

Fiber diameter

Conc. of PLA solu. without PF (wt %)	0.8	1.0	2.0	3.0	4.0	5.0
Fiber diam. (nm)	- [a)]	100-300	150-300	300-800	500-1200	800-2400
Conc. of PLA solu. with 0.8 % PF (wt %)	0.8	1.0	2.0	3.0	4.0	5.0
Fibers diam. (nm)	10-70	50-70	100-300	150-550	400-700	400-1200

[a)] **No fibers but particles were obtained.**

7.4.2 Preparation of PLA / $Pd(OAc)_2$ fibers

Procedure:

Step 1 Preparation of PLA / $Pd(OAc)_2$ solution

Palladium acetate was added to 3 wt % PLA solution in dichloromethane without additive. The weight ratio of solid PLA to palladium acetate was 1:1. The mixture was a dark-brown, non-transparent suspension. In case where higher Pd content is needed, the ratio of PLA to palladium acetate could be increased to 1:2.

Step 2 Electrospinning of the PLA / $Pd(OAc)_2$ solution

The electrospinning of PLA / $Pd(OAc)_2$ solution was carried out according to GEP 1 under the same electrospinning conditions as for PLA fibers.

Morphology

The morphology of the PLA / $Pd(OAc)_2$ fibers from 3 wt % PLA / $Pd(OAc)_2$ solution (the weight ratio of PLA : $Pd(OAc)_2$ is 1:1) was shown in Fig. 7. 3 a. The fibers had average diameter of 200-400 nm.

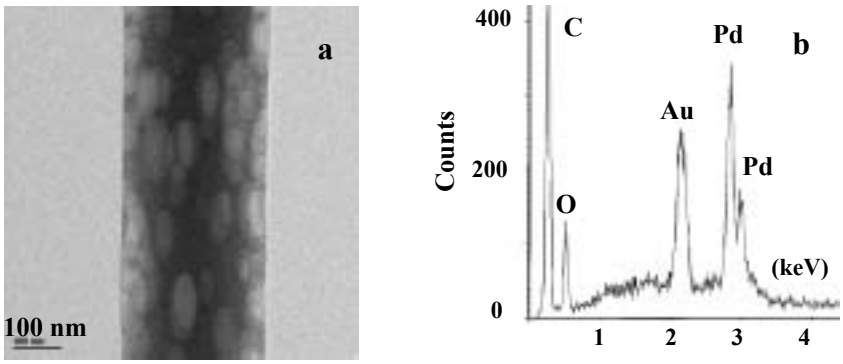

Fig. 7. 3 a: TEM image of PLA / $Pd(OAc)_2$ fibers; b: EDX element analysis pattern

Element analysis

The Element analysis of the PLA / $Pd(OAc)_2$ fibers was performed by EDX equipped on SEM instrument (Fig. 7. 3 b).

7.4.3 Preparation of PLA / $Cu(OAc)_2$ fibers

Procedure:

Step 1 Preparation of PLA / $Cu(OAc)_2$ Solution

PLA solution: 3 wt % in dichloromethane, no additive.

PLA / $Cu(OAc)_2$: 1:1 (weight ratio).

Step 2 Electrospinning of the PLA / $Cu(OAc)_2$ solution:

The electrospinning of the above PLA / $Cu(OAc)_2$ solution was carried out according to the GEP 1 under the same conditions as for PLA fibers.

Morphology

The morphology of the PLA / $Cu(OAc)_2$ fibers from 3 wt % PLA / $Cu(OAc)_2$ solution (the weight ratio of PLA : $Cu(OAc)_2$ is 1:1) was shown in Fig. 7. 4 a. The fibers have average diameters of 200 - 400 nm.

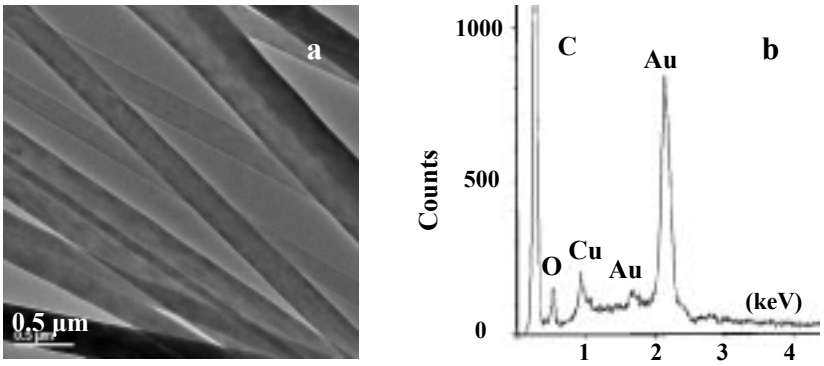

Fig. 7. 4 a: TEM image of the PLA / $Cu(OAc)_2$ fibers, b: EDX pattern

Element analysis

The Element analysis of the PLA / $Cu(OAc)_2$ fibers was performed by EDX (Fig. 7.4 b).

7.4.4 Preparation of PLA / Ag(OAc) fibers

Procedure:

Step 1 Preparation of PLA / Ag(OAc) solution

PLA solution: 3 wt % in dichloromethane, no additive.

PLA / Ag(OAc): 1:1 (weight ratio)

.Step 2 Electrospinning of the PLA / Ag(OAc) solution:

The electrospinning of the above PLA / Ag(OAc) solution was carried out according to the GEP 1 under the same conditions as for PLA fibers.

Morphology

The morphology of the PLA / Ag(OAc) fibers electrospun from 3 wt % PLA / Ag(OAc) solution (the weight ratio of PLA : Ag(OAc) is 1:1) was shown in Fig. 7.5 a. The fibers have average diameter of 200 - 400 nm.

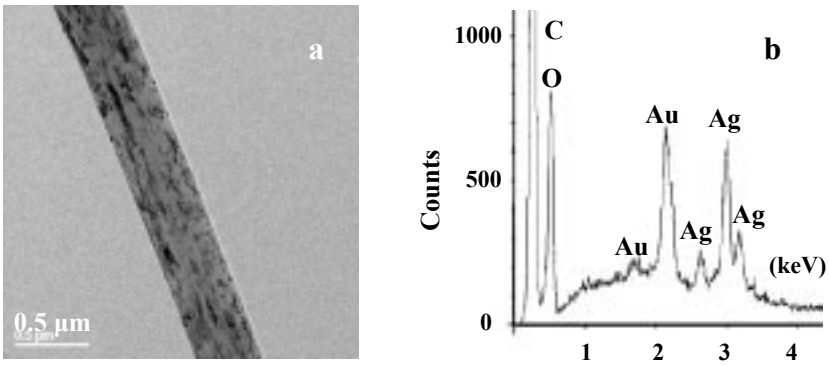

Fig. 7. 5 a: TEM image of PLA / Ag(OAc) fibers, b: EDX pattern

Element analysis

The element analysis of the PLA / $Ag(OAc)_2$ fibers was performed by EDX (Fig. 7.5 b).

7.4.5 Preparation of PEO fibers

Procedure:

Step 1 Preparation of PEO / chloroform solutions

PEO (M_w = 300,000 g/mol) was dissolved in chloroform at RT to prepare 2.5 wt % solution.

Step 2 Electrospinning of the PEO / chloroform solution

The electrospinning of the PEO solution in chloroform was carried out according to the GEP–1 under the following conditions:

Electrical voltage: 40 kV
Distance between the capillary to the substrate: 14 cm
Diameter of the capillary (Φ): Φ = 0.3 mm
Flow rate: 1.0 ml/hr
Temperature: room temperature

7.4.6 Preparation of PEO / NaCl composite fibers

Procedure:

Step 1 Preparation of PEO / NaCl solution in water / isopropanol

PEO (M_w = 300,000 g/mol) was added to a mixture solvent of water / isopropanol (weight ratio 1:9) under strong stirring to prepare 10 wt % PEO solution. To this solution was added 10 wt % NaCl aqueous solution. The amount of the NaCl solution was controlled so that the final concentration of PEO in the mixture was 7 wt %. The ratio of solid PEO to solid NaCl was 4:1.

Step 2 Electrospinning of the PEO / NaCl solution in water / isopropanol:

The electrospinning of PEO / NaCl solution in water / isopropanol was carried out according to the GEP–1 under the following conditions:

Electrical voltage: 45 kV
Diameter of the capillary (Φ): Φ = 0.5 mm
Other conditions were the same as described in 7. 4. 5

Morphology and EDX element analysis

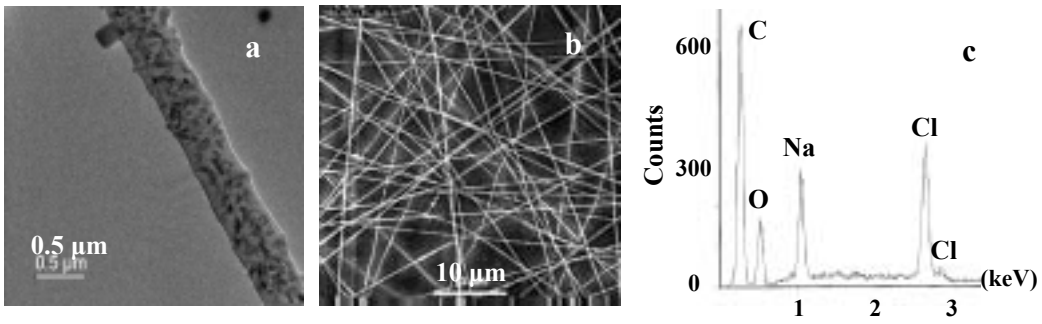

Fig. 7. 6 a: TEM and b: SEM images of PEO / NaCl fibers, c: EDX pattern of PEO / NaCl fibers

Wide-angle x-ray diffraction:

d-space	6.506	5.866	4.617	4.178	3.804	3.257	2.809	1.9
2θ (°)	13	15	19	21	23	27	31	45

7.4.7 Preparation of PVA fibers

Procedure:

Step 1 Preparation of PVA / water solution

3g PVA (Mowiol 28-99) was added in 27 g deionized water to prepare 10 wt % solution. The mixture was heated in a 100ºC oil bath under strong stirring for 3 hrs. After cooling down, a thick, homogeneous solution was obtained. The 10 wt % PVA solution was then diluted to demanded concentrations (ranging from 5wt % to 8 wt %) for electrospinning.

In case of PVA solution with additive, such as NaCl, SDS or Tween 85, the additive was added to the PVA solution directly.

Step 2 Electrospinning of the PVA aqueous solution

The electrospinning of the PVA aqueous solution was carried out according to the GEP 1 under the following conditions:

Electrical voltage: 55 kV
Distance between the capillary to the substrate:12 - 14 cm
Diameter of capillary (Φ):Φ = 0.3 mm for 5 wt %-6 wt % solution and Φ = 0.5 mm for more than 7 wt % solutions.
Flow rate: The PVA solution flowed down under the action of the gravity of the solution.
Temperature: room temperature

Morphology and size of PVA fibers

The morphology of the PVA fibers electrospun from 7 wt % PVA aqueous solution is shown in Fig. 7.7. The fibers have average diameter of 200-400 nm.

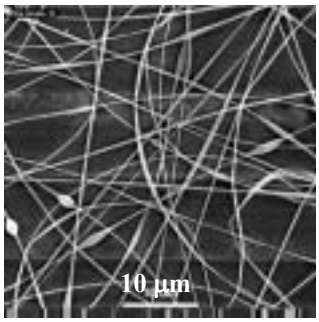

Fig. 7. 7 SEM image of the PVA fibers electrospun from 7 wt % PVA aqueous solution

7.4.8 Preparation of PVA / BSA composite fibers

Procedure:

Step 1 Preparation of PVA / BSA solution in water

3g PVA (Mowiol 56-98, M_w = 195,000 g/mol) was added in 27 g deionized water to prepare 10 wt % PVA solution with the same method as described in 7.4.7. After cooling down, a fluorescence-tagged BSA aqueous solution with the concentration of 1.03 mg/ml was added to the 10 wt % PVA solution. The amount of the BSA solution was controlled so that the weight ratio of the solid PVA to BSA was 100:1. The final concentration of PVA in the solution was about 5 wt %.

Step 2 Electrospinning of the PVA / BSA solution in water

The electrospinning of the above PVA / BSA aqueous solution was carried out according to the GP 1 under the following conditions:

Electrical voltage: 55 kV
Distance between the capillary to the substrate:14 cm
Diameter of the capillary (Φ): Φ = 0.3 mm
Flow rate: the PVA / BSA solution flowed down under the gravity of the solution.
Temperature: room temperature

Morphology and size of the PVA / BSA fibers

The morphology of the PVA / BSA fibers is shown in Fig. 7.8. The fibers have average diameter of 200 - 400 nm.

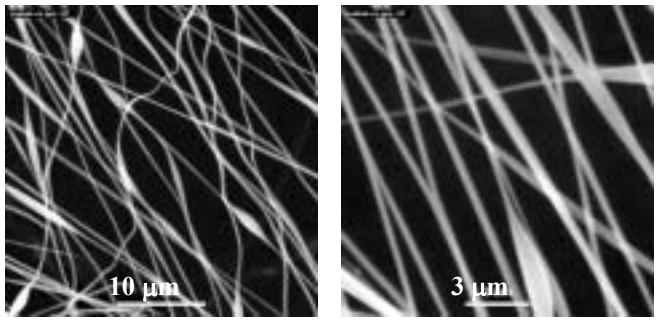

Fig. 7. 8 SEM images of the PVA / BSA fibers

IR spectrum (fibers):

$\tilde{\nu}$ (cm^{-1}) = 3318 s, 2942 s, 1710 w, 1653 w, 1436 m, 1418 m, 1378 m, 1330 m, 1093 m, 918 w, 853 w, 668 w

UV / Vis spectrum: the maximal absorbance at 469 nm.

7.4.9 Release of BSA from PVA / BSA fibers

Standard curve of BSA solutions

The BSA solution with the concentration of 1.03 mg/ml was diluted sequentially into ½, ¼, 1/8, 1/16 of the original concentration. The UV/Vis spectra of these solutions were recorded, respectively (Table 7. 1). A curve of BSA concentration versus UV/Vis absorbance intensity at 469 nm was drawn and used as standard curve.

Table 7. 1 Relationship between the concentration of the BSA solutions and the intensity of the UV absorbance at 469 nm

Conc. BSA solu. (mg/ml)	0.145	0.725	0.363	0.182	0.091
Intensity of the UV absorbance at 469 nm	0.50	0.24	0.12	0.06	0.03

Standard curve

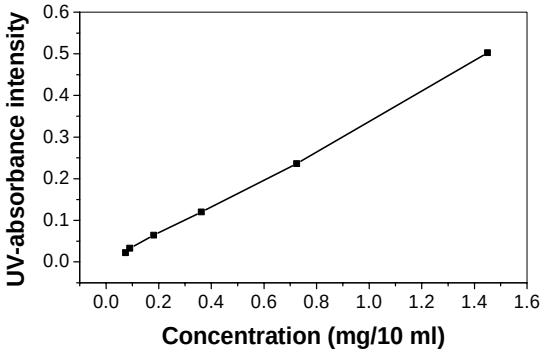

Fig. 7. 9 Relationship between the concentration of the BSA solutions and the intensity of the UV absorbance at 459 nm

Release of BSA from the PVA / BSA fibers

2.8 ml deionized water was added into a quartz cell and about 10 mg of the above produced PVA / BSA fibers were immersed into the water at room temperature. The UV/Vis spectra of the water were recorded at the following immersion time: 1 min, 5 min, 20 min, 1 hr, 3 hr, 1 day, 2 day, respectively. A curve of UV absorbance intensity (at 469 nm) versus immersion time was drawn. Related to the standard curve of BSA solutions, the curve of BSA concentration in the water versus immersion time could be obtained. It is the release rate curve of BSA released from the PVA/BSA fibers.

Table 7.2 Change in UV absorbance at 469 nm with immersion time

Immersion time	2 min	15 min	40 min	8 hrs	28 hrs	56 hrs
Intensity of the UV absorbance at 469 nm	1.32	7.41	12.36	15.20	20.40	20.55

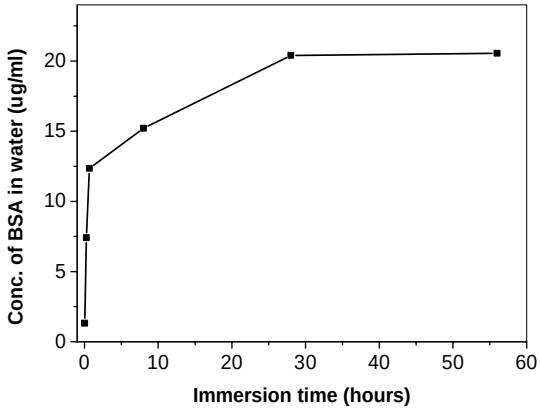

Fig. 7. 10 Release of BSA from PVA / BSA fibers

7.5 Preparation of PPX-coated functional fibers

7.5.1 Preparation of PPX-coated PVA / BSA fibers

The PVA / BSA fibers produced from 7.4.8 were coated with PPX by CVD according to the GEP 2. 500 mg and 100 mg paracyclophane was used, respectively, resulting in PPX coating with 200 - 250 nm thickness and 50 - 80 nm thickness. The morphology of the PPX-coated PVA / BSA fibers is shown in Fig. 7. 11.

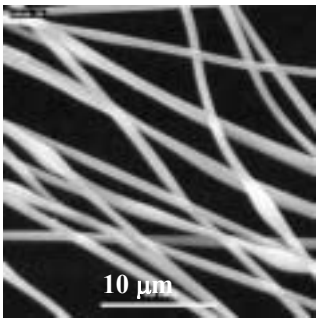

Fig. 7. 11 SEM image of PPX-coated PVA / BSA fibers

7.5.2 Controlled release of BSA from PPX-coated PVA / BSA fibers

PPX-coated PVA / BSA fibers were taken off from the frames and cut off the edges. In a bottle was added 10 ml deionized water and 10 mg of the fibers were immersed into the water. The sealed bottle was kept in a water bath at 37ºC. At different immersion time,

such as 1 day, 5 days, 10 days, 20 days etc, 2.8 ml water was taken out from the bottle and the UV/Vis spectra of the water were recorded. After finishing the UV/Vis spectrum measurement, the water was placed back to the bottle.

7.5.3 Preparation of PPX-coated PEO / NaCl fibers

The PPX coating of the PEO / NaCl fibers were carried out according to the GEP 2. Two samples with different PPX thickness were prepared. One was coated with 70 mg paracyclophane and named 7PXENa; the other was coated with named 140 mg paracyclophane and named 14PXENa. The resulting PPX thickness is 20 - 40 nm and 50 - 80 nm, respectively. The morphology of the PPX-coated PEO / NaCl fibers is shown in Fig. 7. 12.

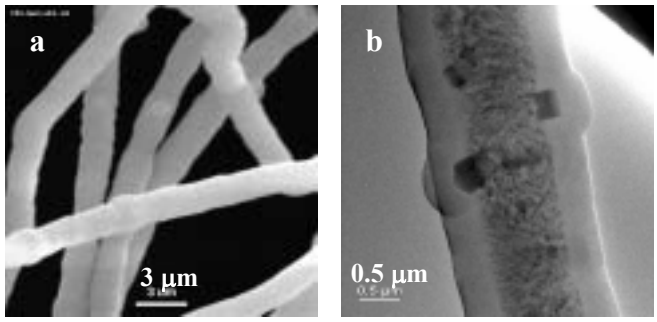

Fig. 7. 12 a: SEM images and b: TEM images of PPX-coated PEO / NaCl fibers

7.5.4 Controlled release of NaCl from PPX-coated PEO / NaCl fibers

Apparatus

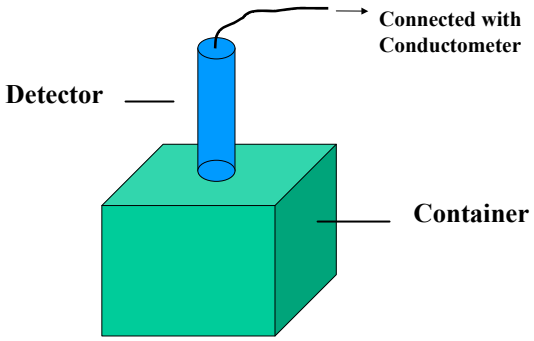

Fig. 7. 13 Apparatus for release of NaCl from PPX-coated PEO / NaCl fibers

The detector of the conductometer was inserted into a container with a hole on the cover. The diameter of the hole was designed to be exactly the diameter of the detector so that a sealed container was formed after the detector was inserted into the container.

Release of NaCl from PPX-coated PEO / NaCl fibers

PPX-coated PEO / NaCl fibers were taken off from the frames and cut into 5 mm x 5 mm small pieces. To the container shown in Fig. 7. 13 was added 65 ml deionized water. 10 mg of the PPX-coated PEO / NaCl fibers were immersed into the water. The electrical conductivity of the water was measured on line and the values at different immersion time were recorded.

Table 7. 3 Change in electrical conductivity of the water with immersion time

Sample: 7PXENa

Immersion time	0 min	1 min	4 min	6 min	13 min	30 min	50 min	1 hr	2 hrs	7 hrs	1 day
Electrical Conductivity (μS/cm)	1.0	37.3	44.8	47.2	52.0	56.2	57.6	58.0	58.5	58.8	59.2

Sample: 14PXENa

Immersion time	0 min	1 min	5 min	10 min	30 min	50 min	70 min	90 min	3 hrs	5 hrs	1 day
Electrical Conductivity (μS/cm)	1.0	3.5	31.6	35.7	41.6	44.4	46.4	48.0	51.5	53.8	56.0

7.6 Preparation of other functional polymer nanofibers

7.6.1 Preparation of water-stable PVA / PAA fibers

Step 1 Preparation of PVA / PAA blend solution

10 wt% PVA (Mowiol 28-99, M_w = 145,000 g/mol) aqueous solution and 10 wt % PAA (Sokalan PA 110S, M_w = 250,000 g/mol) aqueous solution were prepared, respectively. PVA / PAA blend solution was prepared by mixing the above two solutions with the

desired ratio. The weight ratio of PVA / PAA blend varied from 90:10 to 50:50. To accelerate the crosslinking rate of the PVA / PAA fibers, p-toluene sulfonic acid, as an acidic catalyst, was added to the blend solution with the concentration of 5 wt % (related to the solution).

Step 2 Preparation of PVA / PAA blend fibers

The PVA / PAA blend fibers were produced by electrospinning the PVA / PAA blend solution according to GEP 1 under the same condition as for PVA fibers (**7.4.7**). Smooth fibers without beads were obtained. The fiber diameters range from 200 - 500 nm.

Step 3 Crosslinking of the PVA / PAA blend fibers

The PVA / PAA blend fibers were then subjected to annealing in vacuum. In order to search for an optimal crosslinking conditions, that is, higher crosslinking efficiency was achieved at lower temperature and shorter annealing time, the annealing was firstly performed with PVA / PAA blend films with the same components as sample. The film samples were prepared by means of spin-coating of the PVA / PAA solutions on a glass slide.

The annealing temperature was varied from 80ºC to 175ºC, and the annealing time was varied from 30 seconds to a few hours.

Degree of crosslinking of the PVA / PAA blend films

The degree of crosslinking of the PVA / PAA blend film was characterized by swelling degree of the film in water.

Procedures for measurement of swelling degree: the annealed film samples were immersed in water and the water was then heated to boiling. The film samples were kept in the boiling water for 2 hrs and then naturally cooled down. After in water at room temperature for another 2 hrs, the film samples were taken out. The water drops on the film surface were carefully removed by a filter paper. After that, the film samples were weighed. And the swelling degree (SD) was calculated according to the following formula:

$$SD = \frac{W_2 - W_1}{W_1}$$

W_2 is the weight of the films after immersion in water, W_1 is the weight of the annealed films before immersion in water.

Degree of crosslinking of the PVA / PAA nanofibers

The optimal annealing conditions were applied to PVA / PAA fibers. The fibers were then placed in 95ºC steam for 1 hr and were then subjected to SEM observation. The crosslinking degree of the PVA / PAA fibers was characterized by means of the SEM morphology.

7.6.2 Preparation of photo-curable PVA derivatives fibers

Step 1 Synthesis of thienyl acrylic acid

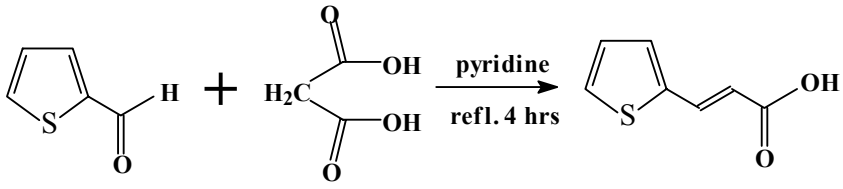

Procedure:

20 ml (0.214 mol) thiophenaldhyde was added to 44.54 g (0.428 mol) malonic acid solution in 160 ml dried pyridine under argon. The mixture was refluxed for 4 hrs. After cooled down, the mixture was kept quiet at room temperature overnight.

The mixture was poured into 500 ml water. The pH of the water was adjusted to 5 - 6 by adding 0.1 N HCl solution. A white, flake-like solid was precipitated out. After filtration, the collected white solid was recrystallized in ethanol / water mixture solvent. Pink-colored, needle-like crystals were obtained.

Yield: 25 g (84.7%)

IR spectrum (KBr):

$\tilde{\nu}$ (cm^{-1}) = 2933 w, 2583 w, 1692 s, 1676 s, 1617 s, 1411 m, 1309 s, 1275 m, 1245 m, 1216 m, 1044 w, 947 w, 859 w, 838 w, 720 w, 704 m, 598 w, 533 w

1H-NMR (300 MHz, $CDCl_3$):

δ (ppm) = 6.2 (d, 1 H, -CH=CH-), 7.84 (d, 1 H, -CH=CH-), 7.01 (t, ThioH), 7.24 (d, ThioH), 7.36 (d, ThioH)

Step 2 Synthesis of thienyl acryloyl chloride

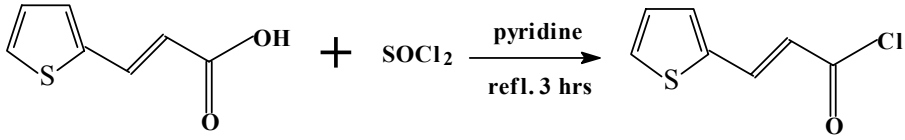

Procedure:

To a 150 ml round-bottom flask was added 10 g thienyl acrylic acid (0.065 mol) and 50 ml thionyl chloride (0.68 mol). After addition of 1 - 2 drops of pyridine, the mixture was refluxed for 3 hrs. The mixture was then cooled down to room temperature. The excess thionyl chloride was distilled out.

The resulting dark-brown mixture was distilled at 120ºC in vacuum (lower than 0.5 mbar) with a air-cooling distillation apparatus). A light-yellowed solid was obtained.

Yield: 10.5 g (95%)

Step 3 Synthesis of partially esterified PVA (PVA-Thio)

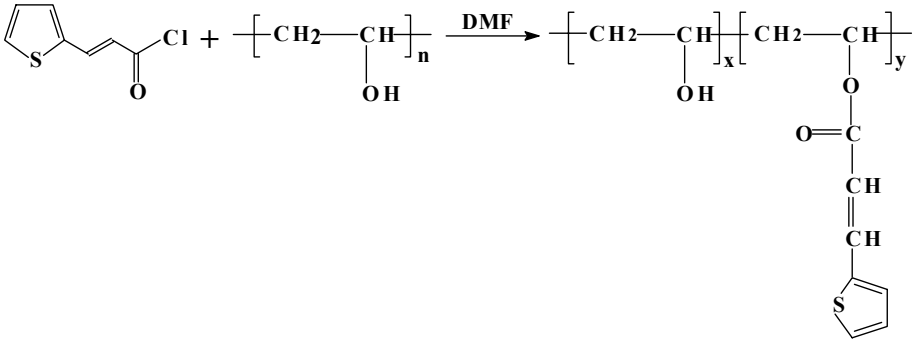

Procedure:

To a 500 ml three-necked flask equipped with a dropping funnel was added 6.38 g PVA (Mowiol 28-99) (0.145 mol) and 250 ml dried DMF. The mixture was heated and strongly stirred at 160ºC for 1 hr to obtain a homogenous solution.

After cooling to 110ºC, 1.25 g thienyl acryloyl chloride (7.25 mmol) in 20 ml dried DMF was added dropwise to the PVA solution within 2 hrs. The mixture was then heated again to 130ºC and stirred at 130ºC for another 4 hrs. A light-yellowed homogeneous solution was obtained.

The warm, clear solution (70 - 80ºC) was poured slowly into 4 l methanol, and a white polymer precipitated out, which was isolated by centrifugation and filtration. After drying in vacuum at 50ºC for one day, a brown polymer was obtained.

Yield: 6.3 g (87 %)

IR spectrum (KBr):

$\tilde{\nu}$ (cm^{-1}) = 3343 s, 2938 s, 1704 w, 1659 s, 1623 w, 1420 m, 1204 w, 1092 s, 849 m, 586 w

1H-NMR (300 MHz, D_2O):

δ (ppm) = 1.64 (m, 15 H, -CH2-), 4.12 (s, 7.5 H, -CH-), 7.56 (1 H, ThioH)

Degree of esterification according to ^{1}H-NMR spectrum

Integration value: (Thio) H 1.58, (-CH_2-) H 23.9, (-CH-) H 11.3

$$Degree\,of\ esterification = \frac{1.58/3}{23.9/2} \times 100\% = 4.40\,mol\,\%$$

Degree of esterification according to titration results

Titration procedure:

To a 200 ml round-bottom flask was added 2 g PVA-Thio and 70 ml deionized water. The mixture was heated till PVA-Thio dissolved. After cooling down to RT, 50 ml 0.1 N KOH standard solution was added to the PVA-Thio solution. The mixture was refluxed for 1.5 hr to hydrolyze the PVA-Thio.

60 ml of the hydrolyzed solution was taken out and titrated with 0.103 N HCl aqueous solution with phenolphthalein as indicator. 14.5 ml HCl solution was consumed. The amount of KOH needed for neutralizing the PVA-Thio is thus calculated as following:

$$A_{KOH} = 0.1 \times 50 \times 60/120 - 14.5 \times 0.103 = 1.0065\,ml$$

Contrast experiment was performed with 1 g PVA (Mowiol 28-99) replacing 2 g PVA-Thio. Other procedure was exactly the same with that for PVA-Thio. 22.5 ml HCl was consumed. The amount of KOH needed for neutralizing the PVA is thus calculated to be 0.1825 mmol.

The amount of thienyl acrylate group is: 1.0065-0.1825 = 0.824 mmol. That is, 1 g PVA-Thio contains 0.824 mmol thienyl acrylate group. **The degree of esterification is thus calculated to be 4.01 mol %.**

UV/Vis spectrum: maximal absorbance at 310 nm

Step 4 Preparation of PVA-Thio electrospun fibers

The PVA-Thio polymer was dissolved in water / DMF mixture solution (90:10). The PVA-Thio fibers were prepared according to GEP 1 under the same condition as for PVA fibers. The produced fibers have diameter ranging from 80 - 200 nm.

Step 5 UV-induced crosslinking of PVA-thio fibers

Reaction:

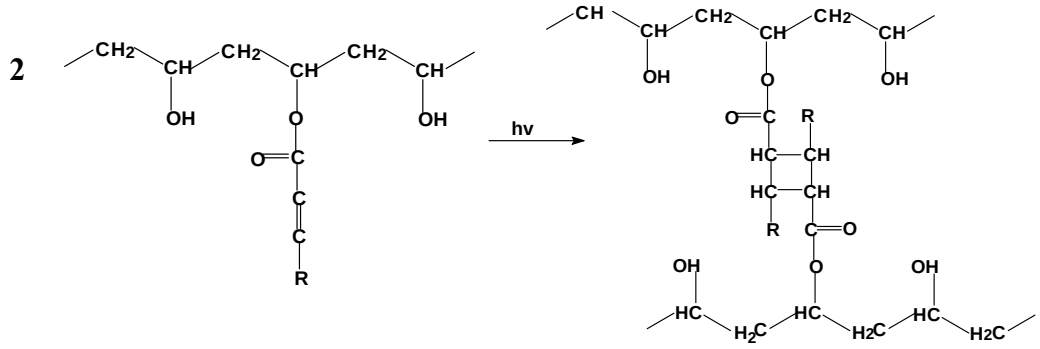

R is thiophene group.

Procedure:

The PVA-Thio fibers were irradiated by a UV lamp (Hg/10, OSRAM, main emission wavelength ranging from 310 to 600 nm) for 1 min, 3 min, 5 min, 10 min, 15 min, and 100 min, respectively.

Water-stability of UV-irradiated PVA-Thio fibers

The PVA-Thio fibers were exposed to steam (95ºC) for 1 hr.

7.6.3 Preparation of photo-curable PVA fibers

Crosslinking agent: tetraethyleneglycol dimethylacrylate (TEGDA)

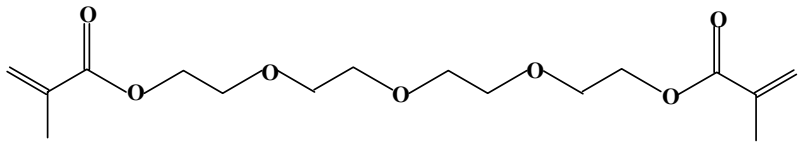

Photoinitiator: ammonium persulfate (APS)

Procedure:

1. To 7 wt % PVA aqueous solution was added TEGDA and APS. Three samples with following components were prepared:

   Sample 1: 7 wt % PVA 10.07 g, TEGDA 0.20 g, APS 0.10 g
   Sample 2: 7 wt % PVA 10.30 g, TEGDA 0.36 g, APS 0.18 g
   Sample 3: 7 wt % PVA 11.28 g, TEGDA 0.21 g, APS 0.20 g

2. PVA / TEGDA / APS fibers were prepared by electrospinning the above solutions, respectively.
3. The fibers were subjected to the irradiation of a mercury lamp (Hg / 10, OSMAR, emission wavelength > 300 nm) under nitrogen atmosphere for different time:30 s, 50 s, 5 min, 10 min.
4. The irradiated fibers were then placed in steam (95ºC) for 1 hr.

7.6.4 Preparation of fluorescent PVA nanofibers

Step 1 Synthesis of anthracenoyl chloride

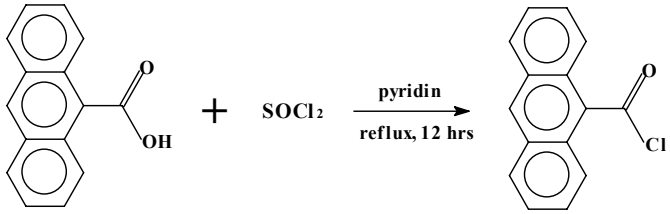

Procedure: the same with **Synthesis of thienyl acryloyl chloride**.

Anthracene carboxylic acid: 4.55 g (0.02 mol)

Thionyl chloride: 15 ml (0.2 mol)

Reflux time: 12 hrs

Sublimed temperature for anthracenoyl chloride: 150ºC

Yield: 3.75 g (76%)

Step 2 Synthesis of partially esterified PVA (PVA-Anth)

Reaction:

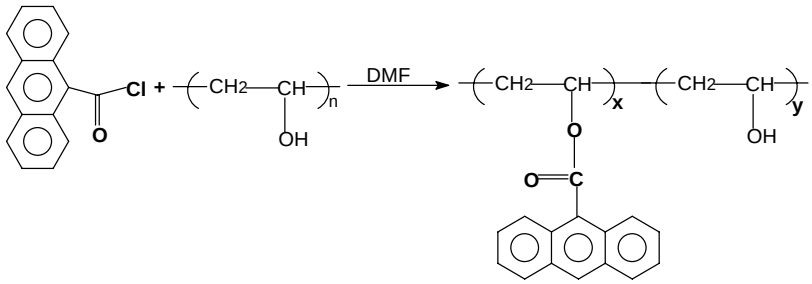

Procedure: the same with **Synthesis of partially esterified PVA (PVA-Thio).**

PVA (Mowiol 28-99): 3.91 g (88.86 mmol)

DMF (dried): 200 ml

Anthracenoyl chloride: 0.5 g (2.08 mmol)

Substitution degree: 1.5 mol % (theoretical 2.28 mol %)

Yield: 65.8 %

IR spectrum (film):

$\tilde{\nu}$ (cm^{-1}) = 3325 s, 2941 m, 1711 w, 1654 m, 1430 m, 1330 m, 1239 w, 1143 m, 1095 m, 918 w, 852 w

UV/Vis spectrum (film): a strong triple absorbance band between 330 nm - 400 nm.

Fluorescence spectrum (film, exciting wavelength 300 nm): the maximal fluorescence emission occurred at 460 nm.

7.6.5 Preparation of fluorescent PAA fibers

Step 1 Synthesis of tert-amine compound (tert-amine-anth)

Reaction:

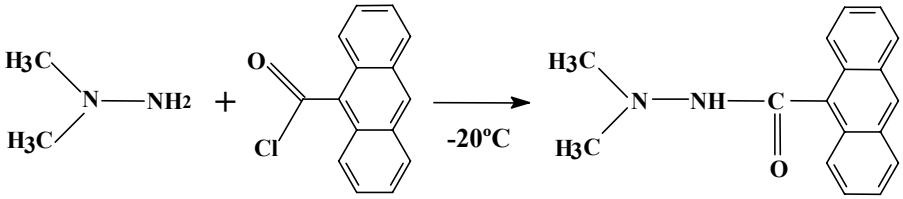

Procedure:

1. To a 150 ml three-necked flask equipped with a dropping funnel was added 1.5 g anthracenoyl chloride (6.24 mmol) and 40 ml dried toluene. The flask was cooled down in a methanol-ice water bath (-24ºC). Under strong stirring, 5 ml (62 mmol) N, N'-dimethylhydrazin in 20 toluene was dropwise added to the flask. The addition rate was controlled so that the bath temperature was kept lower than -20ºC. The addition was finished within 1 hr. The mixture was then naturally warmed up to room temperature. A light-orange colored suspension was obtained.

2. The suspension was filtered, the orange-colored filtrate was washed with ice-water twice, then dried over anhydrous sodium sulfate. The toluene in the mixture was distilled out in a rotating evaporator. A dark orange-colored oil-like solid was obtained. After recrystallized in water / methanol, orange-colored crystals were obtained.

IR spectrum (KBr):

$\tilde{\nu}$ (cm^{-1}) = 3192 m, 3056 w, 2987 w, 2952 w, 2885 w, 1644 s, 1565 m, 1521 s, 1445 s, 1424 m, 1288 m, 1264 m, 1238 s, 1164 s, 1049 m, 1018 w, 902 s, 845 s, 796s, 763 m, 732 s, 681 m

^{1}H-NMR (300 MHz, $CDCl_3$):

δ(ppm) = 3.06 (s, 6 H, $-CH_3$), 7.72 (m, 4 H, anth H), 8.2 (m, 4 H, anth H), 8.67 (d, 1 H, anth-H)

Melting point: 234 – 238ºC

Step 2 Synthesis of PAA-tert-amine salt (PAA-tert-amine)

Reaction:

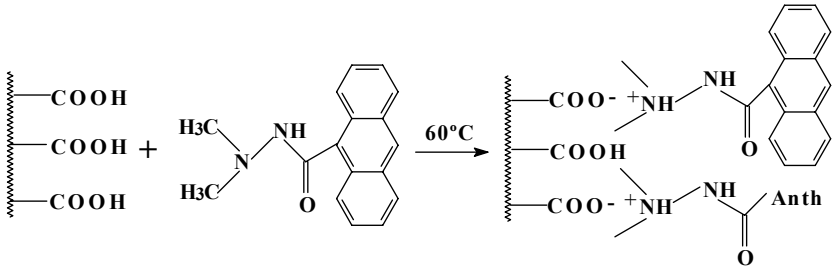

Procedure:

To 35 wt % PAA aqueous solution was added tert-amin-anth with the weight ratio of PAA to tert-amin-anth 100:2). Under a slight heat DMF was added to the mixture until all tert-amin-anth dissolved and a homogenous solution was obtained.

UV/Vis spectrum: a strong triple absorbance band between 330 nm - 400 nm.

Fluorescence spectrum (exciting wavelength 300 nm): the maximal fluorescence emission at 460 nm.

7.7 Functionalization of PPX tubes

7.7.1 Preparation of PPX / PAN composite tubes

Template fibers

PLA fibers spun on metal frames were used as template.

Coating solution

1 wt % PAN solution in DMF was used as dip coating solution.

Air-brush coating

The coating of the PAN solutions on the PLA fibers was performed by using an air-brush apparatus (Scheme. 7. 1)

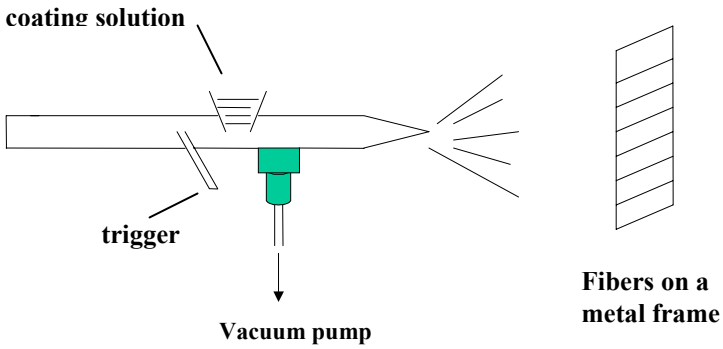

Scheme 7. 1 Apparatus for air-brush coating

For coating, about 3 ml solution was added to the apparatus each time. The coating was performed very slowly in order to disperse the solution on the surface as uniformly as possible. Both sides of the fibers were coated. The coating and drying was repeated for at least 5 times.

PPX coating

After air-brush coating, the dried fibers were subjected to PPX coating by CVD according to GEP 2.

Removal of PLA template

The PLA was removed by means of extraction with chloroform. As PAN is insoluble in chloroform, after extraction, the PLA was removed, while PAN and PPX remained. The product is PPX / PAN composite tubes.

IR spectrum (pressed tubes):

$\tilde{\nu}$ **(cm^{-1}) =** 3015 m, 2921 m, 2855 m, 2244 m, 1513 s, 1453 w, 1417 w, 1204 w, 1140 w, 1084 w, 1019 w, 823 s, 543 s

Element analysis: C: 87.14% C, H: 7.93% H, N: 2.42% N.

7.7.2 Preparation of PPX / PVA / PAA composite tubes

Template fibers: PLA fibers on metal frames

Coating solution

1 wt % PVA (Mowiol 28-99, M_w = 145,000 g/mol) aqueous solution and 1 wt % PAA (Sokalan PA 110S, M_w = 250,000 g/mol) aqueous solution were prepared, respectively. 1 wt % PVA / PAA blend solution was prepared by mixing the above two solutions together with the weight ratio of 75:25.

Air-brush coating: the same as that for PPX / PAN composite tubes.

PPX coating: the same as that for PPX / PAN composite tubes.

Heat-induced crosslinking of PVA / PAA

The PPX / PVA / PAA -coated PLA composite fibers were annealed at 120ºC for 30 min to crosslink PVA / PAA. The resulting crosslinked PVA / PAA coating layer is solvent-resistant.

Removal of PLA template: the same as that for PPX / PAN composite tubes**.**

IR spectrum (pressed tubes):

$\tilde{\nu}$ (cm^{-1}) = 3355 m, 3015 m, 2930 m, 2855 m, 1711 w, 1513 s, 1453 m, 1417 m, 1204 w, 1138 w, 1098 m, 1010 w, 823 s, 543 s

7.7.2.1 Introduction of pyridine group into PPX / PVA / PAA tubes

Structure of PPX / PVA / PAA tubes containing pyridine groups

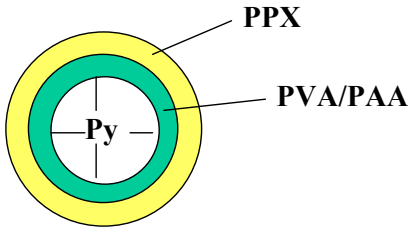

Reaction:

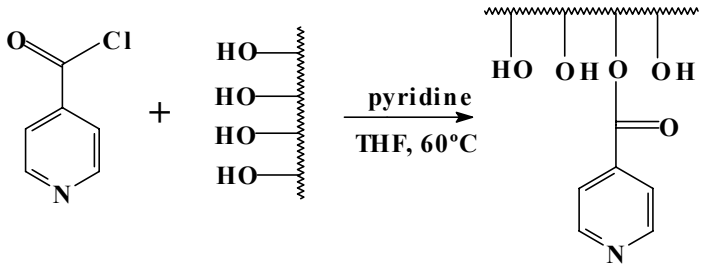

Procedure:

To a 150 ml round-bottom flask was added 2 g isonicotinoyl chloride hydrochloride in 20 ml dried THF. About 20 mg PPX / PVA / PAA tubes were immersed into the mixture. After addition of 40 ml pyridine, the mixture was heated at 50 - 60ºC under slow stirring for 4 hrs. After cooled down, the PPX / PVA / PAA tubes were taken out, washed with chloroform for three times, and dried in the air. The modified PPX / PVA / PAA tubes with pyridine groups on the inner surface were obtained.

IR spectrum:

$\tilde{\nu}$ (cm^{-1}) = 3015 m, 2930 m, 2855 m, 1722 m, 1513 s, 1453 m, 1417 m, 1285 m, 1204 w, 1138 w, 1098 m, 1010 w, 823 s, 758 w, 705 w, 676 w, 543 s

7.7.2.2 Introduction of anthracene group into PPX / PVA / PAA tubes

Reaction:

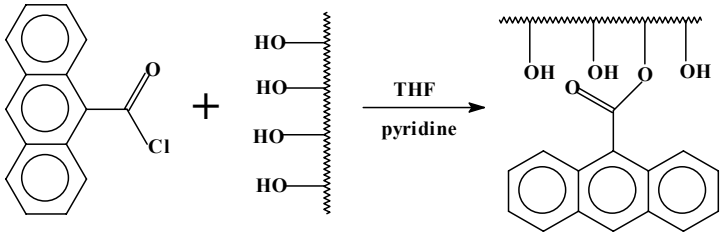

Procedure:

The PPX / PVA / PAA tubes were immersed in 0.5 g anthracenoyl chloride solution in 20 ml dried THF. After addition of 5 - 6 drops of pyridine, the mixture was refluxed for 4 hrs. After cooled down to room temperature, the tubes were taken out, washed with THF 3 time and chloroform 3 times, and then dried in air.

7.7.3 Preparation of PPX / Al composite tubes

PLA electrospun fibers were used as template. The fibers on metal frames were firstly coated with Al according to GEP 7. The thickness of Al coating was controlled by the coating time. In this work, the thickness of Al coating was about 10 - 50nm. After Al coating, the fibers were then subjected to PPX coating according to the GEP 2 and extraction by thermal degradation according to GEP 3.2.

7.7.4 Preparation of PPX / Au composite tubes

The PPX / Au composite tubes were prepared according to the same procedure as for PPX / Al composite tubes.

7.7.5 Preparation of PPX / Pd hybrid tubes

Procedure:

1 PPX coating of the PLA / $Pd(OAc)_2$ fibers

PLA / $Pd(OAc)_2$ fibers were coated with PPX by CVD according to the GEP 2. 500 mg paracyclophane was used, resulting in a thickness of PPX coating of 200nm – 300 nm.

2 Removal of the PLA from PPX-coated PLA / $Pd(OAc)_2$ fibers

Method 1: The PPX-coated PLA / $Pd(OAc)_2$ fibers were subjected to annealing at 365ºC in vacuum for 3 hrs. During the annealing, the PLA decomposed, at the same time, $Pd(OAc)_2$ was reduced to palladium nanoparticles under heat. The produced PPX / Pd hybrid fibers have the following morphology:

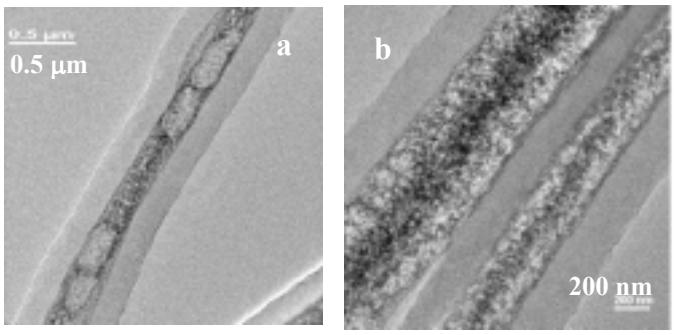

Method 2: The PPX-coated PLA / $Pd(OAc)_2$ fibers were cut into very small pieces (length along the fiber axis was smaller than 1 mm), and then subjected to annealing at 385ºC in vacuum for 5 hrs. The produced PPX / Pd hybrid tubes have the following morphology.

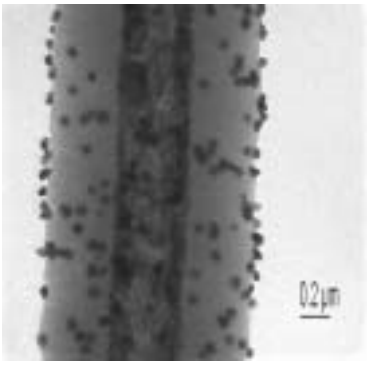

Wide-angle X-ray diffraction

d space	9.419	6.977	4.314	2.996	2.732	2.390	2.269	2.066	1.971	1.451	1.397
2θ (°)	9.3	12	20	29	32	37	39	43	46	64	66

7.7.6 Preparation of PPX / Cu hybrid tubes

Procedure:

1 PPX coating of the PLA / $Cu(OAc)_2$ fibers

PLA / $Cu(OAc)_2$ fibers were coated with PPX by CVD according to the GEP 2. 500 mg paracyclophane was used, resulting in a thickness of PPX coating of 200nm - 300 nm.

2 Removal of PLA from the PPX–coated PLA / $Cu(OAc)_2$ fibers

PLA template was removed from PPX-coated PLA / $Cu(OAc)_2$ fibers according to the same procedures as for **PPX / Pd hybrid tubes – Method 1**.

Wide-angle X-ray diffraction of PPX / Cu hybrid tubes

d space	4.472	3.966	3.358	3.005	2.400	2.305	2.075	1.812
2θ (°)	19	22	26	29	37	39	43	50
d space	1.452	1.278	1.234	1.181	1.089	1.042	1.020	-
2θ (°)	64	74	77	81	89	95	98	-

7.7.7 Preparation of PPX / Ag hybrid tubes

Procedure: PPX / Ag hybrid tubes were prepared according to the same procedure as for PPX / Cu hybrid tubes.

Wide-angle X-ray diffraction of PPX / Ag hybrid tubes

d space	4.363	3.832	2.799	2.604	2.338	2.067	2.028	1.437	1.228	1.176	1.020
2θ (°)	20	23	31	34	38	43	44	64	77	81	98

7.7.8 Preparation of PPX / Pd nanowires

Procedure:

1. Preparation of the PLA / $Pd(OAc)_2$ solution

The PLA / $Pd(OAc)_2$ solution was prepared at RT according to the following ratio.

PLA	$Pd(OAc)_2$	dichloromethane
200 mg	400 mg	20 g

2. Electrospinning of the PLA / $Pd(OAc)_2$ solution

The PLA / $Pd(OAc)_2$ nanofibers were prepared by electrospinning according to GEP 1 under the same conditions as for PLA fibers. A capillary of 0.1 mm in diam. was used.

3. PPX coating of the PLA / $Pd(OAc)_2$ nanofibers

[2, 2] paracyclophane: 120 mg, the thickness of the PPX coating: 50 to 100 nm

[2, 2] paracyclophane: 70 mg , the thickness of the PPX coating: 20 nm to 40 nm

4. Removal of PLA from PPX-coated PLA / $Pd(OAc)_2$ nanofibers

The above produced PPX-coated PLA / $Pd(OAc)_2$ nanofibers were subjected to annealing at 365ºC in vacuum for 3 hrs, resulting in PPX / Pd nanowires.

7.7.9 Surface modification of PPX tubes by chemical reactions

7.7.9.1 Chemical attachment of carboxyl groups onto PPX tubes

Structure:

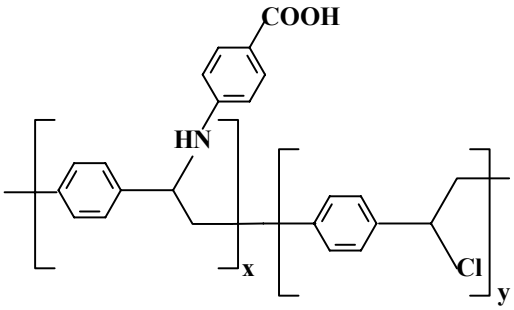

Procedure: see GEP 6.

PPX-Cl tubes	4-aminobenzoic acid	THF	Pyridine
10 mg	1 g	20 ml	5 ml

IR spectrum (pressed tubes):

$\tilde{\nu}$ (cm^{-1}) = 3376 w, 3015 w, 2930 m, 2855 w, 1694 m, 1606 m, 1515 s, 1453 m, 1417 m, 1204 w, 1138 w, 1098 m, 963 m, 831 s, 631 m, 543 m

7.7.9.2 Chemical attachment of cyano groups onto PPX tubes

Structure:

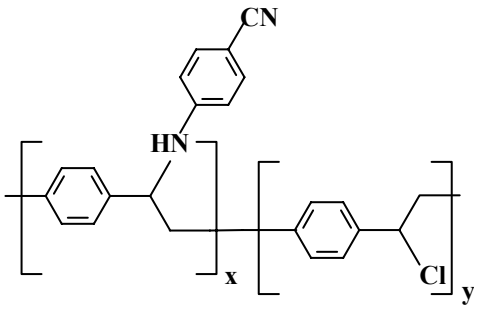

Procedure: see GEP 6.

PPX-Cl tubes	4-cyanoaniline	THF	Pyridine
10 mg	1 g	20 ml	5 ml

IR spectrum (pressed tubes):

$\tilde{\nu}$ (cm^{-1}) = 3417 w, 3015 w, 2930 m, 2855 w, 2244 w, 1606 m, 1515 s, 1453 m, 1417 m, 1204 w, 1138 w, 1098 m,963 m, 831 s, 631 m, 543 m

7.7.9.3 Chemical attachment of hydroxy groups onto PPX tubes

Structure:

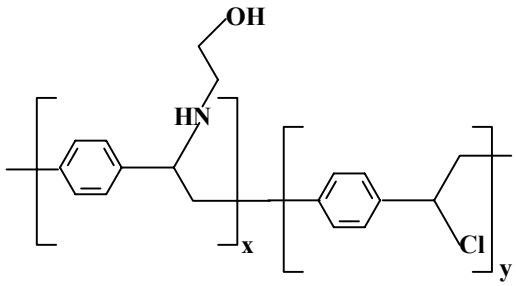

Procedure: see GEP 6

PPX-Cl tubes	2-aminoethanol	THF	Pyridine
10 mg	1 g	20 ml	5 ml

IR spectrum (pressed tubes):

$\tilde{\nu}$ (cm^{-1}) = 3406 w, 3015 w, 2930 m, 2855 w, 1606 w, 1515 s, 1453 m, 1417 m, 1204 w, 1134 m, 1098 m, 963 m, 832 s, 630 m, 541 m

7.7.9.4 Chemical attachment of 15-crownether onto PPX tubes

Structure:

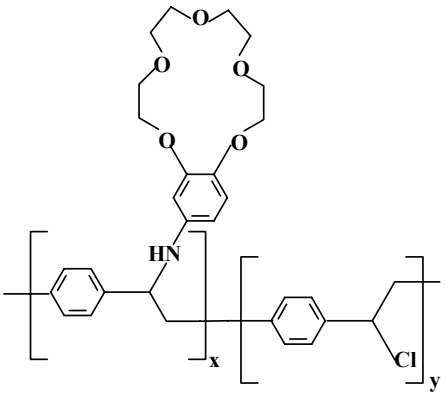

Procedure: see GEP 6

PPX-Cl tubes	4-aminobenzyl-15-crown-5	THF	Pyridine
10 mg	1 g	20 ml	5 ml

IR spectrum (pressed tubes):

$\tilde{\nu}$ (cm^{-1}) = 3391 w, 3015 w, 2930 m, 2855 w, 1606 w, 1515 s, 1453 m, 1417 m, 1204 w, 1134 m, 1059 m, 963 m, 832 s, 630 m, 541 m

7.7.10 Surface grafting of PPX tubes by ATRP

Structure:

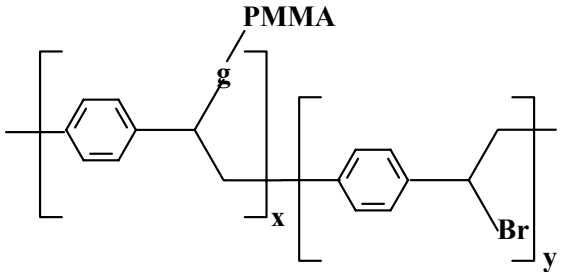

Procedure:

PPX-Br tubes were placed in a 100 ml round-bottom nitrogen flask. To the flask was added 0.16 g CuBr (1.12 mmol), 0.58 g bipyridine (3.71 mmol), 20 ml dried THF and 36.13 ml newly destilled MMA (336 mmol). The mixture was degassed three times, a red-brown homogeneous solution was obtained. After that, the mixture was stirred at 40ºC under argon for 1 day. The mixture became a grey-green suspension.

The PPX-Br tubes were taken out, washed sequentially with THF, $CHCl_3$ and water three times, and immersed in $CHCl_3$ for 2 hrs. After dried in air, a dark-yellow modified PPX-Br tubes were obtained

IR spectrum (pressed tubes):

$\tilde{\nu}$ **(cm^{-1}) =** 3015 w, 2930 m, 2855 w, 1731 s, 1513 s, 1453 m, 1417 m, 1204 w, 1138 w, 1098 m, 1010 w, 831 s, 590 m, 536 w

Element analysis: C 61.35%, H 5.09%, Br 23.32%

7.7.11 Hydrophilication of PPX-C films

Monomer: tetraethyleneglycol dimethylacrylate (TEGDA)
Initiator: azobisisobutylnitrile (AIBN)

Procedure:

15.24 g TEGDA was dissolved in 153.97 g chloroform to prepare 10 wt % TEGDA solution. To the solution was added 0.27 g AIBN. PPX-C films or tubes were immersed in the solution for 2 days.

The PPX-C films or tubes were taken out, dried at room temperature in vacuum for 2 hrs, then annealed at 80ºC under nitrogen for 1 hr.

After annealing, the PPX-C films or tubes were immersed in $CHCl_3$ for 2 hrs and washed with $CHCl_3$ for three times, then immersed in water (50ºC) for 1 day and washed with water for three times, with THF for two times, respectively. At last, the films or tubes were dried in vacuum at 40ºC for 1 day.

IR spectrum (pressed tubes):

$\tilde{\nu}$ (cm^{-1}) = 3017 w, 2922 m, 2856 w, 1730 m, 1513 s, 1453 m, 1415 w, 1266 w, 1182 w, 1138 w, 1020 w, 821 s, 543

8 Conclusion

In this work, meso- and nano-scaled polymer fibers have been produced by means of electrospinning technique. The diameters of the as-spun polymer fibers range from as low as 5 nm to several micrometers. With electrospun fibers as template, polymer tubes with inner diameters ranging from 5 nm to a few micrometers can be fabricated by means of the TUFT process.

It is found that the shape and size of electrospun fibers depend on processing parameters. Solution concentration, solution viscosity, electrical conductivity of polymer solutions, molecular weight and molecular weight distribution of polymers are crucial process parameters. Surface tension of solutions has less influence on the fiber shape and size compared to the above parameters.

Functional polymer fibers were fabricated, including polymer / inorganic compound composite fibers, polymer / protein composite fibers, water-stable PVA fibers, fluorescent nanofibers, polymer / metal compound hybrid fibers. PVA / BSA composite fibers and PPX-coated PVA / BSA composite fibers proved to be promising in applications of drug delivery. PPX-coated PVA / BSA composite fiber system are a potential long-term sustain drug delivery system.

Functionalization of PPX tubes have been achieved by following approaches:

First of all, **PPX / polymer composite tubes have been prepared by means of the modified TUFT process,** for example, PPX / PAN composite tubes and PPX / PVA / PAA composite tubes. The introduction of second polymers containing functional groups increased the reactivity of PPX tubes, which have been proved by reactions taking place inside the PPX / PVA / PAA composite tubes.

Secondly, **PPX / metal composite tubes have been fabricated,** e.g. PPX / Al and PPX / Au composite tubes.

Thirdly, **PPX / metal hybrid tubes have been fabricated, such as PPX / Pd, PPX / Cu, and PPX / Ag hybrid tubes**. In these hybrid tubes, the metal nanoparticles were

wrapped by or finely dispersed in the PPX coatings, which is promising for the application as high efficient catalysts.

Fourthly, by means of **surface chemistry modifications**, various functional groups have been introduced onto the surface of PPX tubes, including carboxyl groups, hydroxyl groups, cyano groups, and crown ether groups. **Surface grafting of polymers** (e. g. PMMA) on PPX-X tubes have been accomplished by means of surface-initiated ATRP.

9 References

[1] Martin, R. V. P. C. R. *Nature* **1994**, 369, 298

[2] Michael H. Huang, Y. W., Hennning Feick, Ngan Tran, Eicke Weber, and Peidong Yang. *Adv. Mater.* **2001**, 13, 113

[3] Chang, B. H. L., Z. Q.; Sun, L. F.; Tang, D. S.; Zhou, W. Y.; Wang, G,; Qian, L. X.; Xie, S. S.; Fen, J. H.; Wan, M. X. *Journal of low Temperature Physics* **2000**, 119, 41

[4] Guangli Che, B. B. L., Ellen R. Fisher and Charles R. Martin. *Nature* **1998**, 393, 346

[5] K. Graham, M. O., T. Raether, T. Grafe, B. McDonald, P. Knauf. The Fifteenth Annual Technical *Conference & Expo of the American Filtration & Separations Society, Galveston, Texas,* April 9-12 **2002**, pp.

[6] Martin, C. R. M., C. P.; Nishizawa, M.; Jirage, K. *Book of Abstracts, 211th ACS National Meeting, New Orleans, LA, United States*, **1996**, pp.

[7] J. C. Hulteen, K. B. J., C. R. Martin. *J. Am. Chem. Soc.* **1997**, 120, 6603

[8] K. B. Jirage, J. C. H., C. R. Martin. *Science* **1997**, 278, 655*658

[9] Martin, Y. K. a. C. R. *Anal. Chem.* **1999**, 71, 3665

[10] G. Che, B. B. L., E. R. Fisher, C. R. Martin,. *Nature* **1998**, 393, 346

[11] Demoustier-Champagne, S. M. S., Pierre-Yves; Delvaux, Marc. *Abstr. Pap. - Am. Chem. Soc. 220th PMSE-240,* **2000**, pp.

[12] Y. Zhang, H. D., I.D. Norris, A. G. MacDiarmid, W. E. Jones. *Abstr. Pap. Am. Chem. Soc.* **2001**,,

[13] C. A. Foss Jr., G. L. H., J. A. Stockert, C. R. Martin. *J. Phys. Chem.* **1992**, 96, 7497

[14] Huaqiang Cao, Z. X., Hai Sang, Dong Sheng, and Chenyang Tie. *Adv. Mater.* **2001**, 13, 121

[15] T. M. Whitney, J. S. J., P. C. Searson, C. L. Chien. *Science* **1993**, 261, 1316

[16] Z. H. Cai, C. R. M. *J. Am. Chem. Soc.* **1989**, 111, 4138

[17] Martin, W. L. a. C. R. *J. Am. Chem. Soc.* **1990**, 112, 9666

[18] Martin, W. L. a. C. R. *J. Am. Chem. Soc.* **1990**, 112, 9666

[19] Martin, C. J. B. a. C. R. *J. Am. Chem. Soc.* **1991**, 113, 3174

[20] Martin, C. R. M. *Book of Abstracts, 210th ACS National Meeting, Chicago, IL*, **1995**, pp.

[21] Martin, C. R. *Acc. Chem. Res.* **1995**, 28, 61

[22] Martin, C. R. *Chem. Mater.* **1996**, 8, 1739

[23] Martin, A. K. a. C. R. *Analytical Chemistry* **1999**, 71, 3665

[24] Martin, C. R. *Chem. Mater.* **1996**, 8, 1739

[25] Li, B. Z., Guangshan; Wang, Xing; Gao, Feifei; Guo, Zhuo; Liu, Chengzhan; Yin, Xiaoju; Wang, Chunlei; Qiu, Shilun. *Abstracts of Papers, 224th ACS National Meeting*, Boston, MA, United States, **2002**, pp.

[26] Steinhart, M. W., J. H.; Greiner, A.; Wehrspohn, R. B.; Nielsch, K.; Schilling, J.; Choi, J.; Goesele, U. *Science (Washington, DC, United States)* **2002**, 296, 1997

[27] Li, B. Z., Guangshan; Wang, Xing; Gao, Feifei; Tu, Shengjiang; Wang, Chunlei; Ben, Teng; Qiu, Shilun; Zhang, Wanjin. *Abstracts of Papers, 224th ACS National Meeting,* Boston, MA, United States, August 18-22 **2002**, pp.

[28] Beck, J. S. V., J. C.; Roth, W. J.; Leonowicz, M. E.; Kresge, C. T.; Schmitt, K. D.; Chu, C. T.-W.; Olson, D. H.; Sheppard, E. W.; McCullen, S. B.; Higgins, J. B.; Schlenker, J. L. *J. Am. Chem. Soc.* **1992**, 114, 10834

[29] Wu, C.-G. B., T. *Science* **1994**, 266, 1013

[30] Wu, C.-G. B., T. *Science* **1994**, 264, 1757

[31] Bruno, F. F. S., Lynn; Roy, Sucharita; Nagarajan, Ramaswamy; Kumar, Jayant; Ziegler, David; Sennett, Michael. *Polymer Preprints (American Chemical Society, Division of Polymer Chemistry)* **2002**, 43, 961

[32] Niu, C. H., Bob; Tennent, Howard. *NASA Conference Publication* **2001**, 210948 (Proceedings of the Sixth Applied Diamond Conference / Second Frontier Carobon Technology Joint Conference, 2001), 652

[33] Ajayan, P. M. V., Robert. *Nano Science Series, Series E: Applied Sciences* **2001**, 372 (Carbon Filaments and Nanotubes: Common Origins, Differing Applications?), 315

[34] Semoustier-Chamagne, S. D., M. *Materials Science & Engineering, C: Biomimetic and Supramolecular Systems* **2001**, C15, 269

[35] QI, Z. L., R. Bruce. *Proceedings - Electrochemical Society* **1997**, 97-5 (Microstructures and Microfabricated Systems), 173

[36] G. Shi, S. J., G. Xue, C. Li. *Science* **1995**, 267, 994

[37] G. Shi, C. L., Y. Liang. *Adv. Mater.* **1999**, 11, 1145

[38] Kobayashi, S. H., Nobuhiro; Suzuki, Masahiro; Kimura, Mutsumi; Shirai, Hirofusa; Hanabusa, Kenji. *Journal of the American Chemical Society* **2002**, 124, 6550

[39] Lakshmi, B. B. D., Peter K.; Martin, Charles R. *Chemistry of Materials* **1997**, 9, 857

[40] Fueters, A. B. *Carbon* **2002**, 40, 1600

[41] G. Che, B. B. L., C. R. Martin, and E. R. Fisher. *Chem. Mater.* **1998**, 10, 260

[42] G. Che, B. B. L., E. R. Fisher, C. R. Martin,. *Nature* **1998**, 393, 346

[43] Guangli Che, S. A. M., Ellen R. Fisher and Charles R. Martin. *Anal. Chem.* **1999**, 71, 3187

[44] Mingxiao Fu, Y. Z., Ruiqin Tan, and Gaoquan Shi. *Adv. Mater.* **2001**, 13, 1874

[45] Martin, C. J. B. a. C. R. *J. Am. Chem. Soc.* **1991**, 113, 3174

[46] Parthasarathy, R. V. M., C. R. *Adv. Mater.* **1995**, 7, 896

[47] T. Kyotani, L.-F. T. A. T. *Chem. Mater.* **1995**, 7, 1427

[48] J. D. Klein, R. D. I. H., D. Palmer, M. J. Sailor, C. J. Brumlik, C. R. Martin. *Chem. Mater.* **1993**, 5, 902

[49] B. B. Lakshmi, P. K. D., C. R. Martin. *Chem. Mater.* **1997**, 9, 857

[50] Jianchun Bao, D. X., Quanfa Zhou, and Zheng Xu. *Chem. Mater.* **2002**, 14, 4700

[51] Haoqing Hou, Z. J., Arndt Reuning, Andreas Schaper, Joachim H. Wndorff, and Andreas Greiner. *Macromolecules* **2002**,,

[52] M. Bognitzki, H. H., M. Ishaque, T. Frese, M. Hellwig, C. Schwarte, A. Schaper, J. H. Wendorff, and A. Greiner. *Adv. Mater.* **2000**, 12, 637

[53] M. M. Bergshoef, G. J. V. *Adv. Mater.* **1999**, 11, 1362

[54] Young-Sic kang, H.-Y. K., Young-Jun Ryu, Douk-Rae Lee, and Soo-Jin Park. *Polymer (Korea)* **2002**, 26, 360

[55] Bin Ding, H.-Y. K., Se-Chul Lee, Chang-Lu Shao, Douk-Rae Lee, Soo-Jin Park, Gyu-Beom Kwag, Kyung-Ju Choi. *Journal of Polymer Science: Part B: Polymer Physics* **2002**, 40, 1261

[56] Wan-Ju Li, C. T. L., Edward J. Caterson, Rocky S. Tuan, Frank K. Ko. *Journal of Biomedical Materials Research* **2002**, 60 (4), 613

[57] Xinhua Zong, K. K., Dufei Fang, Shaofeng Ran, Benjamin S. Hsiao, Benjamin Chu. *Polymer* **2002**, 43, 4403

[58] M. Bognitzki, W. C., T. Frese, A. Schaper, M. Hellwig, M. Steinhart, A. Greiner, and J. H. Wendorff. *Adv. Mater.* **2001**, 13, 70

[59] M. Bognitzki, T. F., J.H. Wendorff, A. Greiner. *Poly. Prepr. (ACS, PMSE)* **2000**, 82, 45

[60] M. M. Demir, L. Y., E. Yilgor, B. Erman. *Polymer* **2002**, 43, 3303

[61] Hao Fong, D. H. R. *Journal of Polymer Science: Part B: Polymer Physics* **1999**, 37, 3488

[62] D. H. Reneker, I. C. *Nanotechnology* **1996**, 7, 216

[63] Yu Wang, S. S., J. J. Santiago-Aviles. *Journal of materials science letters* **2002**, 21, 1055

[64] X. Wang, S.-G. H., M. T. S. Downey, L. Samuelson. *Synth. Met.* **1999**, 107, 117

[65] I. D. Norris, M. M. S., FK. Ko, A. G. MacDiarmid. *Synth. Met.* **2000**, 114, 109

[66] Dong H., J. W. *Polymeric materials: Science & Engineering* **2002**, 87, 273

[67] Christopher J. Buchko, L. C. C., Yu Shen, David C. Martin. *Polymer* **1999**, 40, 7397

[68] J. A. Matthews, G. E. W., D. G. Simpson, and G. L. Bowlin. *Biomacromolecules* **2002**, 3, 232

[69] K. Nagapudi, W. T. B., J. E. Leisen, L. Huang, R. A. McMillan, R. P. Apkarian, V. P. Conticello, E. L. Chaikof. *Macromolecules* **2002**, 35, 1730

[70] L. Huang, R. P. A., E. L. Chaikof. *Scanning* **2001**, 23, 372

[71] L. Huang, K. N., R. P. Apkarian, E. L. Chaikof. *J. Biomater. Sci. - Polym. Ed.* **2002**, 12, 979

[72] Lei Huang, R. A. M., Robert P. Apkarian, Benham Pourdeyhimi, Vincent P. Conticello, and Elliot L. Chaikof. *Macromolecules* **2000**, 33, 2989

[73] Reneker, X. F. a. D. H. *J. Macromol. Sci. - Phys. B* **1997**, 36, 169

[74] H. J. Jin, S. V. F., G. C. Rutledge, D. L. Kaplan. *Poly. Prepr.* **2002**, 43, 743

[75] Shahrzad Zarkoob, D. H. Reneker, R. K. Eby, S. D. Hudson, D. Ertley, W. W. Adams., *Book of Abstracts, 216th ACS National Meeting*, Boston, August 23-27, **1998**

[76] W. Liu, M. G., E. A. Evans, and D. H. Reneker. *J. Material Research* **2002**, 7, 1

[77] P. Gibson, H. S.-G., and D. Rivin. *Colloids and Surfaces A: Physicochemical and Engineering Aspects* **2001**, 187-188, 469

[78] H. Schreuder-Gibson, P. G., K. Senecal, M. Sennett, J. Walker, W. Yeomans, D. Ziegler, P. P. Tsai. *J. Adv. Mater.* **2002**, 34, 44

[79] Jacobsen, M. *Nonwovens Industry* **1991.**

[80] X. Wang, C. D., S. Lee, K. J. Senecal, J. Kumar, L. A. Samuelson. *Polymeric materials: Science & Engineering* **2002**, 87, 284

[81] X. Y. Wang, S. L., C. Drew, K. J. Senecal, J. Kumar, L. A. Samuelson. *Abstr. Pap. Am. Chem. Soc.* **2001**,

[82] E. R. Kenawy, G. L. B., K. Mansfield, J. Layman, D. G. Simpson, E. H. Sanders, G. E. Wnek. *Journal of Controlled Release* **2002**, 81, 57

[83] E. D. Boland, G. E. W., D. G. Simpson, K. J. Pawlowski, and G. L. Bowlin. *J. Macromol. Sci. - Pure Appl. Chem., A* **2001**, 38, 1231

[84] S. Shortkroff. Y. Li, T. S. T., G.C Rutledge. *Polymeric materials: Science & Engineering* **2002**, 87, 457

[85] Reneker, J.-S. K. a. D. H. *Polymer Composites* **1999**, 20, 124

[86] Gorham, W. F. *U. S. Patent*, **1967**, 3, 342, 754

[87] Rayleigh, L. *Phil. Mag. J.* **1882**, 44, 184

[88] Formhals, A. *US Patent*, **1934**, US 1,975,504

[89] Baumgarten, P. K. *J. Colloid Interface Sci.* **1971**, 36, 71

[90] L. Larrondo, a. R. S. J. M. *J. Polymer Sci.: Polymer Phys. Edn.* **1981**, 19, 909

[91] L. Larrondo, a. R. S. J. M. *J. Polymer Sci.: Polymer Phys. Edn.* **1981**, 19, 921

[92] L. Larrondo, a. R. S. J. M. *J. Polymer Sci.: Polymer Phys. Edn.* **1981**, 19, 933

[93] I. Chun, D. H. R., H. Fong, X. Fang, J. Deitzel, N. B. Tan and K. Kearns. *J. Adv. Mater.* **1996**, 31, 36

[94] J. Doshi, G. S., D. H. Reneker. *Polym. News* **1995**, 20, 206

[95] J. Doshi, D. H. R. *J. Electrostatics* **1995**, 35, 151

[96] D. H. Reneker, A. L. Y., H. Fong, S. Koombhongse. *J. Appl. Phys.* **2000**, 87, 4531

[97] M. Bognityki, T. F., M. Steinhart, A. Greiner, J.H. Wendorff, A. Schaper, M. Hellwig. *Polym. Eng. Sci.* **2001**, 41, 982

[98] A. L. Yarin, S. K. a. D. H. R. *Journal of applied physics* **2001**, 89, 3018

[99] J. M. Deitzel, J. K., D. Harris, NCB Tan. *Polymer* **2001**, 42, 261

[100] A. G. MacDiarmid, W. E. J., I. D. Norris, J. Gao, A. T. Johnson, N.J. Pinto, J. Hone, B. Han, FK. Ko, H. Okuzaki, M. Llaguno. *Synth. Met.* **2002**, 119, 27

[101] J. S. Kim, D. H. R. *Polymer Composites.* **1999**, 20, 124

[102] Szwarc, M. *Nature* **1947**, 160, 403

[103] Szwarc, M. *Faraday Society Discussions* **1947**, 2, 46

[104] Szwarc, M. *J. Chem. Phys.* **1948**, 16, 128

[105] H. G. Gilch, W. L. W. *J. Polym. Sci., Part A-1* **1966**, 4, 1337

[106] L. A. Errede, B. F. L. *J. Am. Chem. Soc.* **1957**, 79, 4952

[107] J. M. Pearson, H. A. S., D. J. Williams, M. Levy. *J. Am. Chem. Soc.* **1971**, 5034

[108] O. Schaefer, S. M., E. Arici, G. Luessen, C. Unterlechner, J. H. Wendorff, A. Greiner. *Macromol. Chem. Phys.* **1998**, 199, 807

[109] Beach, W. F. *Encycopadia of Polymer Science and Engineering*; Wiley: New York, 1998

[110] L. A. Errede, N. K. *J. Polym. Sci.* **1962**, 60, 33

[111] R. I. Iwamoto, R. C. B., B. Wunderlich. *J. Polym. Sci., Polym. Phys. Ed.* **1975**, 13, 1925

[112] Gorham, W. F. *J. Polym. Sci., Part A-1* **1966**, 4, 3027

[113] W. F. Beach, T. M. A. *SAMPE Journal* **1988**, 6, 9

[114] R. A. Caruso, J. H. S., A. Greiner. *Adv. Mater.* **2001**, 13, 1577

[115] Grattan, D. W. *Can. Chem. News* **1989**, 25,

[116] Matyjaszewski, J.-S. W. a. k. *Macromolecules* **1995**, 28, 7901

[117] Krzysztof Matyjaszewski, T. E. P., and Jianhua Xia. *J. Am. Chem. Soc.* **1997**, 119, 674

[118] Krzysztof Matyjaszewski, S. M. J., Hyun-jong Paik, and Scott G. Gaynor. *Macromolecules* **1997**, 30, 6398

[119] Krzysztof Matyjaszewski, P. J. M., Nisha Shukla, Boonchuan Immaraporn, Andrew Gelman, Barry B. Luokala, Tiberiu M. Siclovan, Guido Kickelbick, Thomas Vallant, Helmuth Hoffmann, and Tadeusz Pakula. *Macromolecules* **1999**, 32, 8716

[120] M. Save, J. V. M. W., and S. P. Armes. *Macromolecules* **2002**, 35, 1152

[121] Xia, K. M. a. J. *Chem. Rev.* **2001**, 101, 2921

[122] Xiao-song Wang, N. L., Sheng-kang Ying. *Polymer* **1999**, 40, 4157

[123] Xuan Zhang, J. X., and Krzysztof Matyjaszewski. *Macromolecules* **1998**, 31, 5167

[124] Zhu, Y. S. a. S. *Macromolecules* **2001**,,

[125] A. Ersin Acar, M. B. Y., and Lon J. Mathias. *Macromolecules* **2000**, 33, 7700

[126] J. Xia, K. M. *Macromolecules* **1999**, 32, 5199

[127] Jianhua Xia, S. G. G., and Krzysztof Matyjaszewski. *Macromolecules* **1998**, 31, 5958

[128] Jong-Bum Kim, M. L. B., and Gregory L. Baker. *J. Am. Chem. Soc.* **2000**, 122, 7616

[129] Wenxi Huang, J.-B. K., Merlin L. Brening, and Gregory L. Baker. *Macromolecules* **2002**, 35, 1175

[130] H. Fong, I. C., D.H. Reneker. *Polymer* **1999**, 40, 4585

[131] F. Ignatious, J. M. B. PCT Int., **2000**, WO 0154667

[132] Koizumi, S. K., Nobuyuki. (Fuji Photo Film Co., Ltd., Japan). *Jpn. Kokai Tokkyo Koho*, **1988**, JP 63218945 A2 19880912 Application: JP 87-51782 19870306. CAN 110:125500

[133] Koizumi, S. K., Nobuyuki. (Fuji Photo Film Co., Ltd., Japan). *Brit. UK Pat. Appl.*, **1988**, GB 2204315 A1 19881109

[134] Satomura, M. F. P. F. C., Ltd., Japan). *Jpn. Kokai Tokkyo Koho*, **1975**, JP 50005032 19750120 Application No.: JP1973-2539

Acknowledgements

The presented dissertation was performed in the Institute of physical, nuclear, and macromolecular chemistry in Philipps-University Marburg during the period from September 1999 to March 2003.

I am very grateful to all the people who have given me much support and help so that I could successfully fulfill this work.

I am very grateful to Prof. Dr. A. Greiner for his grant of this topic, his strong interest, his continuous encouragement, and his novel ideas, interesting aspects, and helpful suggestions during the work.

I thank my colleague, Dr. Haoqing Hou, for his much help and frequent encouragement during my work. In particular, I thank him for his helpful suggestions in chemical synthesis and PPX coating, and his instruction in the operation of scanning electronic microscopy.

The group of Prof. Dr. J. H. Wendorff gave me much help in the preparation of film samples by spin-coating, measurement of contact angle, and measurement of wide-angle X-ray diffraction. I am very grateful to all the members of AK Wendorff for their friendly help.

The group of Prof. Dr. A. Schaper gave me much support in characterization of my samples by SEM and TEM. I thank Prof. Dr. A. Schaper for his instruction in the operation of the transmission electronic microscopy. Also, I thank Mr. M. Hellwig for his SEM observations and Mr. Zhihong Jia for his TEM observations.

I thank Prof. Massa for his instruction in identification of metal by X-ray diffractograms.

I am grateful to the colleagues in Feinmechanischen-Werkstatt for their perfect techniques in making various devices required by my experiments. Also, I thank the colleagues in Electronikwerkstatt for their help in solving various electrical problems.

Acknowledgements

I thank Dr. M. Bognitzki for the frequent discussion about electrospinning.

Mrs. Schmidt gave me much kindly help to solve many problems which I as a foreign student frequently met in Germany. Here I thank her very much.

I thank my colleague, Dr. Seema Agarwal, for her intensive correction of my thesis.

I thank all the members of the group of Prof. Dr. A. Greiner for the friendly group atmosphere and the together spent happy time, especially the unforgotable experiences in Kleinwassertal.

I thank my parents and my husband for their continuous support and encouragement during my study.